# Efficient Joint Broadband Radar and Communication for Airborne SAR Imaging with Small Platforms

Von der Fakultät für Informatik, Elektrotechnik und Informationstechnik der Universität Stuttgart zur Erlangung der Würde eines Doktor-Ingenieurs (Dr.-Ing.) genehmigte Abhandlung

Vorgelegt von

**Winfried Johannes**

aus Adenau

| | |
|---|---|
| Hauptberichter: | Prof. Dr.-Ing. Ingmar Kallfass |
| Mitberichter: | Prof. Dr.-Ing. Dirk Nüßler |
| | |
| Tag der mündlichen Prüfung: | 12.03.2025 |

Institut für Robuste Leistungshalbleitersysteme der Universität Stuttgart

2024

# Executive Abstract

Integrating multiple functionalities into radio frequency systems becomes more and more interesting for researchers, users and customers. The motivation for this trend is saving energy, size, weight and costs regarding the final product. One important aim is to achieve joint radar and wireless communication systems, because both functions are based on radio frequencies. In this context, designations like radar and communication (RadCom), dual-function radar-communication (DFRC) or joint communication and sensing (JCS) are well known in the community. It can be differentiated whether an approach emphasizes a radar sensor with communication capabilities or a wireless communication system with sensing skills.
This thesis addresses the problem of realizing a joint high-resolution radar sensor with several GHz of bandwidth and simultaneous wireless communication with a data rate on the order of 100 Mbit/s working as a battery-driven airborne system in the millimeter-wave band. Therefore, it is essential to reach a minimal power consumption and also minimal size and weight of the final system for maximizing the operation time. The application behind this problem is for example the continuous, image-based surveillance of an area of interest with a circular synthetic aperture radar (CSAR) and simultaneous radar raw data transmission to a ground station inside the surveillance area.
Thus, a broadband radar considering high power efficiency, low system size and weight and also low cost for the mentioned application is required. It is found that a continuous wave radar with frequency modulation (FMCW) in the millimeter-wave band is the best choice for this problem. Its analog de-ramping capability helps to significantly reduce the sample rate of the analog-to-digital converter (ADC), the usage of a solid-state amplifier and the constant envelope of the time and frequency signal without additional effort.
Regarding the communication in the millimeter-wave band, a robust data link

with a sufficient data rate for transmitting the FMCW radar raw data is required. Here, power efficiency is also an important task. It is found that communication with quadrature phase shift keying (QPSK) is ideal for this scenario, because the peak-to-average power ratio (PAPR) is as low as possible for high power efficiency. Furthermore, a sufficient data rate can be reached and the data transmission is very robust.

Consequently, it is necessary to integrate a data link into an FMCW radar system by using only one high power amplifier (HPA) and a single transmit antenna for saving resources. The best choice for this is shown in this work to be the approach of frequency division multiplexing (FDM) of broadband FMCW radar and single-carrier QPSK communication, because sufficient data rates in a robust behavior and ultra-high synthetic aperture radar (SAR) image resolution can be realized simultaneously with high power efficiency. One competing state-of-the-art approach is orthogonal frequency division multiplexing (OFDM). This is a popular method of realizing radar and high-speed communication simultaneously, but cannot be used in the target application scenario, as shown in this work. This is because of a high peak-to-average power ratio (and hence, poor power efficiency), high challenges regarding the digital signal processing and ultra-high requirements regarding system linearity compared with the proposed technique. Therefore, high-resolution SAR imaging by using small platforms is not possible efficiently with OFDM but with the proposed technique of joint FMCW broadband radar and QPSK communication in FDM.

By using only a single HPA for FDM with two closely related carrier frequencies for FMCW radar and for QPSK communication, it is essential to consider the resulting intermodulation products. This is treated theoretically in a first step. Here, it is found that the resulting overall bandwidth for the SAR scenario is only 5% larger than the radar bandwidth, because of the additional communication bandwidth and a required gap between both frequency bands. While the transmit power of the radar should be as high as possible (dependent on the range to the power of four), the power level of the communication (because of range to the power of two) can be reduced. This helps with suppressing the intermodulation products. In the discussed example, the system performance is optimized with simulations and measurements regarding a minimal error

vector magnitude (EVM) for different power levels of the communication part and different gaps between both frequency bands for saving overall bandwidth. The results are verified quantitatively with radar measurements and with constellation diagrams for the communication.
In summary, this work presents an efficient approach of joint broadband radar and single-carrier communication in FDM for airborne SAR and radar raw data transmission to a ground station in comparison to the state of the art. Here, the resulting overall bandwidth for an assumed SAR scenario is only 5% larger than the radar bandwidth of 2 GHz. It is found to be possible to reduce the gap between the radar band and the communication band based on measurements by 70%. This minimizes also the overall bandwidth of the mentioned approach.

# Zusammenfassung

Mehrere Funktionen innerhalb eines Systems, welches mit Funkfrequenzen arbeitet, werden für Forscher, Anwender und Kunden immer interessanter. Dieses liegt an der Einsparung von Leistungsaufnahme, Größe, Gewicht und Kosten beim Endprodukt. Es ist besonders der Fall bei der gemeinsamen Nutzung eines Radarsensors und der drahtlosen Kommunikation, da beide Funktionen auf der Nutzung von Funkfrequenzen basieren. In diesem Zusammenhang sind in der Community Bezeichnungen wie Radar and Communication (RadCom), Dual-Function Radar-Communication (DFRC) oder Joint Communication and Sensing (JCS) bekannt, wobei zwischen einem Radarsensor mit Kommunikationsfähigkeit und einem drahtlosen Kommunikationssystem mit Sensorfähigkeiten unterschieden werden kann.
Diese Arbeit beschäftigt sich mit der Aufgabe, einen hochauflösenden Radarsensor mit mehreren GHz Bandbreite und gleichzeitiger, drahtloser Kommunikation mit einer Datenrate von einigen 100 Mbit/s in einem System zu erforschen. Dieses soll als batteriebetriebenes, luftgestütztes System im Millimeterwellenband arbeiten. Dafür ist es wichtig, eine minimale elektrische Leistungsaufnahme, eine geringe Baugröße und ein geringeres Gewicht des Endsystems zu erreichen, wodurch die Betriebszeit maximiert werden kann. Eine mögliche Anwendung dafür ist die kontinuierliche, bildbasierte Beobachtung eines Überwachungsgebietes am Boden mit einem luftgetragenen Radar mit zirkularer, synthetischer Apertur (CSAR) und gleichzeitiger Übertragung der Radar-Rohdaten an eine Bodenstation innerhalb des Überwachungsbereichs.
Für die genannte Anwendung ist ein breitbandiges Radar mit hoher Leistungseffizienz, kleiner Systemgröße und geringem Systemgewicht sowie geringen Kosten erforderlich. Es zeigt sich, dass ein Dauerstrichradar mit Frequenzmodulation (FMCW) im Millimeterwellenband die beste Wahl für dieses Problem ist. Dieses ist unter anderem auf die kompakte Bauform, das analoge

de-ramping zur erheblichen Reduzierung der Abtastrate des Analog-Digital-Wandlers (ADC), die Verwendung von Halbleiterverstärkern und die vorhandene, konstante Hüllkurve des Zeit- und Frequenzsignals zurückzuführen.
Für die Übertragung der FMCW-Radar-Rohdaten zu einer Bodenstation ist eine robuste Datenverbindung mit ausreichender Datenrate im Millimeterwellenband erforderlich. Auch hier ist die Energieeffizienz eine wichtige Aufgabe. Es stellt sich heraus, dass die Kommunikation mit nur einem Träger und mit Quadraturphasenumtastung (QPSK) dafür ideal ist, da das Spitzen-zu-Durchschnittsleistungsverhältnis (PAPR) sehr niedrig ist. Darüber hinaus kann eine ausreichende Datenrate erreicht werden. Die sich ergebende Datenübertragung ist zudem sehr robust.
Folglich ist es für das genannte Szenario erforderlich, eine Datenkommunikation in ein FMCW-Radarsystem zu integrieren. Es ist dafür notwendig, nur einen Leistungsverstärker (HPA) und eine einzige Sendeantenne zu verwenden, um Ressourcen zu sparen. Die beste Wahl hierfür ist der neue Ansatz des Frequenzmultiplex (FDM) von Breitband-FMCW-Radar und Einzelträger-QPSK-Kommunikation. Hier können ultrahohe SAR-Bildauflösung und robuste Kommunikation mit ausreichender Datenrate gleichzeitig und mit hoher Leistungseffizienz realisiert werden. Ein häufig angewandter Ansatz ist Orthogonal Frequency Division Multiplexing (OFDM). Dieses ist eine weitere mögliche Methode zur gleichzeitigen Realisierung von Radar und Kommunikation, was hier jedoch nicht verwendet werden kann. Begründet wird dieses mit einem hohen Spitzen-zu-Durchschnittsleistungsverhältnis (schlechte Leistungseffizienz), mit Herausforderungen hinsichtlich einer effizienten digitalen Signalverarbeitung und mit extrem hohen Anforderungen an die Systemlinearität im Vergleich zur vorgeschlagenen Technik. Daher ist eine hochauflösende SAR-Bildgebung unter Verwendung kleiner Plattformen mit OFDM nicht effizient möglich, wohl aber mit der hier vorgeschlagenen Technik eines gemeinsamen FMCW-Breitbandradars und einer QPSK-Kommunikation in FDM.
Durch die Verwendung eines einzelnen HPA für FDM mit zwei dicht benachbarten Trägerfrequenzen für FMCW-Radar und für QPSK-Kommunikation ist es wichtig, die resultierenden Intermodulationsprodukte zu berücksichtigen. Dieses wird zuerst theoretisch behandelt. Die sich ergebende Gesamtband-

breite für ein angenommenes CSAR-Szenario aufgrund der zusätzlichen Kommunikationsbandbreite und einer erforderlichen Lücke zwischen beiden Frequenzbändern ist hierbei nur 5% größer als die Radarbandbreite. Während die Sendeleistung des Radars möglichst hoch sein sollte (abhängig von der Entfernung zur vierten Potenz), kann die Leistung der Kommunikation (abhängig von der Entfernung zur zweiten Potenz) reduziert werden. Dieses führt dann zur Unterdrückung der Intermodulationsprodukte. Im diskutierten Beispiel wird die Systemleistung durch Simulationen und Messungen hinsichtlich einer minimalen Fehlervektorgröße (EVM) für unterschiedliche Leistungspegel der Kommunikation und unterschiedliche Lücken zwischen beiden Frequenzbändern optimiert, um Gesamtbandbreite einzusparen. Die Ergebnisse werden mit Radarmessungen und mit Konstellationsdiagrammen für die Kommunikation quantitativ verifiziert.

Zusammenfassend stellt diese Arbeit einen effizienten Ansatz für die gemeinsame Realisierung von Breitbandradar und Einzelträgerkommunikation in FDM für luftgestütztes SAR und die Radar-Rohdatenübertragung an eine Bodenstation im Vergleich zum Stand der Technik vor. Dabei ist die resultierende Gesamtbandbreite für ein angenommenes SAR-Szenario nur 5% größer als die Radarbandbreite von 2 GHz. Basierend auf Messungen wurde festgestellt, dass es möglich ist, die Lücke zwischen dem Radarband und dem Kommunikationsband um 70% zu verringern. Dies minimiert auch die Gesamtbandbreite des genannten Ansatzes.

# Acknowledgements

It is with great thankfulness that I would like to express my appreciation and recognition for all those who supported me on my way to completing this doctoral thesis.

I would like to express my sincere gratitude to my doctoral supervisor, Professor Ingmar Kallfass. His support and expert advice guided me through the challenges of this research project. Without his commitment this work would not have been possible.
I would also like to thank my second reviewer, Professor Dirk Nüßler, who sacrificed his time and expertise to survey this work.
A special thank you goes to my second supervisor, Dr. Stephan Stanko, who supported me with patience and foresight. His professional expertise and encouragement were invaluable to me.
My sincere thanks also go to my colleagues of the Fraunhofer Institute for High Frequency Physics and Radar Techniques, especially Denis Nötel, Dr. Michael Caris and Frank Klöppel, for their inspiring conversations, their constructive feedback and their constant support.
I would also like to thank the clients, Bundeswehr Technical Center for Information Technology and Electronics (WTD81 – GF320) and the Research and Innovation Hub of the Planning Department of the Federal Ministry of Defense, who provided the financial support and resources.
My family has always shown me support, love and understanding. She gave me the opportunity to focus on my academic goals. Their support and encouragement have been the driving force behind my success.

Finally, I would like to thank everyone who contributed in any way to completing this doctoral thesis. Their support motivated me to do my best.

# Contents


**Abstract** **i**

**Zusammenfassung** **v**

**Acknowledgements** **ix**

**List of Figures** **xv**

**List of Tables** **xxi**

**List of Abbreviations and Symbols** **xxv**

**1 Introduction** **1**

1.1 Motivation . . . . . . . . . . . . . . . . . . . . . . . . . . 1

1.2 State of the Art . . . . . . . . . . . . . . . . . . . . . . . . 3

1.2.1 Orthogonal frequency division multiplexing . . . . . . . . 3

1.2.2 FMCW waveform with integrated communication . . . . 6

1.2.3 Joint SAR and communication . . . . . . . . . . . . . . . 8

1.2.4 Summary . . . . . . . . . . . . . . . . . . . . . . . . . 9

1.3 Scope of this Work . . . . . . . . . . . . . . . . . . . . . . . 10

**2 Introduction to Joint Broadband Radar and Single-Carrier Communication in FDM** **13**

2.1 Introduction to Radar . . . . . . . . . . . . . . . . . . . . . . 14

2.2 Introduction to Wireless Communication . . . . . . . . . . . . . 17

2.3 FDM of Broadband FMCW Radar and Single-Carrier QPSK Communication . . . . . . . . . . . . . . . . . . . . . . . . . 20

2.3.1 Introduction . . . . . . . . . . . . . . . . . . . . . . . . 20

2.3.2 General Description . . . . . . . . . . . . . . . . . . . . 22

2.3.3 Hardware Description . . . . . . . . . . . . . . . . . . . . 24
2.3.4 Simulation Results Based on an Initial Parameter Set. . 28
2.3.5 Measurement Results Based on an Initial Parameter Set 30

**3 Analysis of the Relation Between the Radar Band and the Communication Band in FDM 35**
3.1 Investigation of the Intermodulation Products of the HPA . . . . 36
3.1.1 Fundamental Considerations of Intermodulation Products 36
3.1.2 Third-Order Intermodulation of Radar and Communication in FDM . . . . . . . . . . . . . . . . . . . . . . . . 38
3.1.3 Formulation of the Resulting Overall Bandwidth for the CSAR application . . . . . . . . . . . . . . . . . . . . . 40
3.2 Evaluation of the Gap Width Dependence of the System Performance . . . . . . . . . . . . . . . . . . . . . . . . . . . . 44
3.2.1 Effect of Different Gaps on the Communication Performance . . . . . . . . . . . . . . . . . . . . . . . . . . 44
3.2.2 Effect of Different Gaps on the FMCW Radar Performance 49
3.3 Determination of the Frequency of the Local Oscillator for down-conversion of the QPSK signal . . . . . . . . . . . . . . . . . . 60
3.3.1 Mathematical Deduction . . . . . . . . . . . . . . . . . . 60
3.3.2 Behavior of the IF Signals in the Receive Path . . . . . . 63
3.3.3 Analysis of the Measured Signals After the HPA and the Receiving Mixer . . . . . . . . . . . . . . . . . . . . . . 65
3.4 Discussion and Conclusion . . . . . . . . . . . . . . . . . . . 70

**4 Optimization of the Communication Signal Parameters for Minimum Bandwidth Requirements 73**
4.1 Investigation of Third-Order Non-Linearity Reduction . . . . . . 74
4.1.1 Fundamentals of third-order non-linearities . . . . . . . 74
4.1.2 Power-Balancing Regarding the FMCW Radar Signal . . 77
4.1.3 Power-Balancing Regarding the QPSK Communication Signal . . . . . . . . . . . . . . . . . . . . . . . . . . 79

4.2 Fundamentals regarding the Power of the Third-Order Intermodulation Products . . . 81
4.3 Reducing the Influence of the Third-Order Intermodulation Products . . . 83
4.3.1 Varying the Third-Order Intercept Point . . . 83
4.3.2 Varying the Power of the Communication Signal . . . 85
4.4 Signal-to-Noise Ratio of FMCW Radar and QPSK Communciation in FDM for an assumed CSAR scenario . . . 90
4.5 Discussion and Conclusion . . . 94

**5 Analysis of the Power Efficiency of Joint Broadband Radar and Single-Carrier Communication in FDM 97**
5.1 Introduction to the Complementary Cumulative Distribution Function . . . 98
5.1.1 Behavior of OFDM Regarding the Power Efficiency . . . 99
5.1.2 Comparison of 16-QAM and QPSK Regarding the Power Efficiency . . . 103
5.2 CCDF of FMCW Radar and QPSK Communication in FDM . . 104
5.2.1 Simulative Validation . . . 104
5.2.2 Behavior of an Amplifier Regarding the CCDF . . . 105

**6 Conclusions 109**

**Bibliography 115**

# List of Figures


2.1 Sketch of the FMCW signals with all relevant parameters. . . . . 16
2.2 Visualization of a carrier signal in the complex plane. . . . . . . 17
2.3 Visualization of TDM (left) and FDM (right) in the frequency time plane. . . . . . . . . . . . . . . . . . . . . . . . . . . . 19
2.4 Basic block diagram of the broadband FMCW radar and single-carrier QPSK communication in FDM. . . . . . . . . . . . . . . . 21
2.5 Simulated spectrum of the broadband FMCW radar and single-carrier QPSK communication in FDM. . . . . . . . . . . . . . . . 22
2.6 Photograph of the high power amplifier working in the Ka-band. 25
2.7 Amplification behavior of the amplifier for three different frequency points. . . . . . . . . . . . . . . . . . . . . . . . . 25
2.8 Third-order intercept point at the output of the amplifier ($OIP_3$) at three different frequency points. . . . . . . . . . . . . . . . 26
2.9 Power-added efficiency of the amplifier (PAE) at three different frequency points. . . . . . . . . . . . . . . . . . . . . . . . . 27
2.10 QPSK communication signal generated by the SDR ADALM PLUTO after the up-conversion. . . . . . . . . . . . . . . . . . 28
2.11 Simulated IF of the FMCW radar with and without simultaneous QPSK communication in FDM. . . . . . . . . . . . . . . . . . 29
2.12 Simulated constellation diagram of the QPSK communication with simultaneous FMCW radar in FDM. . . . . . . . . . . . . . 30
2.13 Block diagram of the measurement setup. The ADALM PLUTO is used as the SDR for communication, and the MIRANDA35 front-end for radar. . . . . . . . . . . . . . . . . . . . . . . . 31
2.14 Measured IF of the FMCW radar with and without simultaneous QPSK communication in FDM. . . . . . . . . . . . . . . . . . 32

2.15 Measured constellation diagram of the QPSK communication with simultaneous FMCW radar in FDM. . . . . . . . . . . . . . . 33

3.1 Sketch of the intermodulation products by using two frequencies. 37
3.2 Sketch of the third-order intermodulation products (red and blue), the radar band (black) and the communication band (green). . . 38
3.3 Sketch of joint CSAR and communication scenario with the most important parameters. . . . . . . . . . . . . . . . . . . . . . . . . 41
3.4 Simulated overall bandwidth dependent on the flight altitude for an assumed CSAR scenario. . . . . . . . . . . . . . . . . . . . . . . 44
3.5 Simulated EVM as rms in percentage over different gaps. The gap is shown in percentage of the communication bandwidth. . 45
3.6 Measurement setup for the assessment of the communication performance dependent on different gaps. . . . . . . . . . . . . 47
3.7 Measured EVM as rms in percentage over different gaps. The gap is shown in percentage of the communication bandwidth. . 48
3.8 Top: Sketch of the received FDM signal (black and green) and the local oscillator of the receiving mixer (yellow).
Bottom: Sketch of the resulting radar IF band (gray) with the undesired mixing product (orange). . . . . . . . . . . . . . . . . 49
3.9 Range-Doppler map generated by using the parameters from Table 3.4 and a gap of 1.4 GHz. . . . . . . . . . . . . . . . . . . 52
3.10 Range-Doppler map generated by using the parameters from Table 3.4 and a gap of 700 MHz. . . . . . . . . . . . . . . . . . 53
3.11 Range-Doppler map generated by using the parameters from Table 3.4 and a gap of 0 Hz. . . . . . . . . . . . . . . . . . . . 54
3.12 Block diagram for investigating the radar performance for different gaps. . . . . . . . . . . . . . . . . . . . . . . . . . . . . 55
3.13 Range-Doppler map for the minimal gaps of 1400 MHz. No effect of the undesired signals on the radar measurement is detectable. The SNR amounts to 74.4 dB. . . . . . . . . . . . . 57
3.14 Range-Doppler map for the minimal gaps of 700 MHz. The SNR of the radar measurement is approximately 75.6 dB. . . . . . . 58

3.15 Range-Doppler map for a minimal gap of 0 Hz. The SNR of the radar measurement decreases to 71.7 dB. . . . . . . . . . . . . . 59
3.16 Top: Sketch of the received RF including the radar chirp ($B_1$, black), the communication band ($B_2$, green) as well as the intermodulation products (red and blue).
Bottom: Sketch of the IF with the resulting mixing products for the case of $G = B_2$. . . . . . . . . . . . . . . . . . . . . . . . . 61
3.17 Top: Sketch of the received RF including the radar chirp ($B_1$, black), the communication band ($B_2$, green) as well as the intermodulation products (red and blue).
Bottom: Sketch of the IF with the resulting mixing products for the special case of $G \geq 2 \cdot B_2$. . . . . . . . . . . . . . . . . . . 62
3.18 Spectrum of the RF input signal of the receiving mixer at the time of the last chirp frequency at 36.25 GHz. The center frequency of the communication signal amounts to 37.1875 GHz. Additionally, the upper and the lower intermodulation products and the gap with $G = B_2$ are visible. . . . . . . . . . . . . . . . . . . . . . . 64
3.19 Spectrum of the IF output signal of the receiving mixer at the time of the last chirp frequency. The center frequency of the communication signal amounts now to 2.8125 GHz. Additionally, the upper and the lower intermodulation products are visible. . . 65
3.20 Block diagram of the measurement setup to characterize the signals before and after the receiving mixer and the communication performance with and without FMCW radar operation. . . . . . 67
3.21 Output signal of the high power amplifier with and without the FMCW radar signal. . . . . . . . . . . . . . . . . . . . . . . . . 68
3.22 Output signal of the receiving mixer with and without the FMCW radar signal. . . . . . . . . . . . . . . . . . . . . . . . . . . 69
3.23 Constellation diagram of the QPSK data transmission with (left) and without (right) the FMCW radar signal. . . . . . . . . . . . 70

4.1 Single carrier frequency and the QPSK communication signal in FDM. . . . . . . . . . . . . . . . . . . . . . . . . . . . . . 75

4.2 Single carrier frequency and the QPSK communication signal in FDM to the power of three. . . . . . . . . . . . . . . . . . . . . . 76
4.3 Block diagram for the power-balancing regarding a generator signal with fixed frequency. The HPA output power of the communication signal is reduced from 30 dBm to 12 dBm. . . . . . . 77
4.4 Generator signal in the frequency domain measured at the output of the HPA for three different attenuations of the communication signal and without the QPSK communication signal. . . . 78
4.5 Block diagram for the power-balancing regarding the QPSK communication signal. The HPA output power of the FMCW radar signal is between 30 dBm and 36 dBm. . . . . . . . . . . 79
4.6 QPSK signal in the frequency domain measured at the output of the HPA for two different attenuations of the chirp signal and without the chirp signal. . . . . . . . . . . . . . . . . . . . . . . 80
4.7 Power over frequency for three different power levels of TOI.The blue thin line corresponds to $P_{\mathrm{IP3}} = 35\ \mathrm{dBm}$, the green thin line to $P_{\mathrm{IP3}} = 40\ \mathrm{dBm}$ and the yellow one to $P_{\mathrm{IP3}} = 45\ \mathrm{dBm}$ . . . . 84
4.8 Simulated rmsEVM in percent over the power of the third-order intercept point . . . . . . . . . . . . . . . . . . . . . . . . . 85
4.9 Power over frequency for three different power levels of the communication signal. The radar signal is visualized in black and the three communication signals in red (30 dBm), green (20 dBm) and blue (10 dBm). These signals are in thick lines. The corresponding intermodulation products are in thin lines. . 86
4.10 Simulated rmsEVM in percent over the power of the communication signal. . . . . . . . . . . . . . . . . . . . . . . . . . 87
4.11 Block diagram of the setup for the measurement of the rmsEVM dependent on the power of the communication signal. . . . . . 88
4.12 Measured rmsEVM in percent over the power of the communication signal. . . . . . . . . . . . . . . . . . . . . . . . . . 89
4.13 SNR of the radar part (red) and the communication part with two different power levels (purple and yellow) dependent on the flight altitude. . . . . . . . . . . . . . . . . . . . . . . . . . 94

5.1 Frequency division multiplexing (FDM) of 8 channels. . . . . . . 99
5.2 Orthogonal frequency division multiplexing (OFDM) of 8 channels.100
5.3 CCDF curves for a different amount of carrier frequencies N of an OFDM system. Modified from [BP20]. . . . . . . . . . . . . . 101
5.4 CCDF comparison of two different, non-distortion PAPR reduction techniques for an OFDM system with 1024 carriers. Modified from [RS17]. . . . . . . . . . . . . . . . . . . . . . . . . . . . . 102
5.5 CCDF curves for the two different modulation formats QPSK and 16-QAM after the influence of an AWGN-channel. . . . . . . . . . 103
5.6 Simulated CCDF curve of the joint FMCW radar and QPSK communication signal in FDM. . . . . . . . . . . . . . . . . . . . . 104
5.7 Measurement setup for measuring the FDM signal before and after the HPA in the time domain with an oscilloscope. . . . . . 105
5.8 FDM signal before (left) and after (right) the HPA in the time domain. . . . . . . . . . . . . . . . . . . . . . . . . . . . . . 106
5.9 Measured CCDF curves of the FDM signal before and after the HPA. . . . . . . . . . . . . . . . . . . . . . . . . . . . . . . . 107

# List of Tables


2.1 Parameters used for the SystemVue simulation . . . . . . . . . . 29

3.1 Parameters used for the simulation for the overall bandwidth dependent on the flight altitude. . . . . . . . . . . . . . . . . . . 43
3.2 Parameters used for the simulation of the communication performance. . . . . . . . . . . . . . . . . . . . . . . . . . . . 45
3.3 Parameters used for the measurement for the assessment of the communication performance. . . . . . . . . . . . . . . . . . . 46
3.4 Parameters used for the simulation of the radar performance. . 51
3.5 Parameters used for the measurement for the assessment of the radar performance. . . . . . . . . . . . . . . . . . . . . . . 56
3.6 Parameters used for the simulation for the assessment of the signals before and after the receiving mixer. . . . . . . . . . . . 63
3.7 Parameters used for the measurement for the assessment of the signals before and after the receiving mixer. . . . . . . . . . 66

4.1 Parameters used for the simulation of the third-order intermodulation distortion. . . . . . . . . . . . . . . . . . . . . . . . . 75
4.2 Parameters used for the simulation of the third-order intermodulation products dependent on the third-order intercept point. . . 83
4.3 Parameters used for the simulation of the third-order intermodulation products dependent on the communication power. . . . . 86
4.4 Parameters used for the measurement for the assessment of the communication performance dependent on different power levels. . . . . . . . . . . . . . . . . . . . . . . . . . . . . 89
4.5 Parameters used for the simulation of the SNR of the radar and the communication link. . . . . . . . . . . . . . . . . . . . . 93

5.1 Parameters used for the measurement for the assessment of the signals before and after the HPA. . . . . . . . . . . . . . . . . . 106

# List of Abbreviations and Symbols

| | |
|---|---|
| $A$ | Attenuation |
| ADC | Analog-to-Digital Converter |
| ASK | Amplitude Shift Keying |
| $B$ | Overall Bandwidth |
| $B_1$ | Bandwidth of Lower Band |
| $B_2$ | Bandwidth of Upper Band |
| $B_\mathrm{C}$ | Bandwidth of Communication Signal |
| BPSK | Binary Phase Shift Keying |
| $B_\mathrm{R}$ | Bandwidth of Radar Signal |
| $c$ | QPSK Communication Signal |
| CCDF | Complementary Cumulative Distribution Function |
| CDM | Code Division Multiplexing |
| CSAR | Circular Synthetic Aperture Radar |
| CSS | Chirp Spread Spectrum |
| DAC | Digital-to-Analog Converter |
| DDS | Direct Digital Synthesizer |
| DFRC | Dual-Function Radar-Communication |
| EVM | Error Vector Magnitude |
| $f_1$ | Lowest Frequency of Lower Band |
| $f_2$ | Lowest Frequency of Upper Band |
| $f_\mathrm{bb}$ | Lowest Frequency of Lower Intermodulation Product |
| $f_\mathrm{bu}$ | Highest Frequency of Lower Intermodulation Product |
| FDM | Frequency Division Multiplexing |
| $\mathrm{fdm}$ | FDM Signal |
| $f_\mathrm{LO}$ | Frequency of Local Oscillator |
| FMCW | Frequency Modulated Continous Wave |

| | |
|---|---|
| FSK | Frequency Shift Keying |
| $f_{\mathrm{ub}}$ | Lowest Frequency of Upper Intermodulation Product |
| $f_{\mathrm{uu}}$ | Highest Frequency of Upper Intermodulation Product |
| $G$ | Gap between Frequency Bands |
| GaN | Gallium Nitride |
| HPA | High Power Amplifier |
| $I$ | Integration Gain |
| IF | Intermediate Frequency |
| $\mathrm{IF}_{\mathrm{R}}$ | Intermediate Frequency of FMCW Radar |
| IM | Intermodulation Products |
| JCS | Joint Communication and Sensing |
| LNA | Low Noise Amplifier |
| MPA | Medium Power Amplifier |
| MSK | Minimum Shift Keying |
| MSQP | Multi-Subband Quasi-Perfect |
| $N$ | Amount of Sub-Carriers |
| OCDM | Orthogonal Chirp Division Multiplexing |
| OFDM | Orthogonal Frequency Division Multiplexing |
| OIP3 | Output Third-Order Intercept Point |
| OTFS | Orthogonal Time Frequency Space |
| PAPR | Peak-to-Average Power Ratio |
| $P_{\mathrm{b}}$ | Power of Lower Intermodulation Product |
| $P_{\mathrm{IP3}}$ | Power of Third-Order Intercept Point |
| PRF | Pulse Repetition Frequency |
| PSK | Phase Shift Keying |
| $P_{\mathrm{u}}$ | Power of Upper Intermodulation Product |
| QAM | Quadrature Amplitude Modulation |
| QPSK | Quadrature Phase Shift Keying |
| $R$ | Range |
| $r$ | Chirp Sequence Signal |
| Radar | Radio Detection and Ranging |
| RadCom | Radar Communication |

| | |
|---|---|
| RCS | Radar Cross Section |
| RF | Radio Frequency |
| rms | Root Mean Square |
| SAR | Synthetic Aperture Radar |
| SAW | Surface Acoustic Wave |
| SDM | Space Division Multiplexing |
| SDR | Software Defined Radio |
| SFDR | Spurious Free Dynamic Range |
| SISO | Single-Input Single-Output |
| SNR | Signal-to-Noise Ratio |
| $\mathrm{SNR}_{\mathrm{Com}}$ | Signal-to-Noise Ratio of Communication |
| $\mathrm{SNR}_{\mathrm{Rad}}$ | Signal-to-Noise Ratio of Radar |
| STC | Space-Time Coding |
| TDM | Time Division Multiplexing |
| TOI | Third-Order Intercept Point |
| $T_{\mathrm{R}}$ | Time Duration of Chirp |
| $v$ | Velocity |

# 1 Introduction

## 1.1 Motivation

The image-based surveillance of ground sites with airborne radar systems is an important task in many military and civil applications. This is due to the fact that radar measurements are daylight and largely weather independent. Additionally, measurements through dust are possible. Radar images with resolutions in the lower cm range, independent of the flight altitude, can be acquired based on synthetic aperture radar (SAR) [M I80]. In order to achieve such high image resolutions, a broadband radar with a radio frequency (RF) bandwidth of several GHz is necessary [R J00]. For example, a SAR image resolution on ground of approximately 4 cm requires a RF bandwidth of the radar sensor of 3.75 GHz. By using a single-input single-output (SISO) circular SAR system (CSAR), a continuous airborne surveillance of the scene of interest (for example the protection of a military camp) with 3-D capability is possible with little effort regarding the analog front-end and back-end of the radar system. This is essential for the usage of small airborne platforms, where the maximum payload and the power consumption is limited. Further information regarding the single-channel airborne CSAR can be found in [Pal21]. An additional military scenario is the use of an efficient SISO SAR system for image-based and real-time convoy protection by using a small airborne platform (for example a drone) flying besides the military vehicles during the radar measurements.

By using the frequency-modulated continuous wave (FMCW) radar, the data rate and therefore the amount of raw data can be minimized in comparison to the RF bandwidth of several GHz because of the de-ramping in the receiving mixer. This is also important for small airborne platforms with limited power consumption for the payload. Additionally, real-time processing of the radar data is possible in an easy and efficient way. Basic information about FMCW radar can be found in [Sto92]. Beyond that, FMCW radars have constant signal envelopes in the time and frequency domain, maximizing their power efficiency. This is essential for good SAR image quality and minimal power consumption. The hardware setup and the digital signal processing of a FMCW radar is in a first approach very easy to implement. This reduces development costs. By using radio frequencies in the millimeter-wave region, for example 35 GHz, the weight, size and power consumption of such a radar system can be minimized in comparison to other radar approaches because of the low wavelength. [CSM+14] and [JSW+14] and the mentioned references present examples for such FMCW sensors in the millimeter-wave region for SAR applications.

Because of the computationally intensive processing of the CSAR image, it makes sense to transfer the radar raw data from the small flying platform to the ground station, where the radar images are processed. This ground station can be located inside the measurement area of the CSAR sensor (for example inside a military camp), and the platform can fly a circle around it. Therefore, it is necessary to find a solution to combine a broadband CSAR with a resulting image resolution of a few cm and a wireless communication with a sufficient data rate in the range of several 100 Mbit/s for radar raw data transmission within one system for a minimum flight altitude of approximately 500 m. Here, it is important that the weight, size, and power consumption of the whole system fulfill the stringent requirements of a small airborne platform. Therefore, high efficiency regarding these parameters is essential.

This thesis presents investigations of an efficient joint broadband SAR system with simultaneous wireless communication capability in the millimeter-wave band, which can be a candidate for such an application with the aforementioned conditions. This approach is based on the frequency division multiplexing (FDM) of a broadband FMCW radar signal and a single carrier communication signal with quadrature phase shift keying (QPSK) modulation. Here, only a single HPA, transmit antenna as well as receive antenna and low noise amplifier (LNA) are used in the front-end. This reduces cost, size, weight and power consumption compared to an approach with multiple amplifiers and antennas.

## 1.2 State of the Art

The current scientific activities in the field of joint communication and sensing (JCS), radar communication (RadCom), dual-function radar communication (DFRC), and joint radar communication (JRC) are very important nowadays because of possible requirements for the new mobile communication standard 6G. For example [LMP+20], [LCM+22], [ZLM+21], [ZRW+22], [WBV21], [WLCL23], [MAA20], [GNA+22] as well as [MSH+20b], [MSH+20a], [QQGZ14], [TDJ+21], [MBK+19], [FFW+20], [ZZCW22], [WQW+23] and the references mentioned therein provide among others very good overviews about different kinds of multi-functional systems regarding radar and communication for various applications. One main distinction that can be made is between communication with sensing capability and radar with communication functionality. An important approach frequently mentioned in these publications is the orthogonal frequency division multiplex (OFDM) technique. One of the first publications about OFDM is found in [Bal66], where it is formulated for communication systems. Here, advantages such as high spectrum efficiency are named. The modern mobile communication standard 5G for example is based on OFDM for communication.

### 1.2.1 Orthogonal frequency division multiplexing

OFDM is also an appropriate approach for radar. One of the first publications about OFDM radar is [Lev00] and the references mentioned therein. [SPZW09] describes a novel OFDM radar signal processing technique, where the performance of the radar is completely independent of the carried information. In the case of the static base stations of the new mobile communication standards 5G and 6G, many publications present approaches for JCS based on OFDM. One of them is [LRBV21], which presents an optimized OFDM waveform for 5G-6G communication with sensing. Here, the radar performance is improved with the filling of empty sub-carriers with optimized samples. The necessary trade-off between communication and sensing is considered in this publication. The use of OFDM requires the complete band to be sampled which puts high demands on the analog-to-digital converter (ADC). Processing this ultra high amount of data also requires high computing power and large memories in case of a broadband radar with very fine range resolution. Additionally, the hardware costs are very high. [HKH23] goes into the details of this problem regarding OFDM radar. The suggested approach reduces the ADC sampling rate with sub-Nyquist sampling but needs very high sampling rates for the generation of the OFDM waveform. Additional processing for noise cancellation is necessary. It is compared with three other approaches of OFDM radars with reduced ADC sampling rates. One of them makes use of the possibility to enhance the range resolution without increasing the sample rate and computational effort with the use of a frequency comb OFDM radar [NMMZ20]. The disadvantages of this approach are the increased noise, and the necessity for a high precision and stable calibration. Multiple mixers are needed for the up- and down-conversion of the OFDM signals. Similar to the approach above, [BKRS23] describes a JCS approach for communication base stations which uses a combination of OFDM and FMCW. Here, additional hardware like multiple digital-to-analog converter (DAC) and mixers are necessary. The described simulation of radar and communication works with a carrier frequency of 24 GHz and a bandwidth of only 61.44 MHz. [MSA22] uses overlapped OFDM and FMCW waveforms in the time and frequency domain. Here, the mentioned disadvantages of OFDM are still present. The bandwidth in the simulation is only 122.28 MHz. The approach in [Gen23] reduces the computational complexity and the sensing overhead by using a diagonal waveform structure of the OFDM signal with the disadvantage that ambiguities in range and velocity can occur. The approach described in this thesis is based on a FMCW radar with the de-ramping feature in the receiving mixer and simultaneous single carrier communication in FDM. In the radar case, this reduces the sampling frequency of the ADC significantly to only a few percent of the radar RF bandwidth. The generation of the FMCW waveform can be realized for example with efficient direct digital synthesizers in combination with frequency multiplier to reach the high RF bandwidth in the GHz region and the final carrier frequency.

Another drawback of OFDM is the high PAPR because of multiple, simultaneous carrier frequencies. This reduces the power efficiency of the analog signal

chain of the system and results in inter-carrier interference because of non-linearities of the HPA. The OFDM requirement of high linearity of the analog signal chain is hard to realize especially in the millimeter-wave band and for very broadband signals [MCW+22]. PAPR reduction procedures in the digital domain with more or less computational effort are necessary, which are the subject of many scientific publications. [HL05], [JW08] and [LHN09] for example presented overviews and the comparisons of PAPR reduction schemes only for communications. The optimal technique depends on the system requirements which determines the PAPR reduction performance. Modern communication systems with lots of simultaneous carrier frequencies achieve PAPR values of 10 dB and more by using these reduction techniques [Mul20]. Additional schemes using a constant envelope OFDM can be found in the literature, for example [TAP+08], [MSM10], [HHM+18] and [RSM+18]. These approaches are based on phase modulation and require oversampling of the signal, which increases the computational effort. Nowadays, low-PAPR approaches are developed additionally for the joint use of OFDM for radar and communication [HHM+22] and [VBS23]. Here, the communication subbands are located within a larger bandwidth for radar measurements. Oversampling is also necessary and the algorithm is based on several iterations, which increases the computational effort. The approach mentioned in this thesis uses only two carrier frequencies – one for radar and one for communication. Therefore, the resulting PAPR is only 6 dB without any effort. This saves system resources.
The signals of the orthogonal time frequency space (OTFS) modulation are processed in the delay-Doppler domain as opposed to OFDM with signals in the time-frequency domain. One of the first publications about OTFS and the improvement over OFDM regarding high Doppler is [HRT+17]. The PAPR of OTFS is slightly reduced compared to OFDM, as mentioned in [SAC19], but higher than the approach described in this thesis. [KD21] describes characteristics, advantages and disadvantages of OTFS. The major disadvantage of OTFS is the high receiver complexity.
Another approach for the usage in the millimeter-wave band is the use of multi-subband quasi-perfect sequences (MSQP), where many different subbands are used [MCW+22]. Here, multiple ADCs with low sample rates can be used

to sample these subbands, with the disadvantage that synchronization errors can occur. Additional effort for calibration is needed.

### 1.2.2 FMCW waveform with integrated communication

As mentioned above, it makes sense to use ADCs with low sampling rates to save system resources and costs. An attractive way to realize a broadband radar is to use frequency modulated continuous wave (FMCW) as waveform featuring de-ramping in the receiving mixer [CSM+14]. Thereby, the high RF bandwidth of the radar is reduced to a small bandwidth in the intermediate frequency (IF), which is processable with efficient ADCs with low sample rate. Such an FMCW radar can be extended to realize an integrated communication. The disadvantage of those approaches are the low data rates regarding the communication part.

There are a few possibilities described in the literature to integrate the communication functionality into an FMCW radar. One way is to do a phase modulation of the transmitted chirp with de-ramping in the receiving mixer for interference mitigation e.g. [Uys20], [UO20] and [KPVY23b] or for communication e.g. [MSBM19], [LTAW19], [KPZ+21] and [KPVY23a]. The effect of the phase modulation are range sidelobes dependent on the modulation index and a low data rate. These have to be compensated by adequate post-processing algorithms. Additionally, the deployment of synchronization methods is necessary in case of the use of more than one transceiver [LUT+20].

Another possibility to communicate with chirps is the use of overlapped chirps to enhance the data rate as described in [PBF20] and the mentioned references. This principle is well known as orthogonal chirp division multiplexing (OCDM). The disadvantages of this approach is the need for compensation algorithms for the occurring intersymbol interferences and the sampling of the whole RF bandwidth of the signal in the receiver. [BPG+21] and [BSBF21] describe the OCDM principle for communication in time division multiplexing with several non-overlapping and unmodulated chirps for the radar measurements. Here, simultaneous data transmission and radar measurements is not possible and the whole RF bandwidth must be sampled in the receiver.

Similar to this approach, it is possible to use the chirp spread spectrum (CSS) technique for communication and target detection based on chirps [HLZ+22] and [AON+20]. Here, the LoRa communication principle [Sem25] is used with the disadvantages that the data rate is very low and that it depends on the chirp repetition interval. [DBSF19] uses time division multiplexing of FMCW radar and communication based on the CSS principle with the mentioned disadvantages. Additionally, correction methods for using FFT-based radar signal processing are necessary.
In the case of very short linear frequency modulated pulses, a joint radar-communication system based on different chirp slopes is described in [GCI+16] and [GCI+18]. A major disadvantage is that the whole radar RF bandwidth has to be digitized and elaborated signal processing techniques are necessary. Furthermore, the use of a large radar RF bandwidth is not possible.
One of the first approaches of multifunctional radar and communication systems use surface acoustic Wave (SAW) devices for generating the chirp waveforms with opposite slopes as mentioned in [RB03] and [SSB07]. These systems are characterized through mostly analogous signal processing techniques.
[SFHS15], [SFH+16] and [WA18] describe the combination of frequency shift keying (FSK) communication and FMCW radar. The data rate of these systems is very low and a time and frequency synchronization between multiple stations is necessary. This is because the internal unmodulated chirp of a receiver is mixed with the FSK modulated chirp of another transmitter. An alternating FSK communication and FMCW radar is described in [SJS08], where two stations have to be roughly synchronized. Here, the data rate is very low, but the radar RF bandwidth can be very high. [YWZT18], describes a system, which uses FSK as radar procedure and the two different slopes (up-chirp and down-chirp) of a chirp as its communication principle (Chirp-BOK modulation). The disadvantages of this approach are that the achievable data rate is very low and that the radar performance is limited. [MW13a] and [MW13b] introduce the time multiplexing of FMCW radar and high-speed communication based on phase shift keying (PSK). The downside is the limited RF bandwidth of the radar because of the usage of a direct digital synthesizer (DDS) for generating the chirp without a multiplier for bandwidth enhancement. The front-end hardware

in the form of a transceiver with time multiplexing of the radar and the communication mode is described in [DCJ+23]. Here, a very high bandwidth for the FMCW radar of 30 GHz and a very high bandwidth for the communication of 20 GHz can be reached. The disadvantages are that radar and communication operation cannot be simultaneously, hardware switches with controlling are necessary and the operating range is short. Unidirectional communication between an FMCW radar and a distinct receiver is described in [BEJ07], where amplitude modulation of the chirp is used. Here, the necessary constant envelope for an airborne SAR imaging is not given. [AEK+21] presents a MIMO radar only for near range applications with asynchronous Binary Phase Shift Keying (BPSK) communication.

### 1.2.3 Joint SAR and communication

The focus of this thesis lies on joint SAR imaging and communication with an image resolution of a few cm. To this end, a radar bandwidth of several GHz is necessary. The integrated communication link for radar raw data transmission must handle a data rate of several 100 Mbit/s.

Regarding OFDM, it is possible to realize SAR imaging. [ZX15] describes OFDM SAR imaging without communication. In this case, a receive window between two consecutive pulses is needed and only 150 MHz of bandwidth is used. Another approach is based on the OFDM chirp waveform for SAR imaging [WCL+15] and [ZWD+21]. Here, no integrated wireless communication is described and the bandwidth of the simulation is limited to only 120 MHz and 30 MHz, respectively. [XZD+23] describes an approach based on the OFDM chirp waveform. Here, the maximum radar bandwidth amounts to 4.8 GHz in the simulation and to 3 GHz in the measurement. The range is limited to approximately 100 m in the simulation and 12 m in the measurement. No integrated wireless communication is described. [BMRP16] focuses on a coded OFDM signal which is optimized regarding the radar image quality. Here, the simulation bandwidth is only 20 MHz and communication is not considered. As mentioned here, the drawbacks of OFDM signals are the high PAPR values and the high side lobes in range. Regarding spaceborne SAR, for example,

[JDW+21] presents a scheme for an improved OFDM waveform without integrated communication. The disadvantage is the low bandwidth of only 30 MHz. The approaches described in the publications on the subject of OFDM SAR all share the mentioned disadvantages of OFDM.
This thesis focuses on the topic of joint SAR and communication. Only a few publications are available in this area of research. [WLC+19] describes a joint system based on the space-time coding (STC) approach. Here, the chirp waveform is used for the SAR imaging and OFDM is used for the communication. The disadvantages are the two times higher pulse repetition frequency (PRF) than the Doppler bandwidth and the low bandwidth of 560 MHz for radar and for communication. The performance of the integrated communication link is not described. [TLY+22] embeds the information into a time-frequency spectrum of the phase coded signal for bistatic SAR imaging. The disadvantages of this approach are the additional effort because of the limited coordinate refresh rate of 10 Hz and the higher bit error rate (BER) compared to QPSK. Last but not least, a SAR-communication system using continuous phase modulation codes and mismatched filters and a literature review is described in [CTRO23]. The disadvantages of this approach are the limited bandwidth of 305 MHz, the low data rate of maximal 5 Mbit/s and the very computationally intensive processing.

### 1.2.4 Summary

One of the most published approaches for joint communication and sensing is OFDM at the moment. The drawbacks of OFDM are the high requirements concerning the linearity of the analog signal chain, the very high sampling rates dependent on the bandwidth for the generation and sampling of the OFDM signal and the high PAPR values which reduces the power efficiency of the system. This is the reason why OFDM is not usable as a waveform for the mentioned scenario of this thesis. The main drawback of FMCW with integrated communication is the low data rate if de-ramping with the receiving mixer is used to reduce the bandwidth of the signal. This is unsuitable for the application considered in this thesis, where radar raw data must be transmitted.

The result of the above-mentioned literature review and the current state of the art regarding joint SAR and communication is that no approach is available for the following requirements:

- Broadband airborne SAR with a bandwidth of several GHz.
- Integrated communication link with a data rate of several 100 Mbit/s.
- Simultaneous and real-time operation.
- Highly efficient system in the millimeter wave band for increased operating time.
- Suitable for small aircrafts like drones with a flight altitude of around 500 m.

Therefore, the research and the approach of this thesis is new and essential for the application and scenario with the mentioned requirements.

## 1.3 Scope of this Work

This thesis focuses on joint broadband FMCW radar and single-carrier QPSK communication in FDM for airborne SAR applications.
Chapter 2 gives some basic information about radar and wireless communication and an introduction to the mentioned approach in the form of a block diagram for a possible hardware realization and a description of mathematical fundamentals. Additionally, the most important hardware used for the investigations of this thesis is shown. Finally, an analysis of range profiles of the FMCW radar and constellation diagrams of the QPSK communication generated by a first simulation of the approach with the tool SystemVue [Key24] and by a first measurement with the described hardware is presented.
The following Chapter 3 presents the fundamentals about the intermodulation products of an HPA at the beginning. After that, the minimal gap between the radar band and the communication band without an influence on each other is determined theoretically for the transmitter part behind the HPA. The resulting overall bandwidth for an assumed CSAR application dependent on

the flight altitude is formulated then with the gap determined by the communication band. Afterwards, the effect of different gaps on the communication performance in the receiver is presented by using a simulation and a measurement with the described hardware. After that, the influence of different gaps on the radar performance in the receiver is shown. Here, no band selection filter is used in the RF path of the receiver. The quantitative analysis is done by using range-Doppler maps for different gaps in the simulation and in the measurement. Section 3.3 describes two possibilities for the determination of the local oscillator of the QPSK communication. The first approach uses a minimized gap between the radar and the communication band, whereas the second approach employs a minimized IF of the communication signal. The determination of both possibilities is mathematically derived. The following sub-section presents the simulation of the signals before and after the receiving mixer where the local oscillator is determined by using a minimized gap as described above. The last sub-section shows the measurement of the signals before and after the receiving mixer. Here, the local oscillator is determined by using a minimized IF of the communication signal. The measured constellation diagrams for the two cases with and without the radar chirp is depicted. The chapter ends with a discussion and a conclusion.
Chapter 4 presents the effect caused by non-linearities of the HPA close to the two carrier frequencies. A simulation result shows this effect. The following two sub-sections describe the reciprocal power balancing of the two frequency bands by using measurements to reduce the aforementioned effect. Section 4.2 focuses on the fundamentals of the power of the third-order intermodulation products. The reduction of the influence of the third-order intermodulation products on the two frequency bands is investigated in Section 4.3. First, the third-order intercept point is varied and the effect on the communication performance is shown with simulations by using no gap between both frequency bands. Second, the power of the communication signal is varied and the effect on the communication performance is investigated with a simulation by using a gap of zero between the radar and the communication band. This second result is verified with a measurement of the communication performance dependent on the communication signal power. The following section is about

the investigation of the signal-to-noise ratio (SNR) of the communication part and the radar part for an assumed CSAR-scenario. This chapter ends with a discussion and conclusion.
The following Chapter 5 shows the difference between FDM and OFDM and gives an overview about the power efficiency of an OFDM signal with and without PAPR reduction techniques first. Second, the two modulation formats 16-QAM and QPSK are compared regarding the PAPR. The last section investigates the approach of this thesis regarding PAPR and power efficiency with a simulation. After that the mentioned FDM signal is analyzed regarding the PAPR with measurements before and after the HPA .
The last Chapter 6 gives a conclusion of the thesis.

# 2 Introduction to Joint Broadband Radar and Single-Carrier Communication in FDM

This chapter gives an introduction to the application-specific approach of joint broadband FMCW radar and single-carrier QPSK communication system in FDM. This system can be used for a battery driven airborne CSAR application with small platforms for medium range up to 1000 m. The reason for choosing this waveform is the efficient realization of a high-resolution airborne SAR imaging system with sufficiently integrated communication capability. The communication system on ground is located inside the measurement area of the CSAR part for reception of radar raw data and for transmitting commands to the flying platform. The overall bandwidth of the waveform is dominated by the bandwidth of the broadband radar. The bandwidth for the communication for radar raw data transmission is reduced to a few percent of the radar bandwidth because of the usage of the analog de-ramping of the FMCW radar. A gap between both frequency bands is necessary, but can be reduced by power balancing of the two signal types. The chapter starts with a brief description of the fundamentals regarding radar and wireless communication. Section 2.3 contains the basic idea behind the innovative approach for the mentioned application. In the first Sub-section 2.3.1, this includes the description of a generic block diagram and the new waveform. The second Sub-section 2.3.2 focuses on a general description of the new waveform in terms of mathematics. The measurements conducted for this thesis are based on the hardware described in Sub-section 2.3.3. The Sub-sections 2.3.4 and 2.3.5 present simulations and measurement results with the described hardware with a quantitative analysis regarding the radar and the communication part of the system.

## 2.1 Introduction to Radar

Radio detection and ranging (Radar) systems use electromagnetic waves for detecting, localization and tracking of objects in an environment. This technology is based on the transmitting, reflection and receiving of high RF signals. The received signals of the radar can be analyzed then to get information about objects like range, radial velocity or radar cross-section (RCS). A millimeter-wave radar system is a special kind of radar and uses radio frequencies between 30 GHz and 300 GHz. The approach considered in this thesis works in the frequency band between 32.5 GHz and 37.5 GHz. Because of the use of radio frequencies, the radar measurements are independent of daylight and widely weather. These characteristics of radar systems enables the use in many military and civil applications. One application behind this thesis is the airborne monitoring of an area of interest on the ground with radar images based on the synthetic aperture radar (SAR) principle. Here, a high image resolution is desired, and therefore, a high RF system bandwidth is necessary. One basic measurement of a radar is the determination of the range to the objects with a certain range resolution. This measurement is based on the time delay $T_{\mathrm{D}}$ between the transmit and the receive signal. The range $R$ between the radar and the object can be calculated with the following formula.

$$R = \frac{c_0 \cdot T_{\mathrm{D}}}{2}, \tag{2.1}$$

where $c_0$ is the speed of light. The factor $\frac{1}{2}$ stems from the propagation of the transmit signal to the target and back to the radar.
The resolution of the range measurement $\Delta R$ depends on the RF bandwidth $B_{\mathrm{R}}$ in the following form.

$$\Delta R = \frac{c_0}{2 \cdot B_{\mathrm{R}}}. \tag{2.2}$$

Another basic measurement of radar systems is the determination of the radial velocity of an object with a certain resolution. This measurement is based on the Doppler frequency. The radial velocity $v$ of an object can be calculated with the following formula.

$$v = \frac{f_\mathrm{D} \cdot c_0}{2 \cdot f_\mathrm{R}}, \tag{2.3}$$

whereby $f_\mathrm{D}$ is measured Doppler frequency and $f_\mathrm{R}$ is the RF of the radar system.
The resolution of the radial velocity measurement $\Delta v$ depends on the observation time $T_\mathrm{O}$ in the following form.

$$\Delta v = \frac{c_0}{2 \cdot f_\mathrm{R} \cdot T_\mathrm{O}}. \tag{2.4}$$

The velocity measurement depends on the RF $f_\mathrm{R}$ of the radar system. The higher the frequency, the finer the velocity resolution. This is an advantage of millimeter-wave radar systems.
It can be distinguished between two types of radar principles: pulse radar and continuous-wave radar. A pulse radar uses short pulses with high peak power, making this difficult to generate and to handle. The transmit and the receive process is not simultaneous. In contrast to this, the continuous-wave radar works with continuous waves with relatively low power. This is easier to generate and to handle than high pulse power. Here, transmitting and receiving occurs simultaneously. A prominent example for this type of radar is the FMCW radar. Here, the radar continuously transmits power to the measurement scene in the form of a linear frequency modulated signal (chirp). The advantage of the use of chirps is the constant power envelope in the time- and the frequency domain. This chirp has a certain, application-dependent RF bandwidth $B_\mathrm{R}$ and a time duration $T_\mathrm{R}$. The repetition time of multiple chirps is the time duration $T_\mathrm{Rep}$. Because of the usage of linear chirps it is possible to multiply the transmit chirp with the received chirps with the receiving mixer. The result of this process is the IF $\mathrm{IF}_\mathrm{R}$, which depends on the time duration $T_\mathrm{D}$ to the object and back to the radar, the RF bandwidth $B_\mathrm{R}$ and the time duration of the chirp $T_\mathrm{R}$. This allows the determination of the distance between the radar and the object. The IF is significantly lower than the RF and the RF bandwidth. This reduces the demands on the subsequent digitization and digital signal processing. The following Figure 2.1 shows the transmit chirp (left blue line) and one receive

chirp (second blue line) with the most important signal parameters.

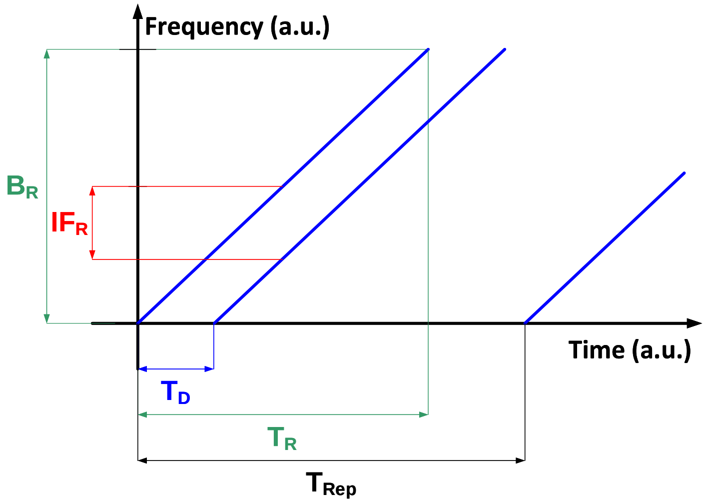


Figure 2.1: Sketch of the FMCW signals with all relevant parameters.

The IF of the radar $\mathrm{IF}_{\mathrm{R}}$ can be calculated with the following equation and is derived by using Figure 2.1 and Equation 2.1.

$$\mathrm{IF}_{\mathrm{R}} = \frac{2 \cdot R \cdot B_{\mathrm{R}}}{T_{\mathrm{R}} \cdot c_0}. \tag{2.5}$$

The higher the RF bandwidth and the range to the target, the higher the IF. Here, the sampling of the Doppler frequency $f_{\mathrm{D}}$ will be done with multiple chirps with the time duration $T_{\mathrm{Rep}}$. The shorter this time duration, the higher the maximal possible Doppler frequency and the higher the IF.

## 2.2 Introduction to Wireless Communication

The focus of wireless communication lies on the robust transmission of digital data by using electromagnetic waves over large distances without a physical connection between the communication devices. This means that the users of such systems can have information anywhere and anytime without a cable connection. Therefore, this technology is very attractive to many kinds of military and civil applications. Common wireless communication standards based on electromagnetic waves like WLAN, Bluetooth or mobile communication use the lower GHz frequency bands, but in the last few years, the millimeter-wave bands have become more and more attractive. The technology of wireless data transmission is very similar to the mentioned radar technology.
For the wireless transmission of discrete information signals it is necessary to modulate a certain carrier signal with the data. A carrier signal for communication $s(t)$ can be considered in the complex plane as follows.

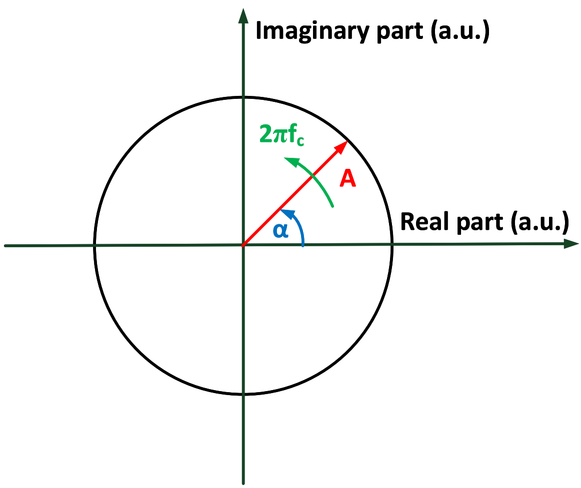


Figure 2.2: Visualization of a carrier signal in the complex plane.

This carrier signal can be expressed mathematically as follows.

$$s(t) = A \cdot \cos(2\pi f_\mathrm{c} t + \alpha). \tag{2.6}$$

It is possible to modulate the signal $s(t)$ dependent on the digital information by varying the following parameter:

- Amplitude $A \Rightarrow$ Amplitude Shift Keying (ASK).
- Frequency $f_\mathrm{c} \Rightarrow$ Frequency Shift Keying (FSK).
- Phase $\alpha \Rightarrow$ Phase Shift Keying (PSK)
- Amplitude $A$ and quadrature Phase $\alpha \Rightarrow$ Quadrature Amplitude Modulation (QAM).
- Frequency $f_\mathrm{c}$ and Phase $\alpha \Rightarrow$ Minimum Shift Keying (MSK).

The most popular modulation format is the varying of the phase corresponding to the information bits. The quadrature phase shift keying (QPSK) is a special kind of the PSK modulation, where the phase of the real and the imaginary part is changed independently. Therefore, it is possible to transmit 2 bits per symbol instead of 1 bit per symbol in case of the binary phase shift keying (BPSK) technique. The well-known advantages of QPSK against QAM for example are the robustness, the easy implementation at the transmitter as well as the receiver and the optimal power efficiency. This is the reason why this thesis focuses primarily on the QPSK modulation.
All linear modulation formats as described above can be mathematically formulated in the base-band in the following form [P A13].

$$c_\mathrm{B}(t) = \sum_k a[k] \cdot g(t - kT), \tag{2.7}$$

where $c_\mathrm{B}(t)$ is the complex communication signal in the base-band, $k$ is the time index, $a[k]$ is the complex data symbol, $T$ is the time duration of a symbol and $g(t)$ is the basic impulse waveform for pulse-shaping. Multiplying this complex base-band signal $c_\mathrm{B}(t)$ with a complex signal with the frequency $f_\mathrm{c}$ results in the complex band-pass signal $c(t)$.

Very important in the field of communication are the multiplexing techniques. Here, multiple signals, for example from many different communication users, can be summarized and transmitted over one single medium. This can be done by using the following techniques:

- Time ⇒ Time Division Multiplexing (TDM).
- Frequency ⇒ Frequency Division Multiplexing (FDM).
- Code ⇒ Code Division Multiplexing (CDM)
- Space ⇒ Space Division Multiplexing (SDM).

The multiplex techniques TDM and FDM are visualized in the following figure.

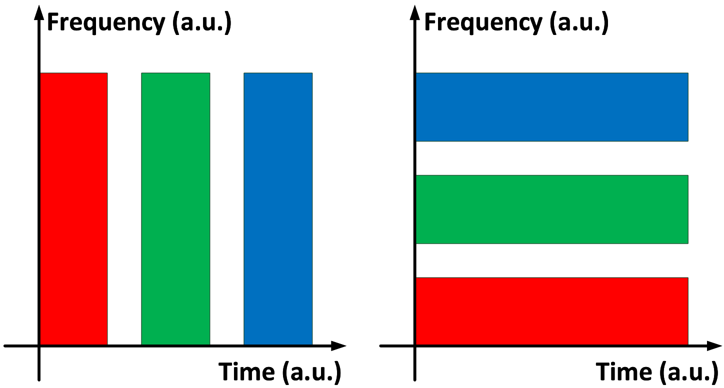


Figure 2.3: Visualization of TDM (left) and FDM (right) in the frequency time plane.

Space division multiplexing requires multiple antennas, which is not possible in this application, where the space for the system is limited. Code division multiplexing requires the same signals with different codes. Therefore, a multiplexing of an FMCW radar and another waveform for communication is not possible. Time division multiplexing of radar and communication achieves only low data rates and the chirp repetition interval for the radar is influenced by the communication part. It can be concluded that the best way to operate efficiently a FMCW broadband radar with simultaneous communication with sufficient data rate within one system is frequency division multiplexing. This is why this thesis focuses on FDM.

## 2.3 FDM of Broadband FMCW Radar and Single-Carrier QPSK Communication

As mentioned in the previous sections, the necessary method for broadband SAR imaging is FMCW and for robust single-carrier communication is QPSK. Both signal types are multiplexed using FDM to realize a simultaneous functionality. This section describes a basic block diagram and a possible spectrum of the described method. After that, a general description of the joint FMCW radar and QPSK communication in FDM technique in an analytical way is presented. The description of the used hardware follows and first overall simulation and measurement results are shown.

### 2.3.1 Introduction

The key components of realizing a dual-band FDM is a power combiner with two input ports and one output port in the transmitter and a power divider with one input port and two output ports in the receiver. Both components are marked in the following Figure 2.4. Additionally, a software-defined radio (SDR) generates a QPSK communication band pass signal. This signal is then up-converted with a mixer to the final frequency band and is denoted with $c(t)$. The chirp waveform is generated with a direct digital synthesizer (DDS) and frequency-multiplied to the final frequency band. This signal is marked with $r(t)$. After power combining, the resulting signal is amplified by a single HPA and radiated by the transmit antenna to the area of interest. Only a single HPA is used for the purpose of saving power, size, weight and cost. The reflected signal and the possible signal of a communication counterpart station is received by the antenna. After amplification with a LNA, the signal is split by a power divider. The received signal is mixed with the transmit chirp on the one hand and with a local oscillator on the other hand. The mixing of two chirps leads to an analog de-ramping. The resulting IF is filtered, amplified and digitized. Mixing the signal in the receiver with a constant frequency to the operating frequency of the SDR is called down-converting. The local oscillators used in the transmitter and in the receiver operate at the same constant frequency. Therefore, the communication band from and to the SDR is automatically the same regarding the frequencies.

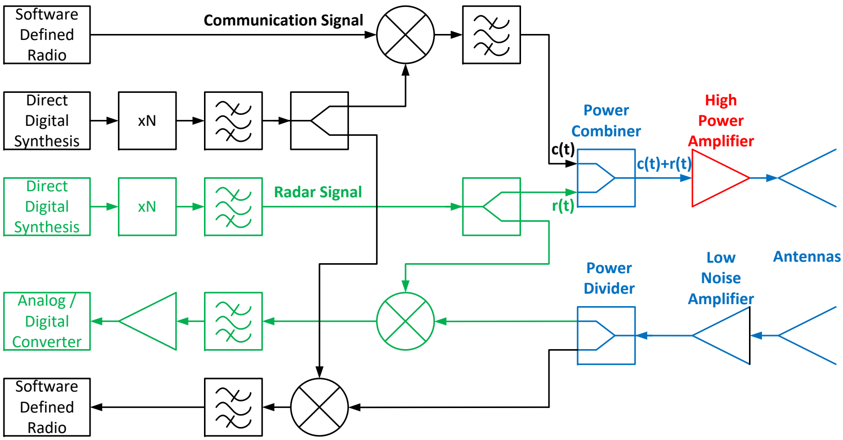


Figure 2.4: Basic block diagram of the broadband FMCW radar and single-carrier QPSK communication in FDM.

The most critical component in this figure is the HPA, because two different frequency bands must be amplified simultaneously. In this case, intermodulation products occur and must be considered. Figure 2.5 shows a simulated spectrum of the aforementioned dual-band FDM without intermodulation products. In this case, the linear chirp of the FMCW radar band shows a center frequency of 34.375 GHz and a bandwidth of 3.75 GHz. The center frequency of the communication signal is 37.1875 GHz. A gap between both frequency bands is necessary as will be mentioned in Chapter 3. The signal of the swept radar signal is simulated in such a way that it provides 30 dBm of power at every frequency step. The power of the single-carrier QPSK communication band is also 30 dBm. But in contrast to the radar signal, this power is spread over the bandwidth of 625 MHz.

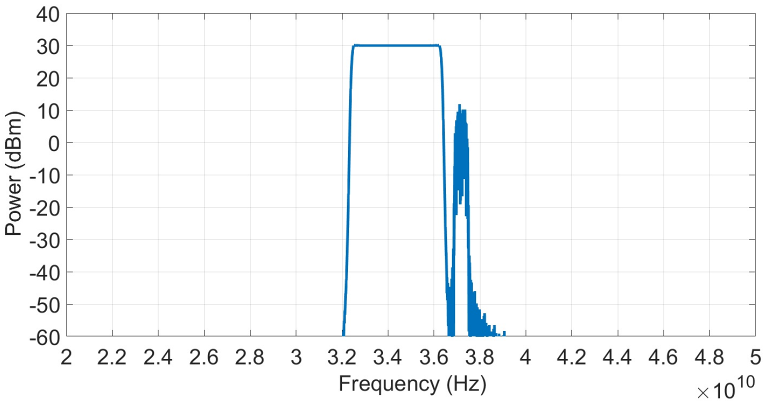


Figure 2.5: Simulated spectrum of the broadband FMCW radar and single-carrier QPSK communication in FDM.

### 2.3.2 General Description

This sub-section gives a mathematical description of the signals of an FMCW radar, of the QPSK modulation and of the FDM of both at the output of the aforementioned power combiner.

A single, complex chirp can be defined as follows. It is based on [KBM17].

$$r_1(t_\mathrm{R}) = A_\mathrm{R} \cdot \mathrm{e}^{j2\pi \cdot (f_\mathrm{R} \cdot t_\mathrm{R} + 0.5 \cdot \frac{B_\mathrm{R}}{T_\mathrm{R}} \cdot t_\mathrm{R}^2)} \cdot \mathrm{rect}\left(\frac{t_\mathrm{R}}{T_\mathrm{R}}\right), \tag{2.8}$$

here $A_\mathrm{R}$ is the signal amplitude, $f_\mathrm{R}$ the center RF, $B_\mathrm{R}$ the radar RF bandwidth and $T_\mathrm{R}$ the time duration of the chirp.

An unlimited chirp sequence can be written like this.

$$r(t_{\mathrm{R}}) = \sum_{m=-\infty}^{\infty} r_1\left(t_{\mathrm{R}} - m \cdot T_{\mathrm{R}}\right), \tag{2.9}$$

where $m$ is the chirp number.

The next step is the definition of the complex QPSK signal. The following mathematical deduction for this is based on [P A13]. It is necessary to define the statistically independent data bits first. This can be done for the real part of the data stream as follows, where $k$ is the time index.

$$u_1[k] \in 0, 1, \tag{2.10}$$

and for the imaginary part of the data stream

$$u_2[k] \in 0, 1. \tag{2.11}$$

The complex data symbol $a[k]$ can then be written for the special case of the QPSK modulation as follows.

$$a[k] = \frac{1}{\sqrt{2}}(1 - 2 \cdot u_1[k]) + j\frac{1}{\sqrt{2}}(1 - 2 \cdot u_2[k]). \tag{2.12}$$

Equation 2.7 shows that the complex data symbol $a[k]$ must be multiplied with the basic impulse $g(t_{\mathrm{C}})$. One possible basic impulse can be the rectangular function $\mathrm{rect}\left(\frac{t_{\mathrm{C}}}{T_{\mathrm{C}}}\right)$ with the time duration of the symbol $T_{\mathrm{C}}$. This results in the following formula for one symbol with the index $k$.

$$c_{\mathrm{k}}(t_{\mathrm{C}}) = \frac{1}{\sqrt{2}} \cdot \mathrm{rect}\left(\frac{t_{\mathrm{C}} - k \cdot T_{\mathrm{C}}}{T_{\mathrm{C}}}\right) \cdot ((1 - 2 \cdot u_1[k]) + j(1 - 2 \cdot u_2[k])). \tag{2.13}$$

Summing up all symbols gives the complex base-band signal in the time domain $c_{\mathrm{B}}(t_{\mathrm{C}})$. The real part of this signal for all symbols can be written like this:

$$c_{\mathrm{Re}}(t_{\mathrm{C}}) = \frac{1}{\sqrt{2}} \cdot \sum_{k=-\infty}^{\infty} \mathrm{rect}\left(\frac{t_{\mathrm{C}} - k \cdot T_{\mathrm{C}}}{T_{\mathrm{C}}}\right) \cdot (1 - 2 \cdot u_1[k]), \tag{2.14}$$

and the imaginary part as

$$c_{\mathrm{Im}}(t_{\mathrm{C}}) = \frac{1}{\sqrt{2}} \cdot \sum_{k=-\infty}^{\infty} \mathrm{rect}\left(\frac{t_{\mathrm{C}} - k \cdot T_{\mathrm{C}}}{T_{\mathrm{C}}}\right) \cdot (1 - 2 \cdot u_2[k]). \tag{2.15}$$

The final communication signal $c(t_{\mathrm{C}})$ can be realized by mixing the complex base-band signal up to the carrier frequency $f_{\mathrm{C}}$ and by adding the resulting two signal components afterwards. This can be written in the following form.

$$c(t_{\mathrm{C}}) = c_{\mathrm{Re}}(t_{\mathrm{C}}) \cdot \sqrt{2} \cdot \cos(2\pi \cdot f_{\mathrm{C}} \cdot t_{\mathrm{C}}) - c_{\mathrm{Im}}(t_{\mathrm{C}}) \cdot \sqrt{2} \cdot \sin(2\pi \cdot f_{\mathrm{C}} \cdot t_{\mathrm{C}}). \tag{2.16}$$

Last but not least, the final FDM signal consisting of the FMCW radar signal $r(t_{\mathrm{R}})$ and the QPSK communication signal $c(t_{\mathrm{C}})$ can be defined as follows.

$$\mathrm{fdm}(t_{\mathrm{R}}, t_{\mathrm{C}}) = r(t_{\mathrm{R}}) + c(t_{\mathrm{C}}). \tag{2.17}$$

The power combiner described in the previous sub-section can be used for adding the radar and the communication signal to realize the FDM signal.

### 2.3.3 Hardware Description

This sub-section describes the most important hardware used for the measurements performed in this thesis. The main focus lies on the HPA. This is a key component for realizing a FDM system with only a single HPA, because the occurring intermodulations have to be considered.
Parts of the high-resolution FMCW SAR system MIRANDA35 described in [CBP+17] are used for the radar measurements of this thesis. This includes the transmitter path without the HPA and the antenna as well as one receiver path without the antenna and the LNA. These components are connected externally. The system works in the Ka-band with a center frequency of 35 GHz and is configured to provide a maximal RF bandwidth $B_{\mathrm{R}}$ of 2 GHz.
The HPA used for the amplification of the FDM signal in the transmitter is specified to work in the frequency range between 32.5 GHz and 37.5 GHz. A photograph of this HPA is depicted in Figure 2.6


Figure 2.6: Photograph of the high power amplifier working in the Ka-band.

This HPA is designed as a Gallium Nitride (GaN) power amplifier with a saturated output power of maximal 36 dBm.

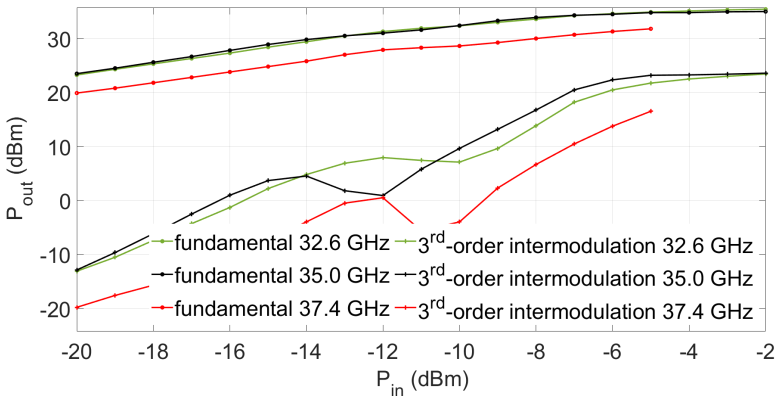


Figure 2.7: Amplification behavior of the amplifier for three different frequency points.

Because of the high importance regarding the achievable performance of the FDM system, the behavior of the amplification of the fundamental signals and of the third-order intermodulation products of the HPA is measured for the following three different frequency points: 32.6 GHz, 35.0 GHz and 37.4 GHz. The result is visualized in Figure 2.7. The output power at 37.4 GHz is 3 dB lower than at the other two frequency points. The behavior of the intermodulation products is very non-linear. To get a better understanding of the third-order intermodulation, the third-order intercept point at the output of the HPA ($OIP_3$) is ascertained. The higher the $OIP_3$, the better the suppression of the intermodulation products. The result is depicted for this HPA in Figure 2.8.

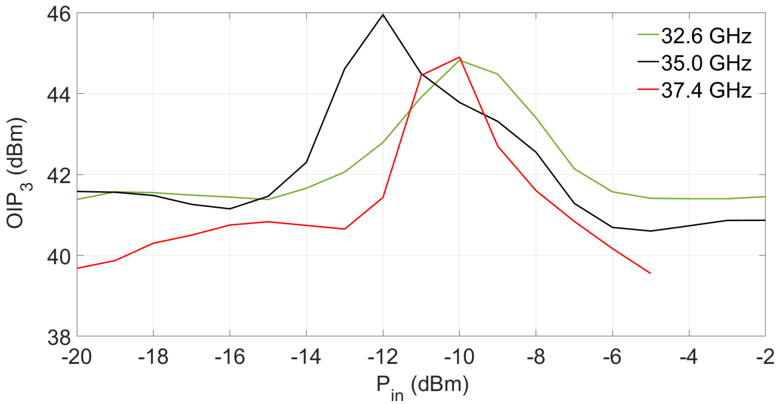


Figure 2.8: Third-order intercept point at the output of the amplifier ($OIP_3$) at three different frequency points.

On average, the $OIP_3$ is approximately 43 dBm for 32.6 GHz and 35.0 GHz and 2 dB lower at 37.4 GHz. The power ratio between the saturated output power of maximal 36 dBm and the $OIP_3$ is maximal 7 dB. Hence, this amplifier is not optimized for optimal linearity over a bandwidth of 5 GHz.
Another quality value of amplifiers is the power-added efficiency (PAE). This value is denoted in percentage and should be as high as possible. The PAE

can be calculated with Equation 2.18.

$$PAE = 100 \cdot \frac{P_{out} - P_{in}}{P_{DC}}, \tag{2.18}$$

where $P_{DC}$ is the power of the supply including the power for cooling the amplifier. The PAE of the HPA was measured and is depicted in dependence on the input power in Figure 2.9.

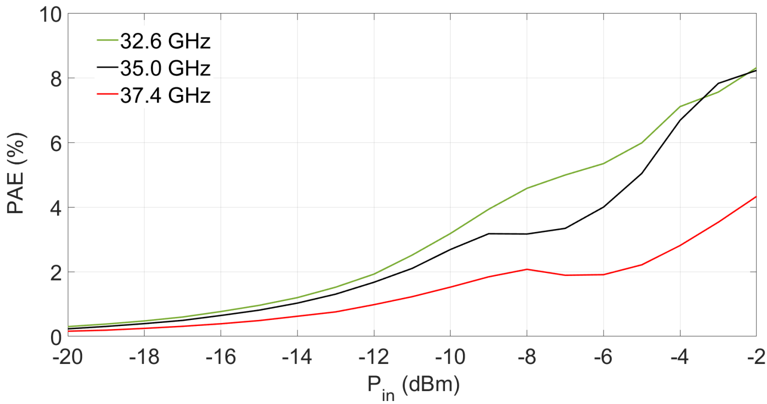


Figure 2.9: Power-added efficiency of the amplifier (PAE) at three different frequency points.

The maximal PAE of the HPA equals 8.2% by operating at the lower frequency limit of 32.6 GHz and at a saturated output power of 36 dBm. The PAE at the upper frequency limit of 37.4 GHz is approximately 4.2%. Thus, the efficiency of this HPA is maximized at lower operating frequencies and higher input power levels.

Regarding the communication part, the QPSK signal is processed at the transmitter and the receiver side with a SDR called ADALM PLUTO. In the transmitter, the base-band signal is generated having a data rate of 0.4 Mbit/s, up-converted to a center frequency of 400 MHz and amplified. A following mixer does the up-conversion to a center frequency of 37.4 GHz. The signal after the following medium power amplifier (MPA) is visualized in Figure 2.10.

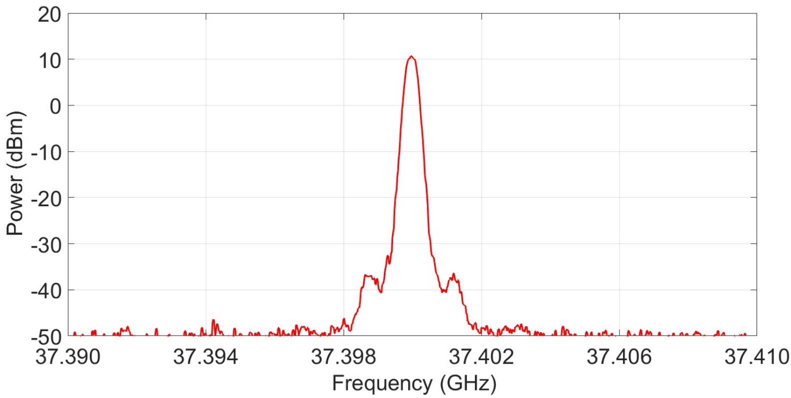


Figure 2.10: QPSK communication signal generated by the SDR ADALM PLUTO after the up-conversion.

The important 3 dB-bandwidth of this QPSK signal by using a pulse-shaping filter with a roll-off of 0.5 amounts to 300 kHz.

### 2.3.4 Simulation Results Based on an Initial Parameter Set.

With the information described in the previous sub-sections it is possible to realize a first simulation with the tool SystemVue based on Figure 2.4 [JSK22]. The chirp of the FMCW radar has a center frequency of 35 GHz and a bandwidth of 2 GHz. The center frequency of the QPSK communication amounts to 37.4 GHz and the data rate equals 0.2 Mbit/s. Table 2.1 summarizes the most important simulation parameters. The simulation with the mentioned parameters requires a high sample rate of 5 GHz. The bit rate of the communication part is only 0.2 Mbit/s, hence the symbols have to be over-sampled by a value of 50000. The result of the IF of the radar after mixing the transmit with the receive chirp, filtering and amplification is shown in Figure 2.11.

Table 2.1: Parameters used for the SystemVue simulation

| **Parameter** | **Value** |
|---|---|
| Simulation sample rate | 5 GHz |
| Samples per symbol | 50000 |
| Radar frequency | 35 GHz |
| Radar bandwidth | 2 GHz |
| Time duration of chirp | 1 ms |
| Communication frequency | 37.4 GHz |
| Bit rate | 0.2 Mbit/s |
| Propagation noise density | -120 dBm |
| Propagation delay | 0.003 ms |
| Propagation loss | 20 dB |

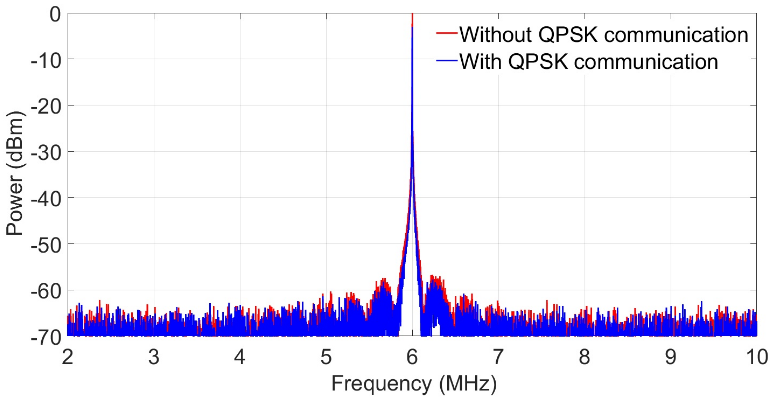


Figure 2.11: Simulated IF of the FMCW radar with and without simultaneous QPSK communication in FDM.

Comparing the two curves of Figure 2.11 shows that the SNR equals in radar-only operation 59.7 dB and in FDM operation of radar and communication 56.6 dB. The difference between both values is founded in the compression of the FDM signal by 3.1 dB through the HPA.

The performance of the communication can be assessed by using the constellation diagrams and the EVM in percentage rms. The four constellation points shown in Figure 2.12 can be clearly detected and represent the four possible symbols of the QPSK communication. Here, the EVM amounts to approximately 2.8%rms.

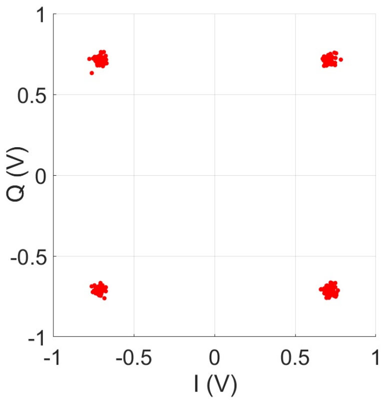


Figure 2.12: Simulated constellation diagram of the QPSK communication with simultaneous FMCW radar in FDM.

The final result of this simulation is that there is no influence in the FDM operation mode of the communication part on the radar part regarding the radar performance and of the radar part on the communication part regarding the communication performance. This is because of a large gap between both frequency bands. The output power of the radar part is 3.1 dB lower in the FDM mode than in the radar-only mode.

### 2.3.5 Measurement Results Based on an Initial Parameter Set

The simulation described in the previous sub-section is now verified with measurements [JSK22]. The parameters of the simulation and the measurement were kept as similar as possible. These parameters are summarized in Table 2.1. Figure 2.13 shows the used measurement setup.

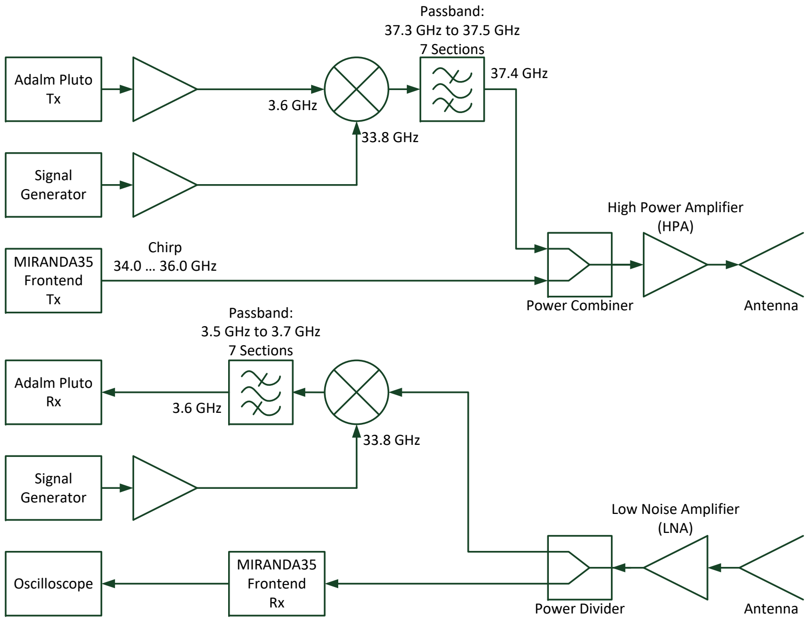


Figure 2.13: Block diagram of the measurement setup. The ADALM PLUTO is used as the SDR for communication, and the MIRANDA35 front-end for radar.

The measurement setup of Figure 2.13 is based on the block diagram of Figure 2.4. At the transmitter side the QPSK signal of the SDR ADALM PLUTO is up-converted to a center frequency of 37.4 GHz and filtered. A power combiner adds this communication signal and the chirp signal coming from the FMCW radar MIRANDA35. An HPA amplifies the resulting FDM signal to the final output power. The transmit antenna radiates the waveform to the measurement scene including a corner reflector in a cluttered environment. The reflected waveform is received by the antenna and amplified with an LNA. A power divider splits this received FDM signal into the radar path and into the communication path. In the radar part, the MIRANDA35 front-end performs the

subsequent analog signal processing. Additionally, the received FDM signal is down-converted to the operating frequency of the SDR ADALM PLUTO and filtered. The SDR does all the appropriate signal processing at the receiver side of the communication part.
Figure 2.14 shows the measured IF of the radar receiver for three constellations: Only receiver noise (black curve), FDM operation with FMCW radar and QPSK communication simultaneously (blue curve) and only FMCW radar operation (red curve).

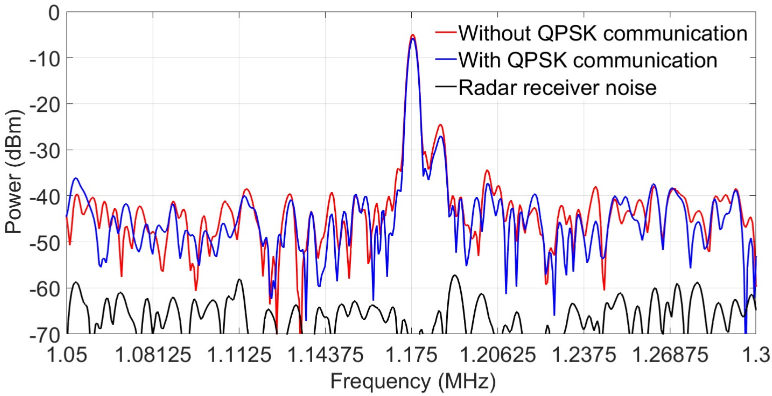


Figure 2.14: Measured IF of the FMCW radar with and without simultaneous QPSK communication in FDM.

The noise floor of the radar receiver has a maximal peak power of -57.2 dBm. The reflection of the corner reflector is represented by the peak at 1.175 MHz. At this point, the SNR is for the radar-only operation 52.5 dB and for the FDM operation with QPSK communication simultaneously 51.5 dB. Similar to the described simulation in the previous sub-section, the HPA compresses the signal by 1 dB. This is a 2.1 dB lower value, because of different operation points of the HPA. All other IF of the red and the blue curves are referable to reflections of the clutter environment.
The constellation diagram of Figure 2.15 is created for this experiment to

assess the communication performance in the FDM operation mode. The QPSK symbols can be clearly detected, with the resulting EVM amounting to 10.5%rms. This EVM is worse than that of the simulation described in the previous sub-section because of multiple reflections from clutter and targets.

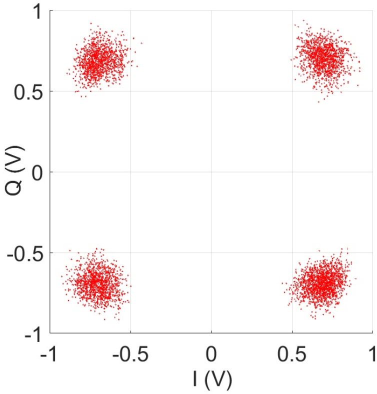


Figure 2.15: Measured constellation diagram of the QPSK communication with simultaneous FMCW radar in FDM.

The final result of this measurement is that there is no influence in FDM operation mode on the radar part and on the communication part. This is because of a large gap between both frequency bands. The output power of the radar part is 1.0 dB lower in the FDM mode than in the radar-only mode. The communication performance is not optimal for this measurement setup because it is based only on reflections coming from the measurement area.

# 3 Analysis of the Relation Between the Radar Band and the Communication Band in FDM

This chapter is about the investigation of the relation between the radar frequencies and the communication carrier frequency as well as the data rate and therefore the communication bandwidth. Here, the overall bandwidth is slightly increased compared to the radar bandwidth because of the additional bandwidth reserved for the communication part and a gap between both frequency bands. While the bandwidth of the radar is resolution-driven and can be several GHz, the resulting communication bandwidth for radar raw data transmission is only a few percent of the radar bandwidth. This is because of the usage of the FMCW radar principle. The approach described in this thesis is about the use of a single HPA for saving weight, size and power consumption. Therefore the intermodulation products of the HPA have to be considered, because they occur during high power amplification of the two carriers simultaneously used by the proposed technique. To this end, the frequency relations and the gap between the radar band and the communication band are mathematically derived and described in Section 3.1. Additionally, the resulting third-order intermodulation products for this approach are presented generally with the focus on the frequencies. The overall bandwidth for a mentioned CSAR scenario is presented in Sub-section 3.1.3. Section 3.2 of this chapter shows the verification of the previous results with simulations and measurements. The corresponding results regarding the influence of the gap on the performance of the communication channel is presented in 3.2.1. The impact of the gap on the radar performance is shown in Sub-section 3.2.2 in the form of the comparison of range-Doppler maps for different gaps in simulation and measurement. Here, the new approach is the use of a two-carrier FDM without any frequency selection filter in the receiver. This increases the flexibility and decreases the gap between both frequency bands. In this case it is necessary to consider the local oscillator of the QPSK communication. The mathematical determination and simulation as well as the measurement results in the form of corresponding spectra and constellation diagrams are presented in Section 3.3. This chapter is finished with a discussion and a conclusion.

## 3.1 Investigation of the Intermodulation Products of the HPA

As mentioned in the previous chapters, this thesis deals with a broadband FMCW radar and single-carrier QPSK communication in FDM. Therefore, it is about a waveform consisting of two simultaneous frequencies. By using a single HPA for amplifying this dual-band signal, it is necessary to consider the resulting intermodulation products. Hence, this section is about the behavior of the resulting frequencies of the intermodulation products.

### 3.1.1 Fundamental Considerations of Intermodulation Products

To characterize an amplifier regarding the harmonics and the intermodulation distortion, a signal composed of two different frequencies is considered as input signal. This can be described mathematically as follows.

$$s_{\mathrm{in}} = A_1 \cdot \cos(2\pi \cdot f_1 \cdot t) + A_2 \cdot \cos(2\pi \cdot f_2 \cdot t). \tag{3.1}$$

Here, the fundamental frequencies of the two-tone input signal are $f_1$ and $f_2$. The output signal of the amplifier can be approximated with a Taylor expansion like this:

$$s_{\mathrm{out}} = C_0 + C_1 \cdot s_{\mathrm{in}} + C_2 \cdot s_{\mathrm{in}}^2 + C_3 \cdot s_{\mathrm{in}}^3 + ... \tag{3.2}$$

The amplification factor for the fundamental frequencies is $C_1$. The second-order intermodulation and the second-order harmonics are amplified with the factor $C_2$. $C_3$ is the amplification factor for the third-order harmonics and third-order intermodulation products. This is continued for all further harmonics and intermodulation products.

Figure 3.1 shows a possible output spectrum of an amplifier including the second, the third and the fifth-order intermodulation products as well as the inherent harmonics.

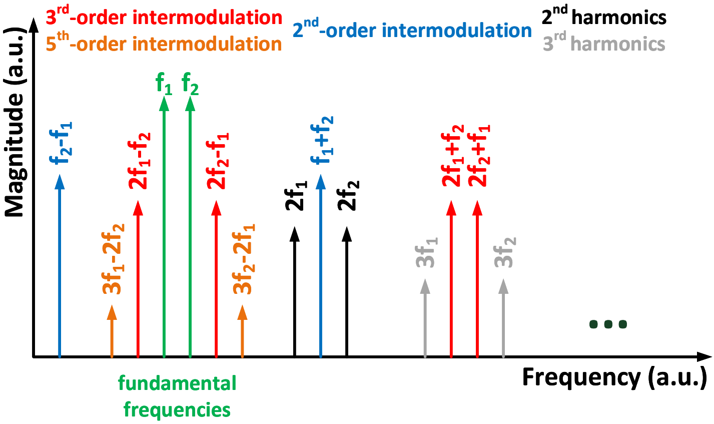


Figure 3.1: Sketch of the intermodulation products by using two frequencies.

The harmonics and many of the intermodulation products can be filtered out, because they are far away from the fundamental frequencies. The most critical intermodulation products lie close to the fundamental frequencies. That is primarily the case for the third-order intermodulation distortion. The fifth-order intermodulation products have a very low amplitude in comparison with the fundamental frequencies and can be neglected at the moment.
This thesis is about FMCW radar with simultaneous single-carrier QPSK communciation in FDM. Therefore, the fundamental frequency $f_1$ sweeps linearly over time within the radar bandwidth and the communication band occupies a certain bandwidth around $f_2$ dependent on the communication data rate. Hence, the intermodulation products have a particular bandwidth and sweep over a certain bandwidth. This effect is considered in Sub-section 3.1.2.

### 3.1.2 Third-Order Intermodulation of Radar and Communication in FDM

As mentioned in the previous Sub-section 3.1.1, the most critical intermodulation distortion is the third-order intermodulation product close to the fundamental frequencies. These are the following two frequencies $f_\mathrm{b}$ and $f_\mathrm{u}$ (please refer to Figure 3.1).

$$f_\mathrm{b} = 2 \cdot f_1 - f_2. \tag{3.3}$$

$$f_\mathrm{u} = 2 \cdot f_2 - f_1. \tag{3.4}$$

Due to the fact that $f_1$ sweeps within a bandwidth of $B_1$ (radar part) and $f_2$ has a bandwidth $B_2$ (communication part), the two third-order intermodulation products also have a bandwidth. This is sketched in Figure 3.2.

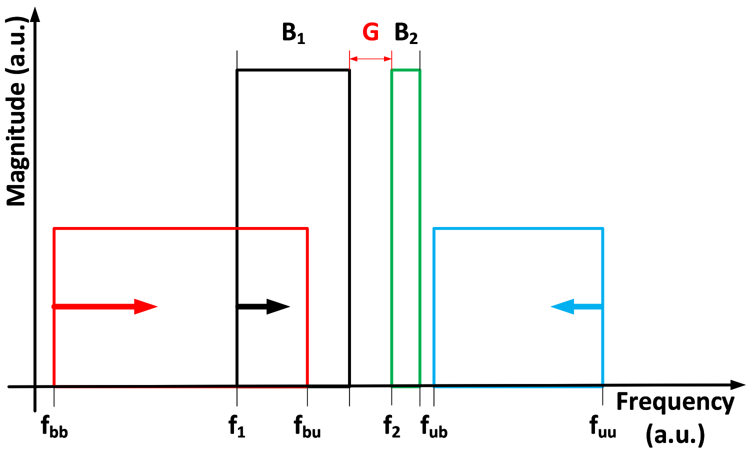


Figure 3.2: Sketch of the third-order intermodulation products (red and blue), the radar band (black) and the communication band (green).

$G$ is the gap between the radar band and the communication band. The radar signal sweeps from the frequency $f_1$ to the frequency $f_1 + B_1$. Therefore, the lower intermodulation product sweeps from $f_{\mathrm{bb}}$ to $f_{\mathrm{bu}}$ and the upper one from $f_{\mathrm{uu}}$ to $f_{\mathrm{ub}}$. The bandwidth of each single frequency step of the lower intermodulation product is $B_2$ and of the upper one $2 \cdot B_2$. It is important at this point of the thesis to ensure that there is no influence of the intermodulation products on the radar and the communication signal by using a sufficiently wide gap. On the other hand, this gap should be as narrow as possible to save overall bandwidth. The first step of a general determination is to calculate the maximal and minimal frequencies of the intermodulation product. This can be formulated for the lower part as follows.

$$f_{\mathrm{bb}} = 2 \cdot f_1 - (f_2 + B_2). \tag{3.5}$$

$$f_{\mathrm{bu}} = 2 \cdot (f_1 + B_1) - f_2. \tag{3.6}$$

And for the upper part like this.

$$f_{\mathrm{ub}} = 2 \cdot f_2 - (f_1 + B_1). \tag{3.7}$$

$$f_{\mathrm{uu}} = 2 \cdot (f_2 + B_2) - f_1. \tag{3.8}$$

The gap $G$ can be calculated in the following form.

$$G = f_2 - (f_1 + B_1) = f_2 - f_1 - B_1. \tag{3.9}$$

For minimizing the gap $G$ it is important that no overlapping of the two carrier frequencies $f_1$ and $f_2$ and the intermodulation products occur.
The next step is to establish the minimal gap regarding the radar band. Here, a band selection filter in the RF path of the receiver is used. The sweep of the FMCW radar starts at $f_1$ and stops at $f_1 + B_1$. The resulting intermodulation product starts at $f_{\mathrm{bb}}$ and stops at $f_{\mathrm{bu}}$. Therefore, overlapping only occurs in the case described as follows:

$$f_{\mathrm{bu}} = f_1 + B_1. \tag{3.10}$$

Substituting $f_{\mathrm{bu}}$ gives this formula.

$$f_2 = f_1 + B_1. \tag{3.11}$$

Inserted in 3.9, this results in $G = 0$. Thus, regarding the radar band the gap must be $G > 0$ to prevent any interactions between the radar carrier and the lower intermodulation product.

The last step is to establish the minimal gap regarding the communication band. Overlapping of the upper intermodulation with the communication band occurs in the following case.

$$f_{\mathrm{ub}} = f_2 + B_2. \tag{3.12}$$

Substituting $f_{\mathrm{ub}}$ gives this formula.

$$f_2 = B_2 + f_1 + B_1. \tag{3.13}$$

Inserted in 3.9 gives the following result.

$$G = B_2. \tag{3.14}$$

As a result for the communication part, the gap must be $G > B_2$ to prevent any interaction between the communication band and the upper intermodulation product.

In conclusion, it can be stated that the minimal gap of the whole FDM system is defined through the gap regarding the communication band and must be $G > B_2$.

### 3.1.3 Formulation of the Resulting Overall Bandwidth for the CSAR application

One possible application for the approach focused on in this thesis is airborne circular synthetic aperture radar (CSAR) with simultaneous data communication. The airborne platform is flying a circle around the area of interest for an image-based surveillance with radar. The pre-processed radar raw data is transmitted to the ground station located inside the measurement area for further computation-intensive CSAR processing. Figure 3.3 shows a sketch of this joint CSAR and communication scenario.

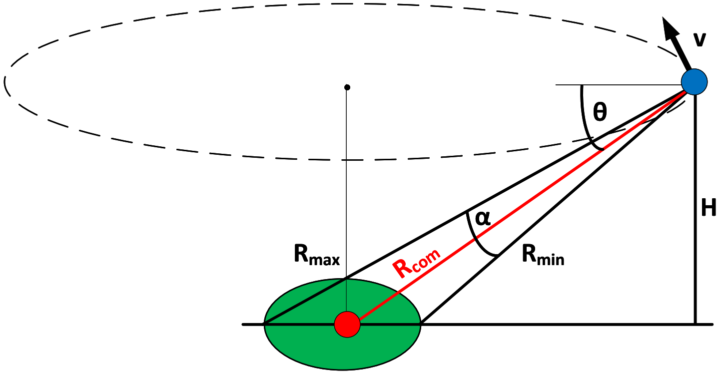


Figure 3.3: Sketch of joint CSAR and communication scenario with the most important parameters.

The blue dot in the figure represents the airborne joint CSAR and communication system and the red dot depicts the ground based communication receiver. The green zone is the measurement area. The mentioned maximal and the minimal range, dependent on the flight altitude $H$ by using a fixed antenna beamwidth $\alpha$ and depression angle $\theta$, is formulated as follows.

$$R_{\max}(H) = \frac{H}{\sin(\theta - \frac{\alpha}{2})}, \tag{3.15}$$

$$R_{\min}(H) = \frac{H}{\sin(\theta + \frac{\alpha}{2})}. \tag{3.16}$$

A key parameter for CSAR is the chirp repetition frequency $f_{\text{Rep}}$, which can be calculated with this equation based on [Pal21].

$$f_{\mathrm{Rep}} = \frac{1}{T_{\mathrm{Rep}}} = 2 \cdot 1.3 \cdot \frac{2 \cdot v \cdot \cos(\frac{\pi}{2} - \frac{\beta}{2}) \cdot f_{\mathrm{R}}}{c_0}, \tag{3.17}$$

here $v$ is the speed of the radar, $\beta$ is the azimuth beamwidth of the antenna, $f_{\mathrm{R}}$ is the radio frequency of the radar part and $c_0$ is the speed of light. No drift angle of the aircraft is considered.
The bandwidth of the integrated communication link $B_C$ for radar raw data transmission to the ground station must be considered to calculate the overall bandwidth. The first step is to calculate the maximal IF of the radar with Equation 2.5 in the following form.

$$\mathrm{IF}_{\mathrm{R_{max}}}(H) = \frac{2 \cdot R_{\mathrm{max}}(H) \cdot B_{\mathrm{R}}}{T_{\mathrm{R}} \cdot c_0}, \tag{3.18}$$

Additionally, a minimum IF can be calculated as follows:

$$\mathrm{IF}_{\mathrm{R_{min}}}(H) = \frac{2 \cdot R_{\mathrm{min}}(H) \cdot B_{\mathrm{R}}}{T_{\mathrm{R}} \cdot c_0}. \tag{3.19}$$

The bandwidth of the IF is defined by

$$B_{\mathrm{IF}}(H) = \mathrm{IF}_{\mathrm{R_{max}}}(H) - \mathrm{IF}_{\mathrm{R_{min}}}(H). \tag{3.20}$$

This signal can be filtered and down-converted to the base-band in a complex manner. The resulting real and complex part can be sampled with two ADC with a resolution of 12 bit respectively. The data rate of the resulting stream of complex data can be formulated as follows:

$$D(H) = 12\ \mathrm{bit} \cdot 2 \cdot B_{\mathrm{IF}}(H). \tag{3.21}$$

The 3 dB-bandwidth of the QPSK signal with an efficiency of 2 bit/s/Hz and with rectangular pulse-shaping used for transmitting the aforementioned data stream without additional data for error correction can be calculated with the following equation.

$$B_{\mathrm{C}}(H) = \frac{D(H)}{2\ \mathrm{bit/s/Hz}} = 12 \cdot B_{\mathrm{IF}}(H). \tag{3.22}$$

By using $T_{\mathrm{R}} = \frac{1}{f_{\mathrm{Rep}}}$ the resulting communication bandwidth for a transmission of the complex radar raw data to the ground station inside the measurement area by using the QPSK modulation technique can be summarized as follows:

$$B_{\mathrm{C}}(H) = 12 \cdot \frac{2 \cdot (R_{\mathrm{max}}(H) - R_{\mathrm{min}}(H)) \cdot B_{\mathrm{R}} \cdot f_{\mathrm{Rep}}}{c_0}. \tag{3.23}$$

On inserting 3.15 and 3.16, this equation shows that the communication bandwidth increases linearly with the flight altitude $H$.
The minimal overall bandwidth without any interaction with the intermodulation products can then be calculated with the following equation (refer to Equation 3.14).

$$B_{\mathrm{min}}(H) = B_{\mathrm{R}} + 2 \cdot B_{\mathrm{C}}(H), \tag{3.24}$$

where $B_{\mathrm{min}}(H)$ is determined by system parameters like the radar bandwidth $B_{\mathrm{R}}$, the depression angle $\theta$, the elevation beamwidth of the antenna $\alpha$, the velocity of the radar $v$, the azimuth beamwidth of the antenna $\beta$, the radar RF $f_{\mathrm{R}}$ and on the the variable flight altitude $H$. Here, the gap is equal to the communication bandwidth as mentioned in 3.14.
This result is now simulated by using the following system parameters.

Table 3.1: Parameters used for the simulation for the overall bandwidth dependent on the flight altitude.

| **Parameter** | **Value** |
|---|---|
| Radar center frequency | 34.375 GHz |
| Radar bandwidth | 3.75 GHz |
| Elevation beamwidth | 12 ° |
| Azimuth beamwidth | 12 ° |
| Depression angle | 35 ° |
| Velocity of radar | 10 m/s |

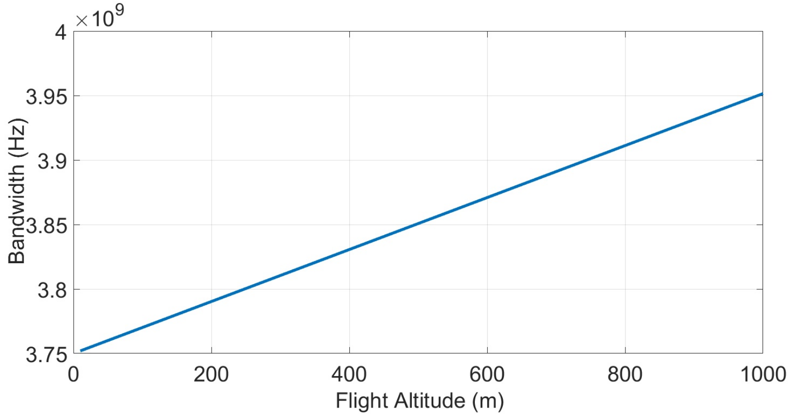


Figure 3.4: Simulated overall bandwidth dependent on the flight altitude for an assumed CSAR scenario.

As expected, Figure 3.4 shows that the overall bandwidth increases linearly with the flight altitude above the radar bandwidth of 3.75 GHz. The overall bandwidth in case of a flight altitude of 1000 m is 3.95 GHz. This exceeds the radar bandwidth only by approximately 5%.

## 3.2 Evaluation of the Gap Width Dependence of the System Performance

This section describes the effect of different gap widths on the communication and on the radar performance of the receiver. This is conducted by varying the gap between the radar band and the communication band.

### 3.2.1 Effect of Different Gaps on the Communication Performance

The communication performance can be assessed with the EVM in percentage rms. For the appropriate assessment in the simulation, the EVM is measured for every gap during the sweep. Here, the minimal gap between both frequency bands is zero and the maximal gap is equal to the radar bandwidth. Table 3.2 summarizes the simulation parameters.

Table 3.2: Parameters used for the simulation of the communication performance.

| **Parameter** | **Value** |
|---|---|
| Center frequency of radar | 34.375 GHz |
| Bandwidth of radar | 3.75 GHz |
| Center frequency of communication | 36.875 GHz |
| Bandwidth of communication | 1.25 GHz |
| Third-order intercept point | 40 dBm |
| Power of radar | 30 dBm |
| Power of communication | 30 dBm |
| Roll-off of pulse-shaping filter | 0.5 |

The radar frequency is increased linearly in the simulation from 32.5 GHz to 36.25 GHz with the effect that the gap in percentage from the communication bandwidth decreases from 300% to 0%. The result is visualized in Figure 3.5.

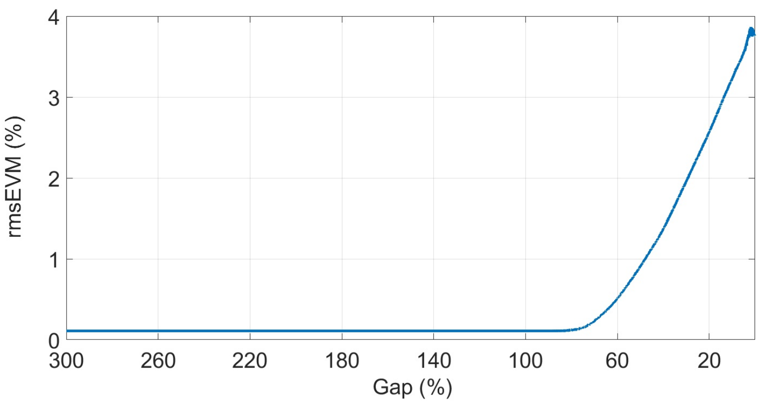


Figure 3.5: Simulated EVM as rms in percentage over different gaps. The gap is shown in percentage of the communication bandwidth.

It is clear from the results at the beginning of this chapter that the intermodulation products have an effect on the communication signal. This effect is visible in Figure 3.5 from 80% to 0%, because the rmsEVM increases from 0.1% to 3.8%. The optimal and minimal gap in percentage from the communication bandwidth calculated with Equation 3.14 is 100%. The simulation shows, that the gap can be 20% lower than the theoretical one because of the usage of a pulse-shaping filter.

This simulation result is now verified with a similar measurement by using the hardware described in Sub-section 2.3.3. The parameter used for the measurement is summarized in Table 3.3.

Table 3.3: Parameters used for the measurement for the assessment of the communication performance.

| **Parameter** | **Value** |
|---|---|
| Frequency range for steps | 37399.6 MHz to 37399.82 MHz |
| Center frequency of communication | 37400 MHz |
| Bandwidth of communication | 300 kHz |
| Third-order intercept point | 40 dBm |
| Power of frequency steps | 30 dBm |
| Power of communication | 30 dBm |
| Roll-off of pulse-shaping filter | 0.5 |

Regarding the QPSK communication a pulse-shaping filter with a roll-off of 0.5 is used. The 3 dB-bandwidth of this communication signal is approximately 300 kHz with a data rate of 0.4 Mbit/s. The lower bound of the communication signal can be calculated by subtracting half of the communication bandwidth from the center frequency of the communication signal to 37399.85 MHz. The amplifier output power of the communication signal and the single frequency steps are equal and amount to 30 dBm. This is approximately 6 dB lower than the saturated output power of the HPA. This power back-off is necessary to prevent a further effect of the non-linearities of the amplifier which is described in the following chapter.

The measurement setup for the assessment of the communication performance dependent on the gap is visualized in Figure 3.6. The up-converted QPSK communication signal coming from the SDR ADALM PLUTO is power-combined with the single frequencies from a signal generator. The resulting FDM signal is amplified in the HPA. The output signal with additional intermodulation products is attenuated and down-converted to the operating frequency of the SDR ADALM PLUTO of 400 MHz. The SDR performs the down-conversion to base-band and the following signal processing steps for QPSK communication. The additional output information is the EVM of the communication signal.

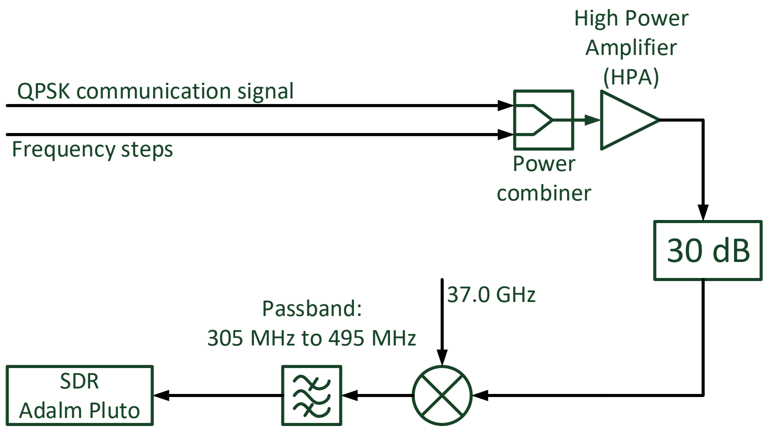


Figure 3.6: Measurement setup for the assessment of the communication performance dependent on different gaps.

The gap between the first mentioned frequency point of 37399.6 MHz and the lower bound of the communication signal of 37399.85 MHz amounts to 250 kHz. This is 83.33% of the communication bandwidth. The gap is decreased during the measurement process by a value of 10 kHz to a minimum of 30 kHz. This minimum value represents 10% of the communication bandwidth. At every step, the EVM is measured. The rmsEVM in percentage over the gap in percentage of the communication bandwidth is depicted in Figure 3.7.

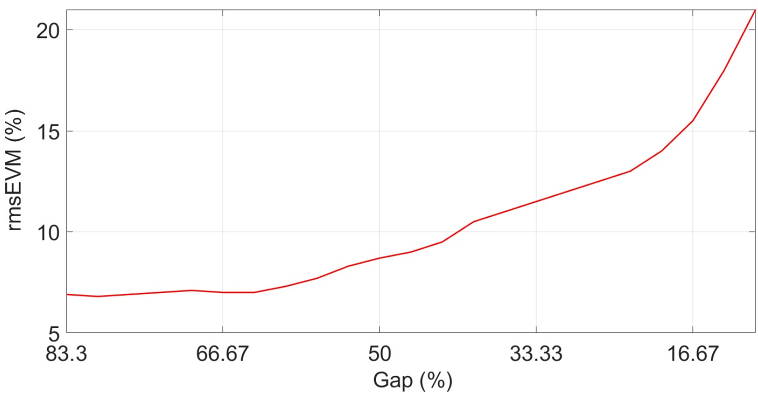


Figure 3.7: Measured EVM as rms in percentage over different gaps. The gap is shown in percentage of the communication bandwidth.

The lowest EVM value amounts to 6.8% at a gap of 80%. This EVM value is 6.7% higher than the corresponding value of the simulation because of additional internal noise and further non-linearity effects of the analog signal processing chain. The EVM increases to 7.0% at a gap of 63.3%. Up to this point, no influence of the intermodulation products on the communication signal is detectable. After further decreasing the gap, the EVM increases because of the intermodulation products. The maximal rmsEVM value of 21% is measured at a gap of 10% of the communication bandwidth.
The minimal gap in the simulation is approximately 20% lower than the theoretical one. In the measurement, the minimal gap without any influence of the intermodulation products on the communication signal is approximately 37% lower than the theoretical one. The difference between both values can be explained by the mentioned offset of the rmsEVM value of 6.7% between the simulation and the measurement. Values below 6.8% rmsEVM cannot be measured with the described setup.

### 3.2.2 Effect of Different Gaps on the FMCW Radar Performance

The performance of the FMCW radar can be assessed with the analysis of range-Doppler maps. This is shown with a quantitative comparison in simulations and measurements for different gaps. In this special case, the necessary FDM signal consists of the radar chirp and a single frequency instead of the communication signal generated by a signal generator. The use of a signal generator instead of the up-converted communication signal allows for the generation of test signals without filtering. In contrast to the theory described at the beginning of this chapter no band selection filter is used in the RF path of the receiver. As a result of this, the whole received FDM signal is mixed with the transmit chirp. This process is depicted in Figure 3.8.

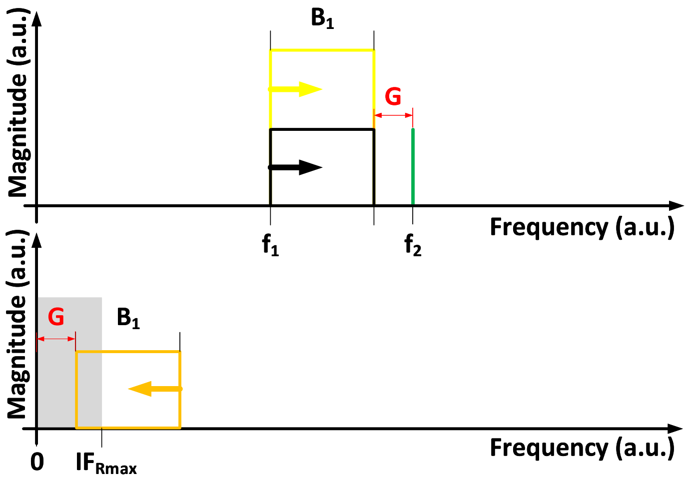


Figure 3.8: Top: Sketch of the received FDM signal (black and green) and the local oscillator of the receiving mixer (yellow).
Bottom: Sketch of the resulting radar IF band (gray) with the undesired mixing product (orange).

The bandwidth of the chirps is denoted with $B_1$, the gap with $G$ and the maximal IF frequency with $\mathrm{IF}_{\mathrm{Rmax}}$. Besides the sum signal from the LO and the signal of the RF path, the receiving mixer also generates the difference of both. Therefore, the useful radar IF is the difference resulting from the mixing process of the transmit chirp and the time-delayed receive chirp. A point target in the measurement area, for example, generates a single frequency in the IF band marked in gray. The undesired mixing product of the transmit chirp and the time-delayed single frequency is also a chirp signal in the IF. In case of using up-chirps this signal is now a down-chirp. Thus, the resulting minimal gap can be expressed as follows.

$$G = \mathrm{IF}_{\mathrm{Rmax}}. \tag{3.25}$$

To prevent any influence of the undesired mixing product on the desired radar signal, the gap must be larger than the maximal IF of the radar ($G > \mathrm{IF}_{\mathrm{Rmax}}$). This signal depends on the RF bandwidth of the radar and the maximal measurement range as mentioned in Equation 2.5.
In this special case, the radar chirp and the single frequency in FDM have the same transmit power. This is the worst case regarding the intermodulation products during the system design. Therefore, the receive power of both signals after reflection at the target is equal. Hence, a power relation between the radar signal and the undesired chirp can be made after the range-Doppler processing. The receive chirp is de-ramped with the transmit chirp and the resulting IF is a signal with a constant frequency and phase in the simplest case. The power of this signal is maximized. The received single frequency is also mixed with the transmit chirp. The result is a chirp signal in the IF. Because of the low-pass filtering of the IF and the digital down-conversion process, the energy of this undesired chirp is lower than the energy of the de-ramped chirp. This can be expressed as a ratio and depends therefore on the RF and IF bandwidth of the radar and the amount of chirps designated for integration and can be formulated for a first approximation as follows.

$$A = \frac{2 \cdot B_{\mathrm{R}} \cdot I}{B_{\mathrm{IF}}}, \tag{3.26}$$

where $B_{\mathrm{R}}$ is the RF bandwidth of the radar chirp, $B_{\mathrm{IF}}$ is the bandwidth of the down-converted IF signal, and $I$ is the amount of chirps to integrate. The factor of 2 results from the separation of the undesired chirp signal into a positive and a negative Doppler frequency.

The effect of the influence of the gap on the desired radar IF is simulated by using the following parameters.

Table 3.4: Parameters used for the simulation of the radar performance.

| **Parameter** | **Value** |
|---|---|
| Frequency range for steps | 37.4 GHz to 36.0 GHz |
| Center frequency of radar | 35.0 GHz |
| Bandwidth of radar | 2 GHz |
| Chirp duration | 150 $\mu$s |
| Maximal IF | 13.996 MHz |
| IF bandwidth | 1.9067 MHz |
| Integration time | 42.9 ms |
| Doppler resolution | 23.31 Hz |
| Doppler bandwidth | 6.67 kHz |
| Power of received FDM signal | -15 dBm |
| Noise power | -95 dBm |

The simulation conducts the mixing of the transmit chirp with the received FDM signal, the IF filtering, the digital down-conversion and the generation of the range-Doppler maps.
By using these parameters, the amount of chirps to integrate can be calculated by dividing the integration time by the chirp duration as follows.

$$I_{\mathrm{Sim}} = \frac{42.9\ \mathrm{ms}}{0.15\ \mathrm{ms}} = 286. \tag{3.27}$$

Now it is possible to calculate the ratio between the undesired chirp signal and the power of the signal corresponding to the target with Equation 3.26.

$$A_{\mathrm{Sim}} = \frac{2 \cdot 2\ \mathrm{GHz} \cdot 286}{1.9067\ \mathrm{MHz}} = 599989.5. \tag{3.28}$$

Expressed in logarithmic scale, this results in a ratio of 57.8 dB between the undesired chirp signal and the power of the desired target reflection. This ratio is only valid for the case that the transmit power of the chirp signal and the single frequency is equal.
Figure 3.9 shows the range-Doppler map generated by using a single frequency of 37.4 GHz. Therefore, the gap equals 1.4 GHz. The mean of the noise floor of section 1 and 2 amounts to -96.3 dBm and the power of a point target marked with the red cross is detected at -14.8 dBm. Therefore, the SNR for this target amounts to 81.5 dB. The used gap of 1.4 GHz is larger than the minimal gap of 13.996 MHz. The whole signal energy of the undesired chirps is filtered out by the low-pass filter in the IF path. Thus, no influence of the undesired mixing product and the desired radar signal is detectable.

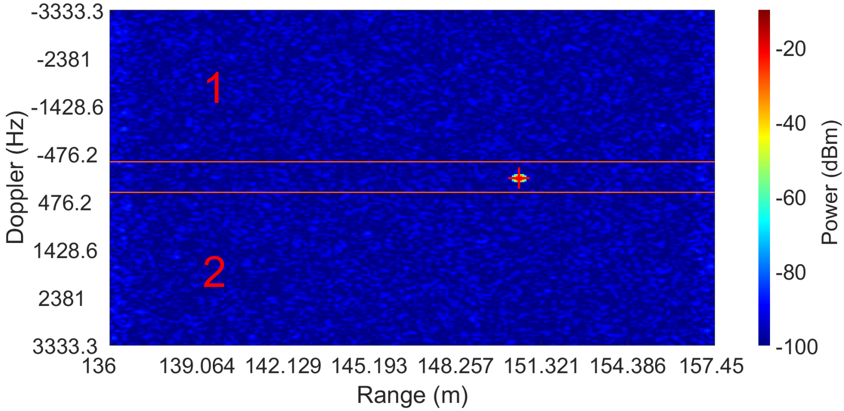


Figure 3.9: Range-Doppler map generated by using the parameters from Table 3.4 and a gap of 1.4 GHz.

The next step is to decrease the gap from 1.4 GHz to 700 MHz. For this, the simulation result is depicted in Figure 3.10. The mean value of the noise floor is also -96.3 dBm and the power corresponding to a point target marked with the red cross amounts to -14.8 dBm. The resulting SNR is 81.5 dB and therefore quite similar to the previous case of a 1.4 GHz gap. The low-pass filter in the IF path has a bandwidth of approximately 14 MHz. The gap of 700 MHz is larger than this. Therefore, the whole signal energy of the undesired chirps is filtered out and no undesired effect is detectable.

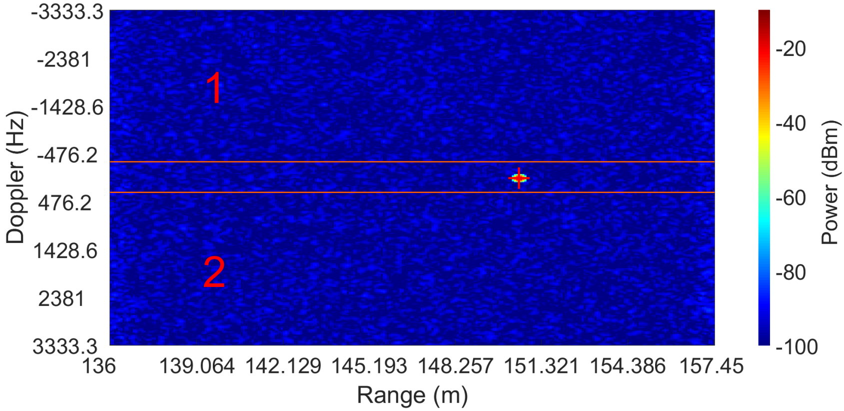


Figure 3.10: Range-Doppler map generated by using the parameters from Table 3.4 and a gap of 700 MHz.

The last simulation uses a minimal gap of 0 Hz. Therefore, the used single frequency is equal to the maximal radar RF of 36 GHz. The resulting range-Doppler map is depicted in Figure 3.11. Now, two additional lines can be detected with a Doppler frequency of +/- 2.2 kHz. These lines result from the mixing of the transmit chirp with the received single frequency. The resulting chirps lie within the IF band of the radar. The Doppler frequencies of these lines are subject to an additional phase shift of $(\frac{2 \cdot \pi}{3})$ of the single frequency. This phase shift is added up for a certain time. The analysis of this gives a mean power level of the noise floor of section 1 and 2 of -91.1 dBm. The power level reflected from the target still yields -14.8 dBm. The resulting SNR is found to be reduced to only 76.3 dB, approximately 5 dB lower than in the case discussed previously. Equation 3.28 shows that the ratio between the power of the targets and the mean power of the undesired chirp amounts to 57.8 dB. The mean power of the mentioned lines in Figure 3.11 is -75.3 dB. This power level can be explained by the power of the strongest point target in the middle of the range-Doppler map marked with the red cross with a power level of -14.8 dBm. The difference between both power levels amounts to 60.5 dB. This is approximately 3 dB lower than the theoretical value of 57.8 dB, because this value is based only on a first approximation.

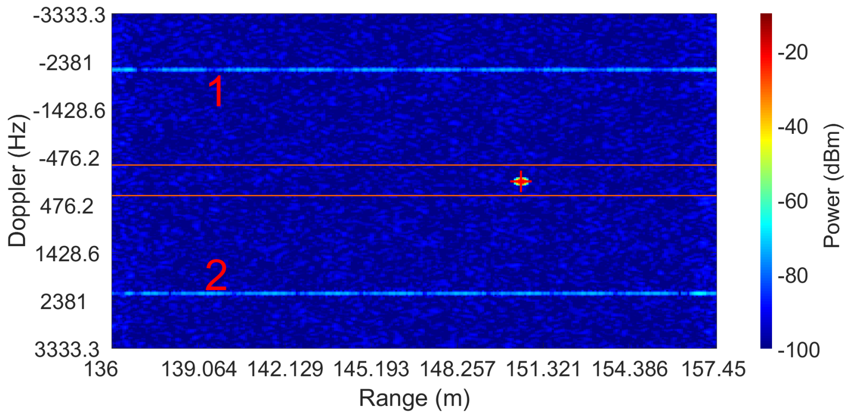


Figure 3.11: Range-Doppler map generated by using the parameters from Table 3.4 and a gap of 0 Hz.

This consideration is true if the power of the radar chirp and the power of the single frequency is equal and the gap is lower than the maximal IF of the radar (Equation 3.25). Decreasing the power of the single frequency decreases also the power of the undesired chirp in the IF. The power difference between the radar chirp and the single frequency must be added to Equation 3.26. In case of a gap larger than the maximal IF of the radar, the undesired chirp in the IF is filtered out by the IF filter.

The simulation results are verified in the following with radar measurements and range-Doppler processing of the radar data. Here, similar parameters are used as in the simulations described above. Figure 3.12 shows the measurement setup used for the assessment similar to the described simulations.

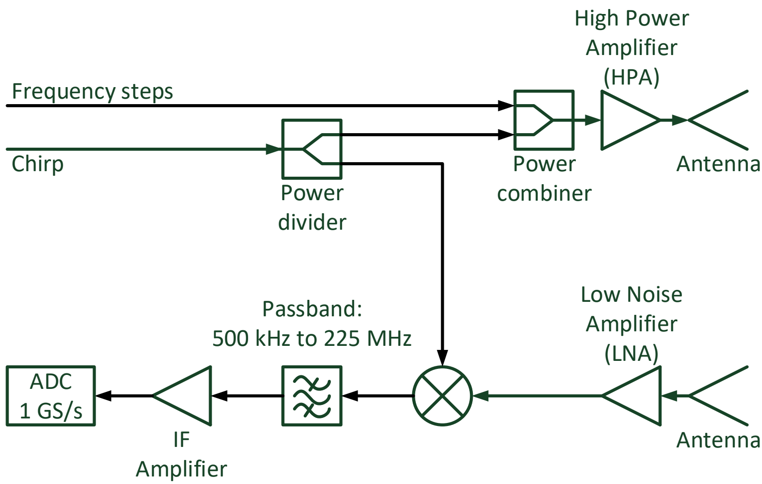


Figure 3.12: Block diagram for investigating the radar performance for different gaps.

The chirp in the frequency range from 34.0 GHz up to 36.0 GHz, generated from the mentioned MIRANDA35 radar system, is power-combined with three different single frequencies coming from a signal generator one after another. These static frequencies are not synchronized to the radar signals. The use of a signal generator instead of the up-converted communication signal allows the generation of test signals without filtering. Therefore, a higher frequency range for this can be used. The resulting FDM signal including the chirp and the single frequencies is then amplified in the HPA. The amplifier generates additional intermodulation products, which are radiated together with the amplified FDM signal by the transmit antenna. The reflected signal coming from the targets, including clutter and a corner reflector, is received by an antenna. The LNA amplifies the received signal including the chirps, the single frequency and the intermodulation products. As opposed to the theory described at the beginning of this chapter, no band selection filter is used in the RF path of the receiver. The LNA is followed by the receiving mixer, making the transmit chirp the only local oscillator. The received signals are mixed with the transmit chirp, and the IF results. After that mixing process, the resulting signal is now band-limited by the IF filter with a bandwidth of 0.5 MHz to 225 MHz and digitized by an ADC. The ADC unit performs the digital down-conversion to base-band including an additional band limitation. The following range-Doppler processing is conducted offline.

Table 3.5 summarizes the most important parameters for the assessment of the radar performance.

Table 3.5: Parameters used for the measurement for the assessment of the radar performance.

| **Parameter** | **Value** |
|---|---|
| Frequency range for steps | 37.4 GHz to 36.0 GHz |
| Center frequency of radar | 35.0 GHz |
| Bandwidth of radar | 2 GHz |
| Chirp duration | 982.04 $\mu$s |
| Pass band of IF filter | 0.5 MHz ... 225 MHz |
| Digital IF bandwidth | 0.24414 MHz |
| Integration time | 219.98 ms |
| Doppler resolution | 4.54 Hz |
| Doppler bandwidth | 1.0172 kHz |
| Power of received FDM signal | -15 dBm |

The upper frequency bound of the radar signal amounts to 36 GHz, because it is designed as an up-chirp. Therefore, the minimal gap between the radar chirp and the discrete frequency steps within 37.4 GHz and 36.0 GHz is in the range between 1.4 GHz and 0 Hz. The chirp duration used in the simulation is shorter than that in the measurement because of memory limitations of the used computer. Therefore, the Doppler bandwidth is higher in the simulation than in the measurement. Hence, different IF bandwidths of simulation and measurement have to be considered in Equation 3.26. Similar to the simulation, one prominent point target with a RCS of 1000 $m^2$ is used.

The first measurement is conducted using a gap of 1.4 GHz. Hence, the used static frequency amounts to 37.4 GHz. Figure 3.13 shows the resulting range-Doppler map. Here, the mentioned corner reflector in the middle, marked with a red cross, is visible. The line in the middle of the range-Doppler map around the point target represents the clutter with low Doppler. There are some system internal spurious signals detectable in the sections 1 and 2. These signals are not referable to the FDM signal including the radar chirp, the single frequency and the intermodulation products generated by the HPA.

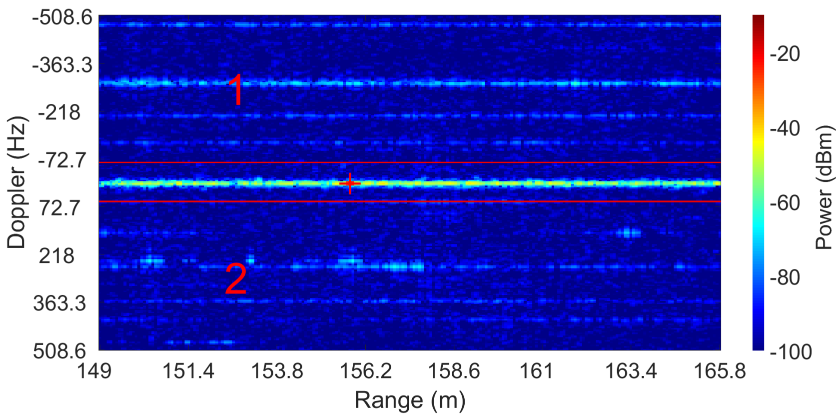


Figure 3.13: Range-Doppler map for the minimal gaps of 1400 MHz. No effect of the undesired signals on the radar measurement is detectable. The SNR amounts to 74.4 dB.

The power level of the point target at Doppler zero amounts to -15 dBm. The mean value of the noise floor including the spurious signals of section 1 and 2 is -89.5 dBm. Therefore, the SNR for this target is 74.4 dB.
Similar to the simulation, the next radar measurement is done by using a gap of 700 MHz. The resulting range-Doppler map is depicted in Figure 3.14. As expected, the undesired chirp signal in the IF, caused by the mixing process of the received single frequency with the transmit chirp, is not detectable. Only the system internal spurious signals in section 1 and 2 are visible. These signals

are not comparable to the FDM signal of the previous measurement. The power corresponding to the corner reflector, marked with the red cross, equals -15 dBm. The mean value of the noise floor, including the spurious signals, is approximately at -90.6 dBm. Hence, the SNR is 75.6 dB. These values are approximately equal to the values found in the previous measurement.

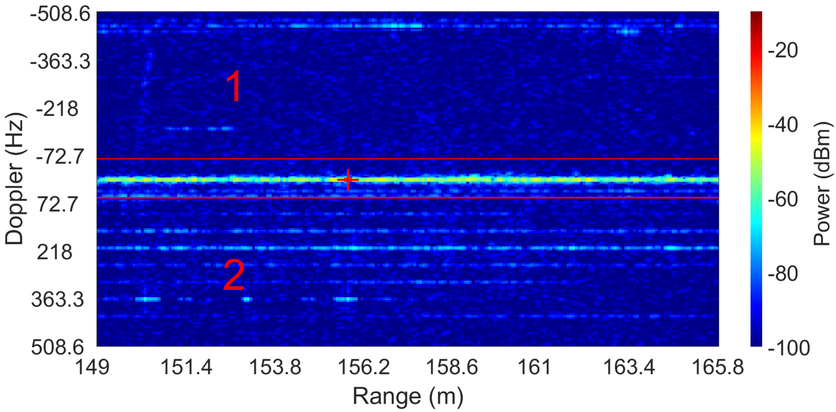


Figure 3.14: Range-Doppler map for the minimal gaps of 700 MHz. The SNR of the radar measurement is approximately 75.6 dB.

The last measurement is done by using a minimal gap of 0 Hz. The resulting range-Doppler map is visualized in Figure 3.15. As expected, the two additional lines with a Doppler shift are recognizable. These lines are part of the undesired chirp caused by the mixing process of the transmit chirp with received single frequency. The power of the point target, marked with a red cross inside the clutter environment, amounts to -15.4 dBm. The mean value of the noise floor including the system internal spurious signals and the undesired chirp signal increases to -87.1 dBm. Therefore, the SNR of this target is only 71.7 dB. This is approximately 3 dB worse than the values of the measurements above. It can be stated that the mentioned undesired chirp signals are clearly detectable, and the corresponding ratio can be calculated with the Equation 3.26. By using the parameters stated in Table 3.5 for the measurements, the amount of chirps to integrate can be calculated by dividing the integration time by the chirp duration as follows.

$$I_{\text{Meas}} = \frac{219.98 \text{ ms}}{0.98204 \text{ ms}} = 224. \tag{3.29}$$

Now it is possible to calculate the ratio between the power of the undesired chirp signal and the power of the signals corresponding to the targets by using Equation 3.26.

$$A_{\text{Meas}} = \frac{2 \cdot 2 \text{ GHz} \cdot 224}{0.24414 \text{ MHz}} = 3670025.4. \tag{3.30}$$

Expressed in logarithmic scale, this gives a ratio of 65.7 dB between the undesired chirp signal and the power of the desired targets. This is true in the case that the transmit power of the chirp signal and the single frequency is equal. The mean power of the two undesired lines equates to -78.7 dBm. By using the power of the point target of -15.4 dBm, the measured ratio of these undesired signals equates to approximately 63.3 dB. This represents a 2 dB increase over the theoretical value.

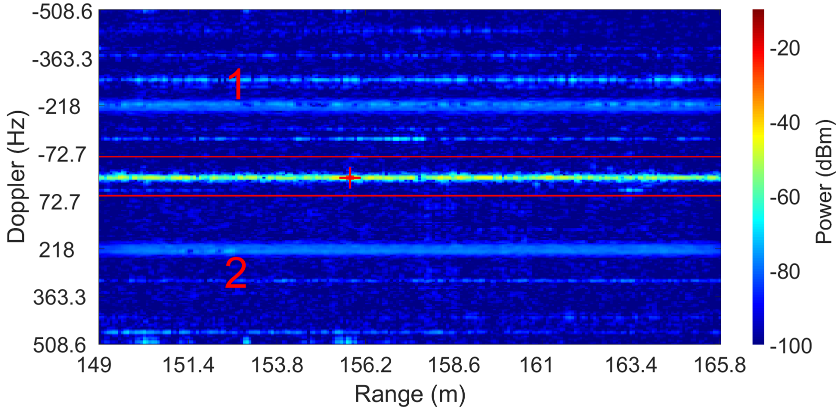


Figure 3.15: Range-Doppler map for a minimal gap of 0 Hz. The SNR of the radar measurement decreases to 71.7 dB.

The reason for the shift of the undesired chirp to both Doppler directions (one line has positive Doppler and the other has negative Doppler) is, that the radar chirp and the single frequencies are not synchronized. If the two signals are synchronized, the undesired chirp signal will be at low Doppler frequencies.

## 3.3 Determination of the Frequency of the Local Oscillator for down-conversion of the QPSK signal

The communication part of the system uses a down-converter in the receiver for transforming the received high millimeter-wave frequency band down to the operational frequency of the SDR. Additionally, the radar chirp and the third-order intermodulation products are down-converted into the frequency band of the SDR, because no band selection filters are used. This section describes two different methods for determining the fixed frequency of the local oscillator for the down-converter. The first can be used for realizing a minimized gap and the second for a minimized communication frequency.

### 3.3.1 Mathematical Deduction

Figure 3.16 shows a sketch of the spectrum of the received RF signals including the radar chirp with the bandwidth $B_1$, the communication signal with the bandwidth $B_2$ as well as the intermodulation products (top) and the resulting IF signal after mixing with the frequency $f_{\mathrm{LO}}$ (bottom). Here, the gap $G$ is as narrow as possible, as mentioned in Equation 3.14. The interesting mixing product is the difference between the local oscillator frequency and the received RF signal. Additionally, the resulting communication band in the IF must fit into the frequency band of the SDR. Therefore, the only location of the frequency of the local oscillator in the spectrum is inside the upper intermodulation product. For calculating the frequency of the local oscillator, the following assumption can be made. In this way, no influence of the upper intermodulation product on the communication band in the IF occurs.

$$f_{\mathrm{uu}} - f_{\mathrm{LO}} = f_{\mathrm{LO}} - (f_2 + B_2) \tag{3.31}$$

After rearranging, the frequency of the local oscillator can be calculated by using the equations of Section 3.1.2 with the following equation.

$$f_{\mathrm{LO}} \geq \frac{f_{\mathrm{uu}} + f_2 + B_2}{2}. \tag{3.32}$$

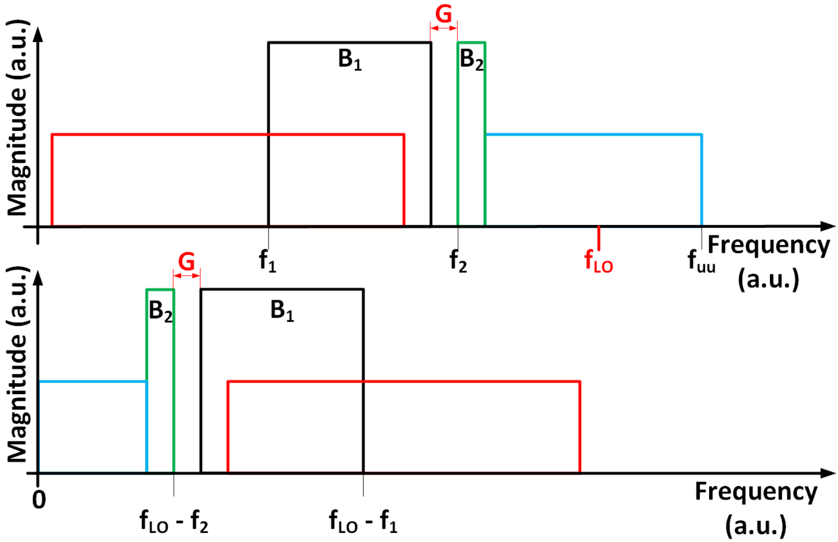


Figure 3.16: Top: Sketch of the received RF including the radar chirp ($B_1$, black), the communication band ($B_2$, green) as well as the intermodulation products (red and blue).
Bottom: Sketch of the IF with the resulting mixing products for the case of $G = B_2$.

The disadvantage of this solution is that the center frequency of the resulting communication band in the IF can be very high depending on the bandwidth of the two desired frequency bands. If it is possible to realize larger gaps then the frequency of the local oscillator can be at another location in the spectrum. Figure 3.17 shows a sketch of the spectrum of the received RF signal including the radar chirp with the bandwidth $B_1$, the QPSK communication signal with the bandwidth $B_2$, as well as the intermodulation products and the resulting IF signal after mixing with the frequency $f_{\mathrm{LO}}$. Here, the gap $G$ is larger than twice the communication bandwidth $B_2$. In this special case, the local oscillator can be determined as follows.

$$f_{\mathrm{LO}} \leq f_2 + \frac{G}{2} \quad \text{and} \quad f_{\mathrm{LO}} \geq f_2 + B_2 \quad \text{for} \quad G \geq 2 \cdot B_2. \tag{3.33}$$

The frequency of the local oscillator can be chosen within the described bounds. If this is the case, the communication band in the IF is not influenced by any other signal components of the spectrum.

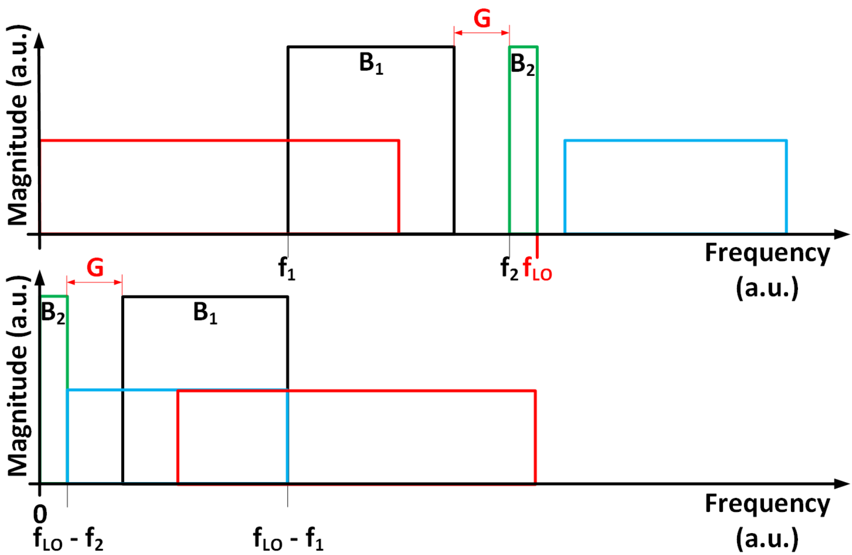


Figure 3.17: Top: Sketch of the received RF including the radar chirp ($B_1$, black), the communication band ($B_2$, green) as well as the intermodulation products (red and blue).
Bottom: Sketch of the IF with the resulting mixing products for the special case of $G \geq 2 \cdot B_2$.

### 3.3.2 Behavior of the IF Signals in the Receive Path

This sub-section describes the behavior of the signals before and after the receiving mixer based on simulations. As mentioned above, the local oscillator has a fixed frequency for converting the QPSK communication signal down to a frequency band suitable for the following SDR. The radar chirp is simulated as an up-chirp and the intermodulation products are also converted down with the local oscillator, because no band selection filter is used in the RF path of the receiver. Table 3.6 summarizes the major parameters used for the simulation.

Table 3.6: Parameters used for the simulation for the assessment of the signals before and after the receiving mixer.

| **Parameter** | **Value** |
|---|---|
| Start frequency of radar chirp | 32.5 GHz |
| Center frequency of radar chirp | 34.375 GHz |
| Bandwidth of radar chirp | 3.75 GHz |
| Start frequency of communication | 36.875 GHz |
| Center frequency of communication | 37.1875 GHz |
| Bandwidth of communication | 625 MHz |
| Power of radar chirp | 30 dBm |
| Power of communication | 30 dBm |
| Third-order intercept point | 40 dBm |

The minimal gap between the radar chirp and the communication band is equal to the communication bandwidth. Therefore, no influence of the intermodulation products on the usable communication and radar signals occurs. (Refer to Section 3.1.2 and Equation 3.14).

Figure 3.18 shows the simulated output signal of the HPA including the radar chirp as well as the communication signal and the upper and lower third-order intermodulation products. Here, the signal constellation of the last chirp frequency of the up-chirp at 36.25 GHz is depicted. This signal is used directly in the simulation for down-conversion with the receiving mixer. As mentioned in Section 3.1.2, the upper intermodulation product at the time of the last chirp frequency of 36.25 GHz ranges from 37.5 GHz to 38.75 GHz. At the time of the first chirp frequency of 32.5 GHz, the upper intermodulation product is between 41.25 GHz and 42.5 GHz. Therefore, the maximal frequency range of the upper intermodulation product is from 37.5 GHz to 42.5 GHz.

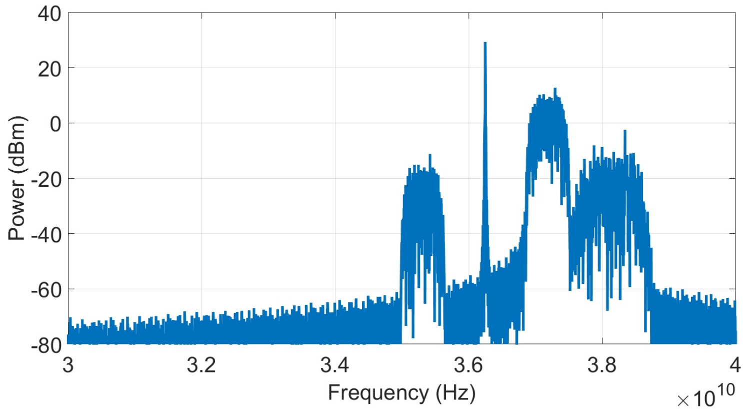


Figure 3.18: Spectrum of the RF input signal of the receiving mixer at the time of the last chirp frequency at 36.25 GHz. The center frequency of the communication signal amounts to 37.1875 GHz. Additionally, the upper and the lower intermodulation products and the gap with $G = B_2$ are visible.

The next step is now to determine the frequency of the local oscillator used for down-conversion of the RF signal. By comparing Figure 3.16 with Figure 3.18 and the description above, the following determination can be made.

$$\begin{aligned} f_{\mathrm{uu}} &= 42.5 \text{ GHz}, \\ f_2 &= 36.875 \text{ GHz}, \\ B_2 &= 625 \text{ MHz}. \end{aligned} \tag{3.34}$$

The frequency of the local oscillator can be calculated with Equation 3.32 as follows.

$$f_{\mathrm{LO}} = \frac{42.5 \text{ GHz} + 36.875 \text{ GHz} + 625 \text{ MHz}}{2} = 40 \text{ GHz} \tag{3.35}$$

By using this frequency as local oscillator for the receiving mixer, the IF depicted in Figure 3.19 results.

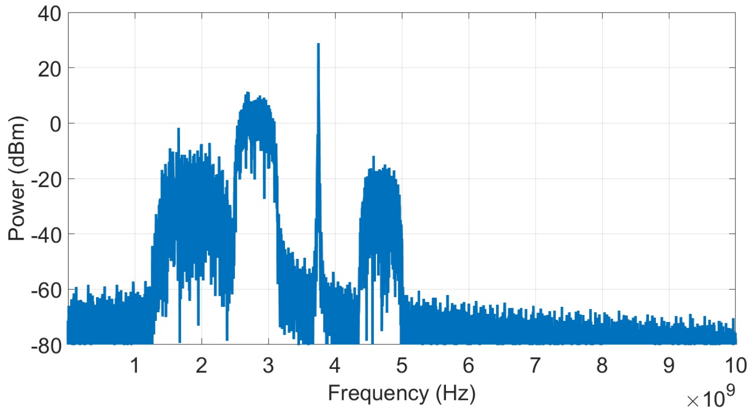


Figure 3.19: Spectrum of the IF output signal of the receiving mixer at the time of the last chirp frequency. The center frequency of the communication signal amounts now to 2.8125 GHz. Additionally, the upper and the lower intermodulation products are visible.

Visualized is the difference of the frequency of the local oscillator and the RF input signal. The last frequency of the radar chirp in the IF amounts to 3.75 GHz. The communication center frequency in the IF equates to 2.8125 GHz. Additionally, the intermodulation products become visible. The communication signal can be processed now with the following SDR without any limitations regarding the communication performance.

### 3.3.3 Analysis of the Measured Signals After the HPA and the Receiving Mixer

As mentioned in Section 3.3.1, the frequency of the resulting QPSK communication band in the IF can be reduced by increasing the gap and choosing a lower frequency of the local oscillator for the receiving mixer. This is described in this section by conducting a measurement [JSK23a]. Additionally, the performance of the QPSK communication is analyzed with and without FMCW radar operation [JSK23a]. The system parameters listed in Table 3.7 are used for the measurement.

Table 3.7: Parameters used for the measurement for the assessment of the signals before and after the receiving mixer.

| **Parameter** | **Value** |
|---|---|
| Start frequency of radar chirp | 34.0 GHz |
| Center frequency of radar chirp | 35.0 GHz |
| Bandwidth of radar chirp | 2.0 GHz |
| Start frequency of communication | 37.399850 GHz |
| Center frequency of communication | 37.4 GHz |
| Bandwidth of communication | 300 kHz |
| Power of radar chirp | 30 dBm |
| Power of communication | 10 dBm |
| Third-order intercept point | 40 dBm |

The minimal gap between the radar band and the communication band is now $G = 1.399850\ \mathrm{GHz}$ and therefore greater than 2 times the communication bandwidth. Therefore, Equation 3.33 can be used for determining the frequency of the local oscillator as follows.

$$\begin{aligned} f_{\mathrm{LO}} &\leq 37.399850\ \mathrm{GHz} + \frac{1.399850\ \mathrm{GHz}}{2} \quad \text{and} \\ f_{\mathrm{LO}} &\geq 37.399850\ \mathrm{GHz} + 300\ \mathrm{kHz} \quad \text{for} \\ 1.399850\ \mathrm{GHz} &\geq 2 \cdot 300\ \mathrm{kHz} \end{aligned} \tag{3.36}$$

The result of this can be described as follows.

$$\begin{aligned} f_{\mathrm{LO}} &\leq 38.099775\ \mathrm{GHz} \quad \text{and} \\ f_{\mathrm{LO}} &\geq 37.400150\ \mathrm{GHz} \quad \text{for} \\ 1.399850\ \mathrm{GHz} &\geq 600\ \mathrm{kHz} \end{aligned} \tag{3.37}$$

The frequency of the local oscillator is then determined to be 37.8 GHz. Therefore, the center frequency of the communication band lies in the IF at 400 MHz. Figure 3.20 shows the measurement setup for characterizing the signals before and after the receiving mixer and the QPSK communication performance with and without FMCW radar operation. The communication signal is generated by the SDR ADALM PLUTO and up-converted to a center frequency of 37.4 GHz. The MIRANDA35 front-end generates the chirp with a center frequency of 35 GHz and a bandwidth of 2 GHz. Both signals are power-combined and amplified by the HPA. After attenuating, the signal is mixed with the receiving mixer down to a 400 MHz center frequency of the communication band. The SDR ADALM PLUTO performs the ensuing processing of the communication signal.

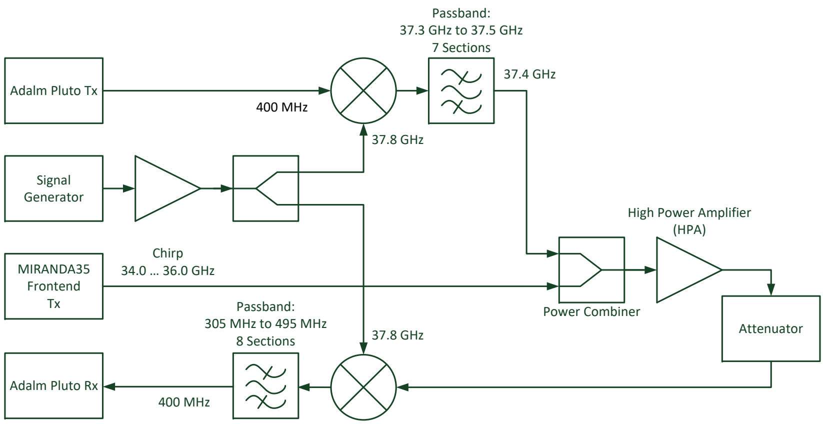


Figure 3.20: Block diagram of the measurement setup to characterize the signals before and after the receiving mixer and the communication performance with and without FMCW radar operation.

The output signal of the HPA is measured after the attenuator with a spectrum analyzer and is depicted in Figure 3.21. The chirp signal from 34 to 36 GHz with and without the communication signal at a frequency of 37.4 GHz is shown. Additionally, one of the two third-order intermodulation products from approximately 30.6 GHz to 34.6 GHz in the two-tone case is visualized. While the chirp starts at 34 GHz, the third-order intermodulation product starts at approximately 30.6 GHz. If the chirp stops at 36 GHz, then the third-order intermodulation product lies at about 34.6 GHz. Therefore, no overlapping of these two signals occurs. The minimal spurious free dynamic range (SFDR) of the chirp signal and the lower intermodulation product is 31 dB. The second third-order intermodulation product lies in the range between approximately 40.8 and 38.8 GHz and is not detectable, because the power of the communication signal is only about -21 dBm in comparison to the radar chirp signal with a power of approximately -2 dBm. Here, the SNR of the communication band amounts to approximately 32 dB.

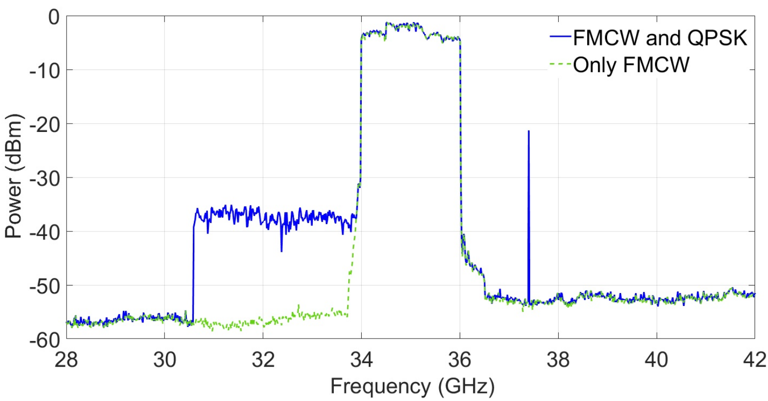


Figure 3.21: Output signal of the high power amplifier with and without the FMCW radar signal.

This signal is now mixed with a local oscillator with a frequency of 37.8 GHz down to the IF, where the difference of the local oscillator and the signal shown in Figure 3.21 is of special interest. The resulting IF is visualized in Figure 3.22. The narrow-band communication signal now lies at 400 MHz, the chirp signal ranges between 3.8 GHz and 1.8 GHz, and the third-order intermodulation products, as mentioned above, lie between approximately 7.2 GHz and 3.2 GHz as well as between approximately 3.0 GHz and 1.0 GHz. The communication signal at 400 MHz can be clearly separated in the frequency domain from the chirp signal and the third-order intermodulation products. The communication signal can be filtered out easily. All the mentioned frequency bands can also be found after comparison with Figure 3.17. The SNR of the communication signal without the chirp signal is 41.5 dB and with the chirp signal 37.5 dB. These values are both higher than the SNR in the RF as mentioned above. This is because of different measurement dynamics in high and low frequency bands of the spectrum analyzer. The filtered communication signal at 400 MHz will be converted to base-band and digitized with the SDR ADALM PLUTO. A subsequent digital signal processing decodes the transmitted data.

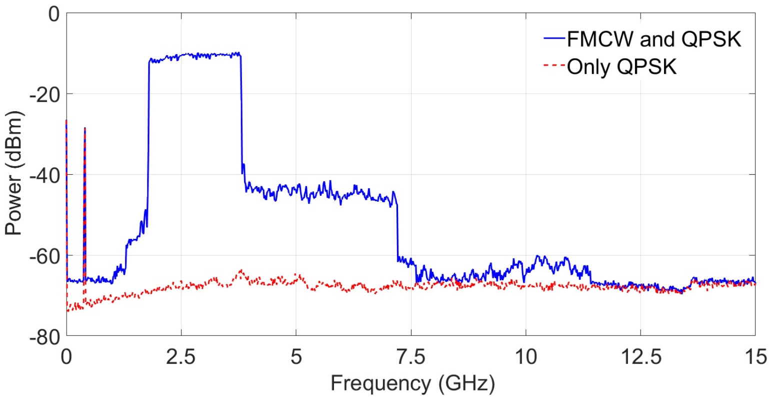


Figure 3.22: Output signal of the receiving mixer with and without the FMCW radar signal.

On the right hand side of Figure 3.23, the constellation diagram of the QPSK transmission without FMCW radar operation is visualized. The typical four constellation points can be clearly detected. In this case, the EVM is calculated to be 4%rms. The constellation diagram of the QPSK data transmission with FMCW radar is shown on the left. Here, the four constellation points can also be clearly detected. The EVM increases by 1%rms to 5%rms. The influence of the radar operation on the communication is therefore very low.

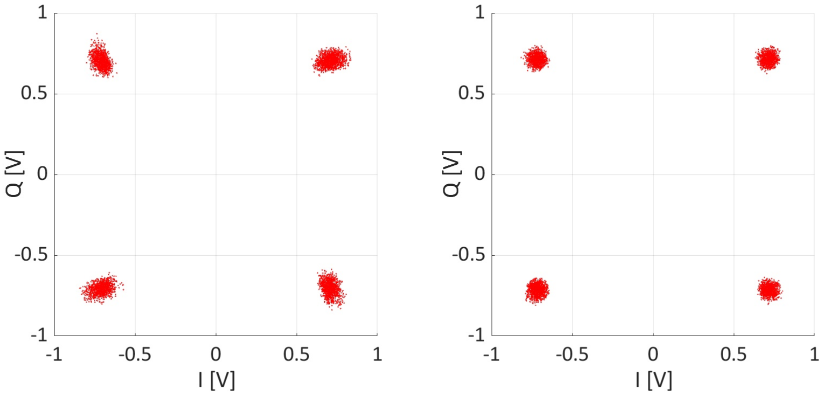


Figure 3.23: Constellation diagram of the QPSK data transmission with (left) and without (right) the FMCW radar signal.

## 3.4 Discussion and Conclusion

This chapter is about the relation of the radar band and the communication band working simultaneously in FDM by using only a single HPA in the transmitter for the amplification of both frequency bands. Therefore, the behavior of the occurring intermodulation products need to be considered. The first section describes these intermodulation products in theory. Section two goes into the details regarding the third-order intermodulation products for the relevant signals by using band selection filters in the receiver. It turned out that the gap between the radar band and the communication band must be equal or larger than the communication bandwidth to prevent any interaction between the intermodulation products and the radar band as well as the communication band.

An important point of the FDM signal to consider is the overall bandwidth of the system for the CSAR scenario with given parameters. The result is that the overall bandwidth is only 5% larger than the radar bandwidth. Including the

minimal gap and the communication bandwidth for a flight altitude of 1000 m, an image resolution of approximately 4 cm and a platform velocity of 10 m/s. Here, the raw data transmission of the FMCW radar to a ground station with simultaneous QPSK communication is assumed.
The effect of different gaps on the communication performance is presented in Sub-section 3.2.1. A theoretical minimal gap of 1.25 GHz is assumed. In simulation, a minimal gap of approximately 80% of the communication bandwidth can be reached, because the EVM of the communication increases from this point from 0.1% to 3.8%. The gap in the simulation is lower than the minimal gap in theory because of the usage of a pulse-shaping filter. The result of a measurement is presented with the focus on the communication performance, dependent on the gap between the radar and the communication band. Here, the theoretical minimal gap is 300 kHz, because the 3 dB-bandwidth of the communication band equals 300 kHz. The minimal measured gap amounts to approximately 63% of the communication bandwidth at an rmsEVM value of approximately 7%. Up to this point, no influence of the intermodulation product on the communication band is verifiable. Here, the measured gap is approximately 37% lower than the theoretical one, because the minimal measurable rmsEVM value is only 6.8% and a pulse-shaping filter is used.
The next Sub-section 3.2.2 describes the effect of different gaps on the FMCW radar performance by way of comparing range-Doppler maps. For this consideration, no band selection filters in the receiver are used. It turned out in this case that the minimal gap amounts to the maximal IF of the radar. The first step in this section is to consider the first approximation of the theoretical ratio of the power of the resulting spurious in the range-Doppler map from the power of the targets. For the parameter set used for the simulations, this ratio amounts to 57.8 dB by using a gap of 0 Hz. In the simulation a ratio of 60.5 dB can be reached. Regarding the parameter set used for the measurements, the theoretical ratio in the first approximation gives 65.7 dB by using a gap of 0 Hz. The measurement results show that the ratio between the power of the spurious chirp signal in the IF and the power of the signals corresponding to the targets are found to be approximately 63.3 dB.
The last section describes the determination of the local oscillator for the com-

munication part of the FDM signal. Here, no band selection filter is used in the receiver. Two possibilities are described mathematically: One by using a minimal gap between the mentioned frequency bands, and another by using larger gaps. The difference between the frequency of the local oscillator and the received FDM signal is the frequency of the resulting communication band in the IF. If the resulting frequency of the communication band gets too high, then the gap can be increased and the resulting communication band gets lower by using another local oscillator frequency. Simulations and measurements are presented to show the effect. Additionally, the communication performance is assessed with measurements with and without the FMCW radar by using a loop-back cable and an attenuator between the transmitter and the receiving mixer. It turns out that the EVM increases by only 1%rms after including the FMCW radar band into the spectrum of the transmit signal.

# 4 Optimization of the Communication Signal Parameters for Minimum Bandwidth Requirements

This chapter describes a new approach of reducing the overall bandwidth of the proposed FDM of broadband radar and communication by minimizing the gap between the two frequency bands. The idea behind this is to increase the ratio between the power of the communication signal and the closest intermodulation product. This can be maximized by increasing the third-order intercept point or by reducing the communication power. This is possible, because the propagation attenuation for the communication part depends on $R^2$ and for the radar part on $R^4$. Therefore, less transmit power is required for the communication than for the radar for the same operation range $R$ and for similar performances. Beyond that, the proposed new FDM technique of broadband FMCW radar and single-carrier QPSK communication allows the usage of different power levels of the two frequency bands. This deviates from the common usage of FDM in communications, where the same power for all channels is required. An additional effect of the non-linearities of the HPA by using digital modulation formats like QPSK in the regions of the carrier frequencies is presented first and, in a second step, minimized with power balancing of the radar and the communication signal. The result of these investigations is that a power back-off of both signals is required. The fundamentals of the power of the third-order intermodulation products will be presented mathematically. Therefore, the influence of the third-order intermodulation products on the communication signal can be reduced by increasing the third-order intercept point and by minimizing the communication power. Simulations of the resulting spectrum and regarding the EVM of the communication signal are shown. Measurements regarding the communication performance with a quantitative analysis of the data is presented. As mentioned earlier, the power of the communication part can be decreased in case of the same operation range. For this case, the behavior of the SNR of the radar and the communication in relation to the the flight altitude of the CSAR system is investigated in section 4. This chapter concludes with a discussion.

## 4.1 Investigation of Third-Order Non-Linearity Reduction

As investigated in Chapter 3, the influence of the third-order non-linearities can be a problem for the radar and the communication part of the system, depending on the gap between both frequency bands. This section describes the investigation of a third-order non-linearity effect close to the two simultaneous carrier frequencies in FDM. This effect can be reduced by power-balancing the two desired frequency bands.

### 4.1.1 Fundamentals of third-order non-linearities

To characterize the third-order intermodulation distortion, a signal with two different frequencies is considered as input signal for the following step. This can be described mathematically in the form of a single frequency and a QPSK communication signal comparable to Equation 2.16 as follows.

$$s_{\mathrm{in}} = A_1 \cdot \cos(2\pi \cdot f_1 \cdot t) + c(t_{\mathrm{C}}), \tag{4.1}$$

where both signal types show different behavior in the time and in the frequency domain. The following output signal of the third-order intermodulation distortion is based on Equation 3.2 and can be written like this.

$$s_{\mathrm{out}} = C_3 \cdot s_{\mathrm{in}}^3. \tag{4.2}$$

The parameter $C_3$ is a constant and can be calculated as follows [Mar25].

$$C_3 = \frac{4}{3 \cdot A_{\mathrm{IP3}}^2}, \tag{4.3}$$

where $A_{\mathrm{IP3}}$ is the third-order intercept point stated as a voltage. Section 4.2 gives more details for the necessary calculation of this parameter.
These two signals are simulated by using the parameters of Table 4.1.

Table 4.1: Parameters used for the simulation of the third-order intermodulation distortion.

| **Parameter** | **Value** |
|---|---|
| Single frequency | 32.5 GHz |
| Communication center frequency | 36.875 GHz |
| Bandwidth of communication | 1.25 GHz |
| Power of single frequency | 30 dBm |
| Power of communication | 30 dBm |
| Third-order intercept point | 40 dBm |

The following Figure 4.1 shows the input signal $s_{\mathrm{in}}$ without any intermodulation distortion. While the power of the single frequency is 30 dBm, the power of the QPSK communication signal is lower in the frequency domain due to the power is spread over the bandwidth of the signal.

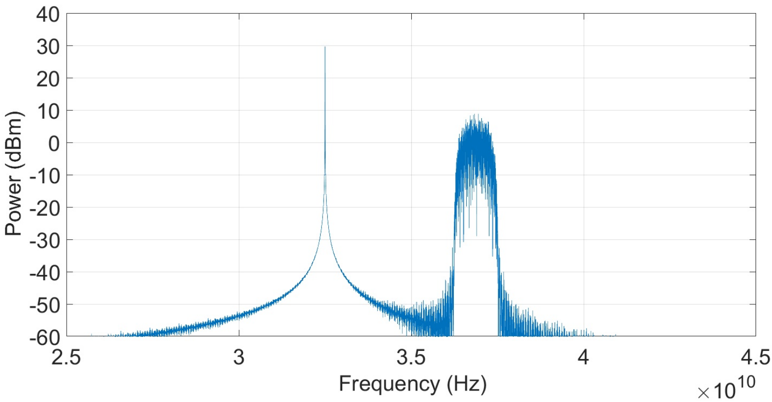


Figure 4.1: Single carrier frequency and the QPSK communication signal in FDM.

The bandwidth of the QPSK communication signal at the right hand side of Figure 4.1 amounts to 1.25 GHz with a center frequency of 36.875 GHz. The input signal $s_{\mathrm{in}}$ to the power of three multiplied with the constant $C_3$ gives the output signal $s_{\mathrm{out}}$. This is visualized in Figure 4.2.

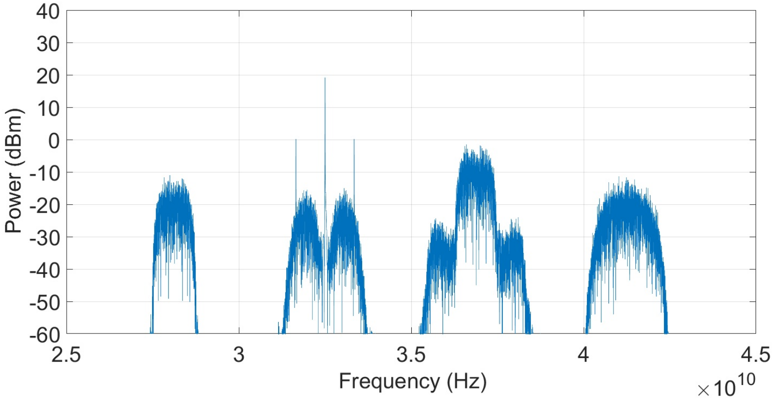


Figure 4.2: Single carrier frequency and the QPSK communication signal in FDM to the power of three.

The input signal (Figure 4.1) is still present in the spectrum at the output at 32.5 GHz and at a center frequency of 36.875 GHz. The power of these signals is approximately 10 dB lower than the power of the original signal. The upper and the lower intermodulation products, as mentioned previously, are detectable between approximately 27.5 GHz and 28.75 GHz as well as between approximately 40.0 GHz and 42.5 GHz. Additional spectral components occur at the left and at the right side of the desired signals. These distortions are close to the useful signals and influence the radar and the communication performance. This effect can be reduced by power balancing the input signals. The next sub-section describes the dependency of this effect from the power level of the communication signal to a signal with a fixed frequency without modulation. The last sub-section shows the dependency of the effect on the communication signal from the chirp signal of the radar.

### 4.1.2 Power-Balancing Regarding the FMCW Radar Signal

The aforementioned effect of distortions close to the carrier frequencies at the output of the HPA can be optimized by power-balancing of the input signals of the HPA. Therefore, this sub-section is about the power-balancing of the communication signal to reduce the distortions of the FMCW radar signal. It is necessary for the analysis of the mentioned effect that the frequency of the signal is static and not sweeping like the chirp of the FMCW signal. Hence, a signal with a fixed frequency is used instead of the chirp of the MIRANDA35 system. Figure 4.3 shows the block diagram used for optimizing the quality of the generator signal at the output of the HPA with a spectrum analyzer by power-balancing of the communication signal at the input of the HPA.

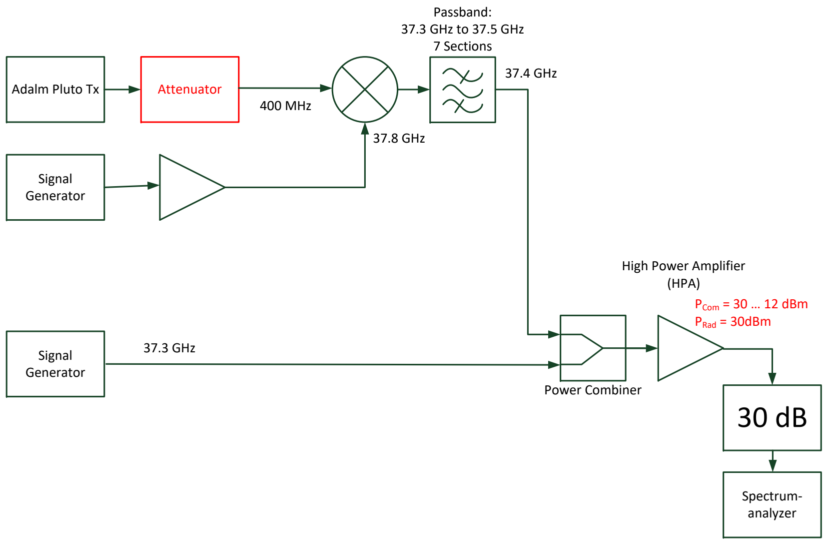


Figure 4.3: Block diagram for the power-balancing regarding a generator signal with fixed frequency. The HPA output power of the communication signal is reduced from 30 dBm to 12 dBm.

The block diagram shows that the communication signal is generated by the ADALM PLUTO SDR and is up-converted to a center frequency of 37.4 GHz. The signal generator provides a signal with a fixed frequency of 37.3 GHz. Both signals are power combined and amplified. The power level of the generator signal at the output of the HPA is approximately 30 dBm and that of the QPSK communication signal is varied between 30 dBm and 12 dBm. This power level can be adjusted by the attenuator at the output of the SDR. After attenuation of the output signal of the HPA, the signal is measured with a spectrum analyzer. Figure 4.4 shows the generator signal at the output of the HPA for four different constellations: 0 dB, 12 dB as well as 18 dB attenuation of the communication signal and without the QPSK communication signal.

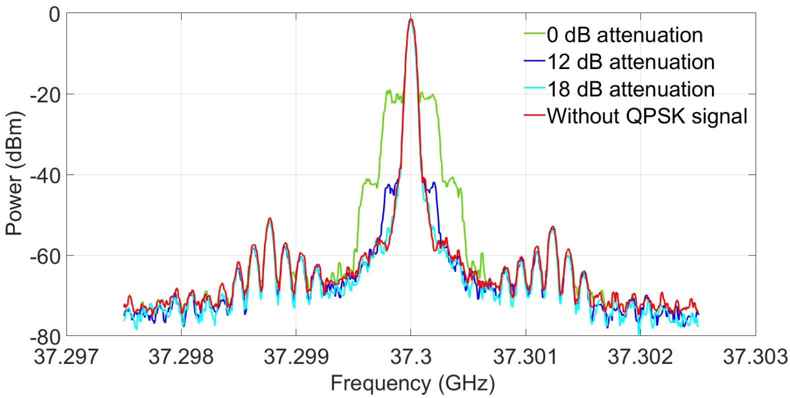


Figure 4.4: Generator signal in the frequency domain measured at the output of the HPA for three different attenuations of the communication signal and without the QPSK communication signal.

The red curve shows the generator signal without the QPSK signal as a reference. The mentioned effect because of the non-linearities of the HPA is clearly visible in the case of an attenuation of 0 dB (green curve). Here, the power levels of the generator signal and the QPSK signal are equal and 6 dB lower than the saturating output power of the HPA. This effect can be reduced by attenuating the communication signal. The best signal quality of the generator signal can be reached by using 18 dB attenuation (light blue curve). 12 db attenuation is also possible, because the undesired effect is reduced by approximately 23 dB in comparison to 0 dB attenuation and approximately 8 dB worse than the curve by using the optimal value of 18 dB attenuation.

### 4.1.3 Power-Balancing Regarding the QPSK Communication Signal

It is important for radar measurements that the corresponding output power is maximal. Therefore, this sub-section is about the maximizing of the radar output power by using the reduced communication output power of 12 dBm [JSK22]. Figure 4.5 shows the corresponding block diagram.

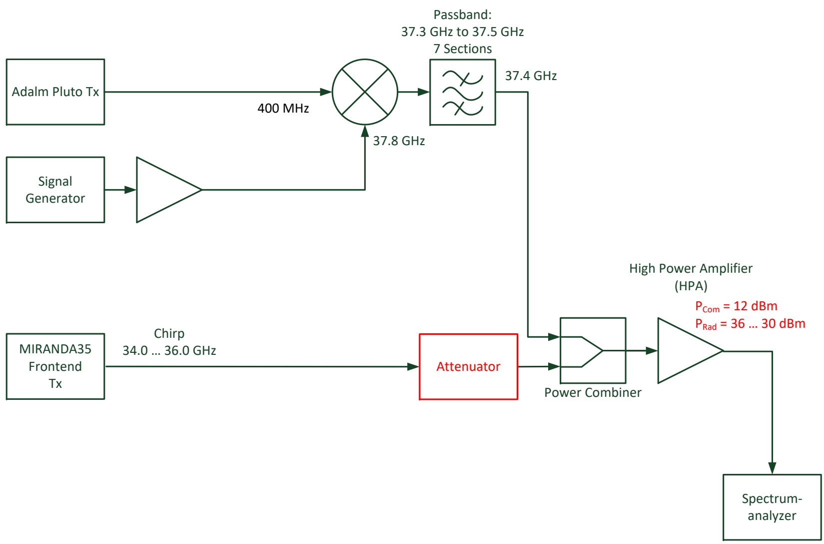


Figure 4.5: Block diagram for the power-balancing regarding the QPSK communication signal. The HPA output power of the FMCW radar signal is between 30 dBm and 36 dBm.

The communication signal is generated by the SDR ADALM PLUTO and is up-converted to 37.4 GHz. The MIRANDA35 front-end generates a chirp in the frequency range between 34 and 36 GHz. The power level of this radar chirp can be adjusted with an attenuator. The resulting signal after the power combiner is amplified with the HPA. A spectrum analyzer measures the communication signal at the output of the HPA. Figure 4.6 depicts this signal for two different attenuations of the chirp signal and without the chirp signal.

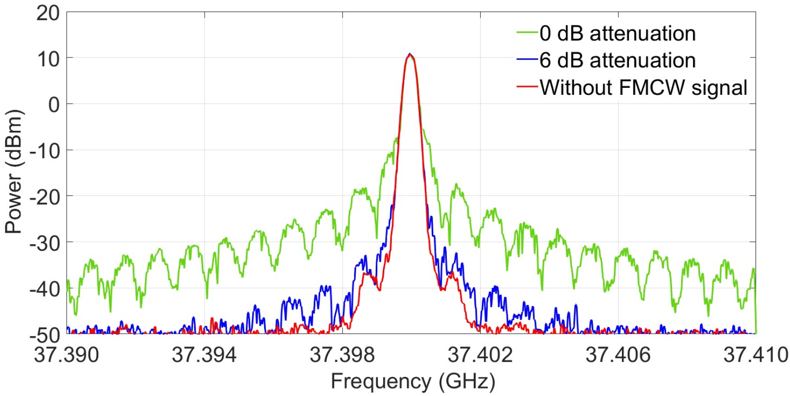


Figure 4.6: QPSK signal in the frequency domain measured at the output of the HPA for two different attenuations of the chirp signal and without the chirp signal.

The red curve shows the communication signal without the FMCW radar signal in FDM as a reference. The blue curve shows a similar constellation as in the previous sub-section: 12 dBm communication output power and 30 dBm radar output power. This is an optimal parameter set, because the influence of the radar chirp on the communication signal is as low as possible. The result of increasing the output power of the radar to 36 dBm (green curve with 0 dB attenuation) are distortions close to the QPSK communication signal.
Therefore, a power back-off of approximately 6 dB to the saturated output power of the HPA for the radar signal is necessary to get an optimal operation point.

The communication power must be reduced to a value lower than 18 dBm for an optimal operation. This is possible for the mentioned joint CSAR and communication application as described later in this chapter.

## 4.2 Fundamentals regarding the Power of the Third-Order Intermodulation Products

The only way to reduce the overall bandwidth of the mentioned two-tone FDM signal by using a single HPA is to minimize the gap $G$ and hence the influence of the upper intermodulation product to the communication signal as mentioned earlier. This can be done by reducing the power of the upper intermodulation product in comparison to the power of the communication signal. Thus, the first step is to consider the power of the two intermodulation products.
The two-tone input signal of an amplifier can be formulated with the following Equation 4.4.

$$s_{\text{in}} = A_1 \cdot \cos(2\pi \cdot f_1 \cdot t) + A_2 \cdot \cos(2\pi \cdot f_2 \cdot t). \tag{4.4}$$

The output signal of the amplifier depending on the input signal and the third-order intermodulation products can be written like Equation 4.5.

$$s_{\text{out}} = C_1 \cdot s_{\text{in}} + C_3 \cdot s_{\text{in}}^3. \tag{4.5}$$

The next step is to calculate the third power of the input signal to obtain information about the third-order distortion. The lower and the upper third-order intermodulation products ($\mathrm{IM_b}$ and $\mathrm{IM_u}$) can then be calculated with the following equations [Mar25].

$$\mathrm{IM_b} = \frac{3}{4} \cdot C_3 \cdot A_1^2 \cdot A_2 \cdot \cos(2\pi \cdot (2 \cdot f_1 - f_2) \cdot t), \tag{4.6}$$

$$\mathrm{IM_u} = \frac{3}{4} \cdot C_3 \cdot A_1 \cdot A_2^2 \cdot \cos(2\pi \cdot (2 \cdot f_2 - f_1) \cdot t). \tag{4.7}$$

The third-order intercept point is where the amplitude of the desired tone is equal to the amplitude of the intermodulation product. By considering the amplitude of $\mathrm{IM_u}$, the tone with the amplitude $A_1$ can be chosen. The result can be written as described in Equation 4.8.

$$\frac{3}{4} \cdot C_3 \cdot A_1 \cdot A_2^2 = C_1 \cdot A_1. \tag{4.8}$$

Here, $A_1$ cancels out, $A_2^2$ is equal to $A_{\mathrm{IP3}}^2$ and $C_1$ can be set to 1. This results in the following equation for $C_3$.

$$C_3 = \frac{4}{3 \cdot A_{\mathrm{IP3}}^2}. \tag{4.9}$$

Inserting this result in Equations 4.6 and 4.7, the amplitudes of the two intermodulation products for the lower and the upper case can be calculated by these two equations.

$$A_{\mathrm{b}} = \frac{A_1^2 \cdot A_2}{A_{\mathrm{IP3}}^2}, \tag{4.10}$$

$$A_{\mathrm{u}} = \frac{A_1 \cdot A_2^2}{A_{\mathrm{IP3}}^2}, \tag{4.11}$$

By squaring these two equations one obtains the power of the two intermodulation products as follows (The resistor $R$ cancels out).

$$P_{\mathrm{b}} = \frac{P_1^2 \cdot P_2}{P_{\mathrm{IP3}}^2}, \tag{4.12}$$

$$P_{\mathrm{u}} = \frac{P_1 \cdot P_2^2}{P_{\mathrm{IP3}}^2}. \tag{4.13}$$

Thus, the power of the intermodulation products depends on the power of the two tones $P_1$ as well as $P_2$ and the power of the third-order intercept point $P_{\mathrm{IP3}}$.

The power of the upper modulation product $P_{\mathrm{u}}$ can be efficiently reduced by increasing the power of the third-order intercept point and by reducing the power of the communication signal as marked with $P_2$. Therefore, the gap between the two frequency bands can be reduced as described later in this chapter. The reduction of the communication signals in comparison to the radar signal is possible for the mentioned CSAR application consisting of a broadband SAR sensor with simultaneous QPSK radar raw data transmission to a ground station. This is also described in this chapter.

## 4.3 Reducing the Influence of the Third-Order Intermodulation Products

This section is about the reduction of the third-order intermodulation products by increasing the third-order intercept point and decreasing the power of the communication signal. The third-order intercept point is hardware-dependent and the influence can only be investigated with simulations. The power of the communication signal can be reduced in the simulation and in a measurement.

### 4.3.1 Varying the Third-Order Intercept Point

This sub-section describes the influence of the third-order intercept point on the performance of the communication signal by using simulations. The simulation result of Figure 4.7 shows the dependency of the upper and lower intermodulation products from the third-order intercept point first. The parameters listed in Table 4.2 are used for the simulation.

Table 4.2: Parameters used for the simulation of the third-order intermodulation products dependent on the third-order intercept point.

| **Parameter** | **Value** |
|---|---|
| Radar center frequency | 34.375 GHz |
| Bandwidth of radar | 3.75 GHz |
| Communication center frequency | 37.1875 GHz |
| Bandwidth of communication | 0.625 GHz |
| Power of single frequency | 30 dBm |
| Power of communication | 30 dBm |
| Third-order intercept point | 35 dBm, 40 dBm, 45 dBm |

The simulation result is visualized in Figure 4.7. While the power of the radar signal (black) is 30 dBm for every chirp frequency, the power of the communication signal (red) is spread over a certain bandwidth and therefore lower than the declared power level. The power of the communication signal and the two intermodulation products are visualized as rms within the respective bandwidth in the frequency domain. As expected, the power of the upper and the lower intermodulation products decreases by 10 dB after increasing the third-order intercept point by 5 dB. Hence, the higher the third-order intercept point of an amplifier, the lower the intermodulation products.

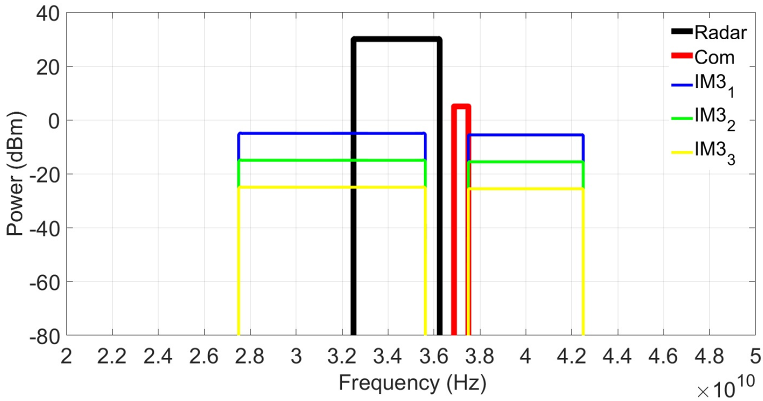


Figure 4.7: Power over frequency for three different power levels of TOI.The blue thin line corresponds to $P_{\mathrm{IP3}} = 35\ \mathrm{dBm}$, the green thin line to $P_{\mathrm{IP3}} = 40\ \mathrm{dBm}$ and the yellow one to $P_{\mathrm{IP3}} = 45\ \mathrm{dBm}$

To measure an influence of the intermodulation product on the communication performance in the simulation it is necessary to decrease the gap between the radar band and the communication band from the gap described in Equation 3.14. Therefore, a center frequency of 36.875 GHz and a bandwidth of 1.25 GHz of the communication signal is used. The minimal gap between both frequency bands is 0 Hz in this case. The third-order intercept point is varied from 30 dBm to 50 dBm by using 20 steps. With every TOI the EVM in percentage of the communication is measured. The result of this simulation is visualized in Figure 4.8. As expected, the EVM at 30 dBm has a high value of 40% and decreases quadratically by increasing the TOI linearly.

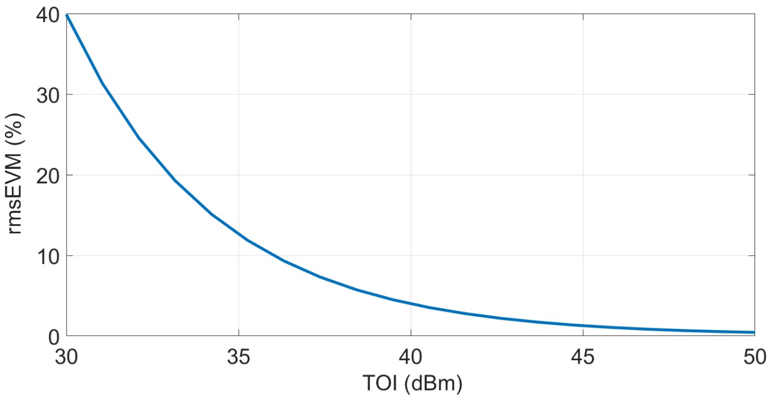


Figure 4.8: Simulated rmsEVM in percent over the power of the third-order intercept point

### 4.3.2 Varying the Power of the Communication Signal

This sub-section describes the dependency of the intermodulation products on the power of the communication signal with simulations and measurements. The objective is to reduce the overall bandwidth of the system by using a reduced gap and an optimal power of the communication signal with optimal communication performance.

The first simulation uses the parameters of Table 4.3. The results in the frequency domain are shown in Figure 4.9. While the TOI is determined to 40 dBm, the power of the communication signal is decreased from 30 dBm to 10 dBm in three equal steps. The power of the communication signal and the two intermodulation products are visualized as rms within the respective bandwidth in the frequency domain. As expected, the upper intermodulation product decreases rapidly by 20 dB after decreasing the communication power by 10 dB. The lower intermodulation product decreases only by 10 dB per step of the communication power.

Table 4.3: Parameters used for the simulation of the third-order intermodulation products dependent on the communication power.

| **Parameter** | **Value** |
|---|---|
| Radar center frequency | 34.375 GHz |
| Bandwidth of radar | 3.75 GHz |
| Communication center frequency | 37.1875 GHz |
| Bandwidth of communication | 0.625 GHz |
| Power of single frequency | 30 dBm |
| Power of communication | 30 dBm, 20 dBm, 10 dBm |
| Third-order intercept point | 40 dBm |

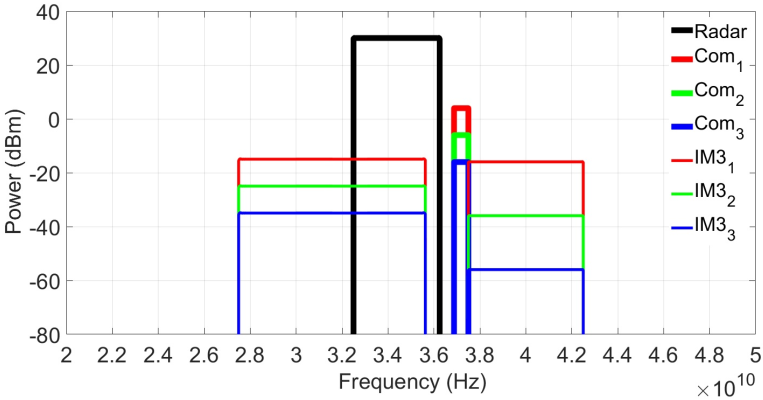


Figure 4.9: Power over frequency for three different power levels of the communication signal. The radar signal is visualized in black and the three communication signals in red (30 dBm), green (20 dBm) and blue (10 dBm). These signals are in thick lines. The corresponding intermodulation products are in thin lines.

To measure an influence of the intermodulation product on the communication performance in the simulation, dependent on the communication power, it is necessary to decrease the gap between the radar band and the communication band from the gap described in Equation 3.14. Therefore, a center frequency of 36.875 GHz and a bandwidth of 1.25 GHz of the communication signal is used. The minimal gap between both frequency bands is now 0 Hz. The power of the communication signal is increased from 0 dBm to 30 dBm by using 31 steps. With every step the EVM in percentage of the communication is measured. The result of this simulation is visualized in Figure 4.10.

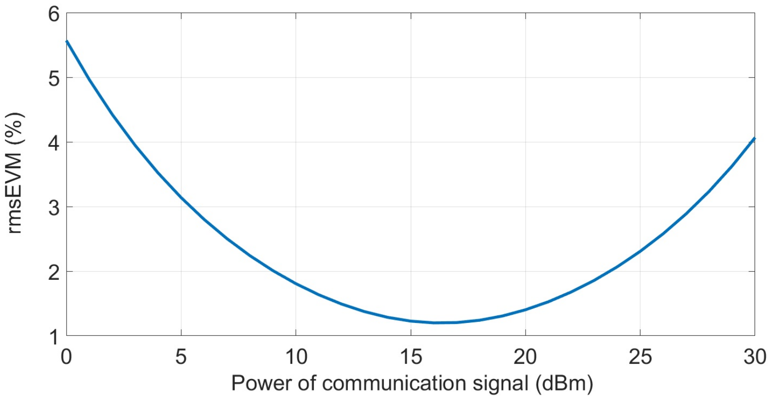


Figure 4.10: Simulated rmsEVM in percent over the power of the communication signal.

The EVM at 0 dBm communication power has a value of 5.5% and decreases to 1.2% by increasing the communication power to 17 dBm. At this section the EVM is influenced by the noise. After further increasing the communication power to 30 dBm the EVM increases to 4%. Here, the EVM is affected by the upper third-order intermodulation product. As a consequence of this, the best operating point for an amplifier with a third-order intercept point of 40 dBm, a radar power of 30 dBm and a gap of 0 GHz is by using a communication power of approximately 17 dBm.

This simulation result is now verified with a measurement. For this purpose, the measurement setup of Figure 4.11 is used.

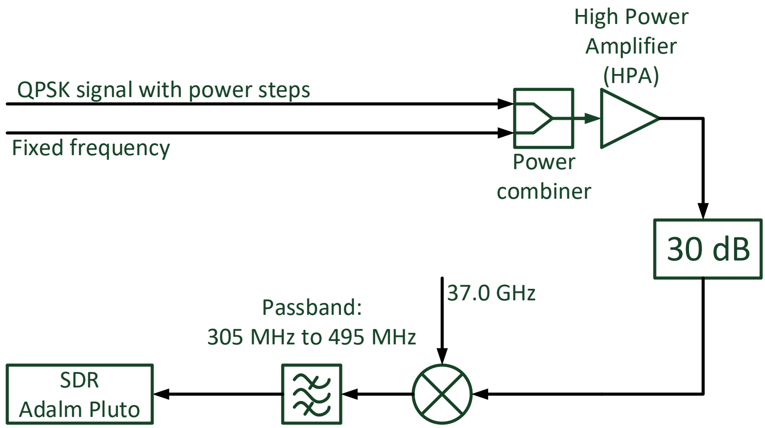


Figure 4.11: Block diagram of the setup for the measurement of the rmsEVM dependent on the power of the communication signal.

For the measurement of the rmsEVM in percentage of the communication signal dependent on its power in dBm, a generator signal with a fixed frequency of 37399.76 MHz and the QPSK signal using a center frequency of 37400 MHz and with different power values are used as input signals to the HPA. The minimal frequency gap between both signals amounts to approximately 30% of the communication bandwidth. Further non-linearities of the HPA described at the beginning of this chapter prevent narrower gaps at higher power levels of the communication signal. The output signal of the HPA is down-converted, filtered and processed by the SDR. The parameters used for the measurement are summarized in Table 4.4. The power of the fixed frequency is 30 dBm and the power of the communication signal is increased from 10 dBm to 30 dBm in 21 steps. With every step the EVM is measured. The result of these measurements are depicted in Figure 4.12.

Table 4.4: Parameters used for the measurement for the assessment of the communication performance dependent on different power levels.

| **Parameter** | **Value** |
|---|---|
| Fixed frequency | 37399.76 MHz |
| Center frequency of communication | 37400 MHz |
| Bandwidth of communication | 300 kHz |
| Third-order intercept point | 40 dBm |
| Power of fixed frequency | 30 dBm |
| Power of communication | 10 dBm to 30 dBm |
| Roll-off of pulse-shaping filter | 0.5 |

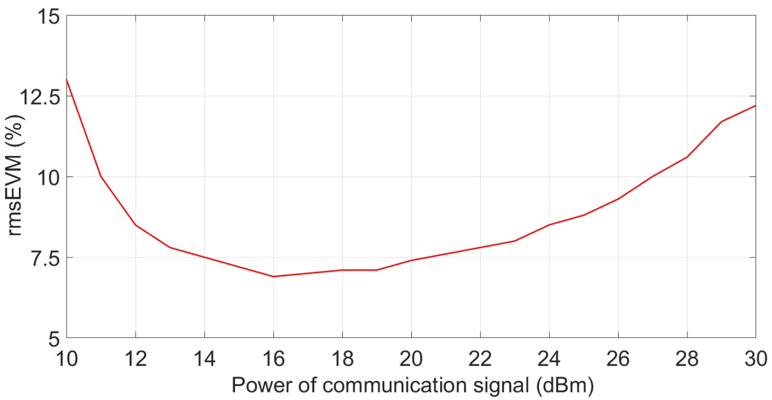


Figure 4.12: Measured rmsEVM in percent over the power of the communication signal.

By using a power level of 10 dBm of the communication signal, the influence of the system noise on the EVM becomes visible. This is very similar to the simulation, except the offset of approximately 7% because of additional noise and further non-linear effects of the analog signal processing and the SDR in the measurement setup. Increasing the power to 16 dBm leads to a decreased EVM value of minimal 7%. Here, again the offset between the simulation and the measurement of approximately 6% is detectable. With further increasing the power of the communication signal, the influence of the upper intermodulation product rises. As a consequence, the EVM value increases to 12% by using a power level of 30 dBm. This is approximately 8% worse than the simulation because of the mentioned reasons. Except for the offset of the gap of 30% of the communication bandwidth and of the EVM of approximately 7%, the simulation and the measurement show good agreement.

## 4.4 Signal-to-Noise Ratio of FMCW Radar and QPSK Communciation in FDM for an assumed CSAR scenario

As described in the previous chapters, the output power of the communication part can be reduced compared to the radar part for the mentioned airborne CSAR application. This is due to the fact that the attenuation of the wave propagation depends on the range to the power of four for the radar part and to the power of two for the communication part. Therefore, it makes sense to investigate the SNR of the radar and the communication link to find an optimal value for the flight altitude of the airborne joint communication and CSAR system.

The following study is based on the results of Sub-section 3.1.3 and is further developed for the calculation of the SNR. Regarding the radar it is based on the radar equation [Wol25] and the thermal noise. Thus, the SNR for the radar can be calculated in the following way.

$$\mathrm{SNR}_{\mathrm{Rad}}(H) = \frac{P_{\mathrm{Rad}} \cdot G_{\mathrm{Tx}} \cdot G_{\mathrm{RadRx}} \cdot c_0^2 \cdot \mathrm{RCS} \cdot I_{\mathrm{SAR}}(H)}{f_{\mathrm{Rad}}^2 \cdot R_{\mathrm{max}}^4(H) \cdot (4\pi)^3 \cdot k \cdot T \cdot \mathrm{IF}_{\mathrm{Rmax}}(H) \cdot \mathrm{NF}}, \tag{4.14}$$

here $P_{\mathrm{Rad}}$ is the transmit power of the radar, $G_{\mathrm{Tx}}$ the gain of the transmit antenna, $G_{\mathrm{RadRx}}$ the gain of the receive antenna, $c_0$ is the speed of light, $\mathrm{RCS}$

is an assumed minimal radar cross-section, $I_{\mathrm{SAR}}(H)$ the integration gain, $f_{\mathrm{Rad}}$ is the carrier frequency of the radar, $R_{\max}(H)$ the maximal range calculated by 3.15 dependent on the flight altitude $H$, $k$ is the Boltzmann constant, $T$ is the operating temperature, $\mathrm{IF}_{\mathrm{Rmax}}(H)$ the maximal IF to be digitized, calculated by Equation 3.18, dependent on the flight altitude $H$ and the noise figure $\mathrm{NF}$. This formula is based on the radar equation to calculate the receive power of the radar and the formula for the calculation of the power of the thermal noise. The integration gain $I_{\mathrm{SAR}}(H)$, dependent on the flight altitude $H$ is derived based on Figure 3.3 now. Therefor, the flight time for one circle $T_{Circle}(H)$ can be formulated as follows.

$$T_{Circle}(H) = \frac{2 \cdot \frac{H}{\tan(\theta)} \cdot \pi}{v}, \tag{4.15}$$

where $H$ is the flight altitude, $\theta$ is the depression angle and $v$ the speed of the radar respectively the airborne platform relative to the ground. The dwell time $T_{\gamma}(H)$ for the integration angle $\gamma$ can be written like this:

$$T_{\gamma}(H) = \frac{T_{Circle}(H) \cdot \gamma}{360°} = T_{Rep} \cdot I_{\mathrm{SAR}}(H). \tag{4.16}$$

Here, $T_{Rep}$ is the chirp repetition interval. Inserting Equation 4.15 in 4.16 and rearranging give the integration gain as follows.

$$I_{\mathrm{SAR}}(H) = \frac{2 \cdot \frac{H}{\tan(\theta)} \cdot \pi \cdot \gamma \cdot f_{\mathrm{Rep}}}{360° \cdot v}, \tag{4.17}$$

where $f_{\mathrm{Rep}}$ is the chirp repetition frequency calculated with Equation 3.17.

Very similar to the SNR of the radar, it is possible to calculate the SNR of the communication link as follows.

$$\mathrm{SNR}_{\mathrm{Com}}(H) = \frac{P_{\mathrm{Com}} \cdot G_{\mathrm{Tx}} \cdot G_{\mathrm{ComRx}} \cdot c_0^2}{f_{\mathrm{Com}}^2 \cdot R_{\mathrm{Com}}^2(H) \cdot (4\pi)^2 \cdot k \cdot T \cdot B_{\mathrm{C}}(H) \cdot \mathrm{NF}}, \tag{4.18}$$

here $P_{\mathrm{Com}}$ is the transmit power of the communication link, $G_{\mathrm{Tx}}$ the gain of the transmit antenna, $G_{\mathrm{ComRx}}$ the gain of the receive antenna, $c_0$ is the speed of light, $f_{\mathrm{Com}}$ is the carrier frequency of the radar, $R_{\mathrm{Com}}(H)$ the range of the communication link dependent on the flight altitude $H$, $k$ is the Boltzmann constant, $T$ is the operating temperature, $B_{\mathrm{C}}(H)$ the bandwidth of the communication link calculated by 3.23 dependent on the flight altitude $H$ and the noise figure $\mathrm{NF}$. The range $R_{\mathrm{Com}}(H)$ can be calculated like this.

$$R_{\mathrm{Com}}(H) = \frac{H}{\sin(\theta)}. \tag{4.19}$$

With all the mentioned equations regarding the CSAR application, it is possible to simulate the SNR of the radar and the communication link. The parameters listed in Table 4.5 are used for the simulation. While the power of the radar part is fixed at a maximum value of 30 dBm, the power of the communication part can be reduced in the simulation from a maximum value of 30 dBm to a minimum value of 13.4 dBm. This is important for the mentioned investigations regarding the intermodulation products of the HPA. The flight altitude is varied in the simulation from 10 m to 1000 m.

The simulation results are visualized in Figure 4.13. Here, a threshold of 12 dB is marked as a blue line. This corresponds to a BER for the QPSK communication of approximately $10^{-4}$ as described in [SRI06] and a detection probability of 0.82 as well as a probability of false alarms of $10^{-4}$ for the radar as mentioned in [M I80]. The SNR of the radar (red curve) lies above this threshold for flight altitudes up to approximately 520 m. The minimal power for the communication part is 13.4 dBm. Here, communication with an SNR of 12 dB and more is possible for flight altitudes of up to approximately 520 m (purple curve). If the power of the communication part is increased to 30 dBm, then communication is possible with higher SNR as shown in 4.13 (yellow curve). As expected, the SNR of the radar decreases much faster than the SNR of the communication because of range to the power of four for the radar part and to the power of two for the communication part. The green curve of this figure is the SNR limit regarding the Shannon-Hartly theorem dependent on the flight altitude which is defined as follows [Lil25].

$$\mathrm{SNR}_{\mathrm{Shannon}}(H) = 10 \cdot log10(2^{\frac{C(H)}{B}} - 1). \tag{4.20}$$

Here, $C(H)$ is the maximal data rate corresponding to the actual flight altitude and $B$ is the maximal possible bandwidth of 625 MHz reserved for the communication part dependent on the maximal bandwidth of the system of 5 GHz. As shown in the Figure 4.13, the SNR of the communication part lies above the Shannon-Hartly limit for flight altitudes of up to 1000 m. Thus, communication is theoretically possible with the resulting data rates.

For the parameters given in Table 4.5 the minimal power of the communication part is 13.4 dBm by using a radar power of 30 dBm. For this constellation, the maximal flight altitude is approximately 520 m, because the minimal SNR of the communication and that of the radar is 12 dB.

Table 4.5: Parameters used for the simulation of the SNR of the radar and the communication link.

| **Parameter** | **Value** |
|---|---|
| Transmit power of radar | 30 dBm |
| Max. Transmit power of radar of communication | 30 dBm |
| Min. Transmit power of radar of communication | 13.4 dBm |
| Bandwidth of radar | 3.75 GHz |
| Max. bandwidth of system | 5 GHz |
| Noise figure | 3 dB |
| Beamwidth elevation | 12° |
| Beamwidth azimuth | 12° |
| Depression angle | 35° |
| Gain of transmit antenna | 24 dB |
| Gain of receive antenna radar | 24 dB |
| Gain of receive antenna communication | 4 dB |
| Assumed radar cross-section | -10 dBm² |
| Speed of radar | 10 m/s |
| Assumed integration angle | 15° |

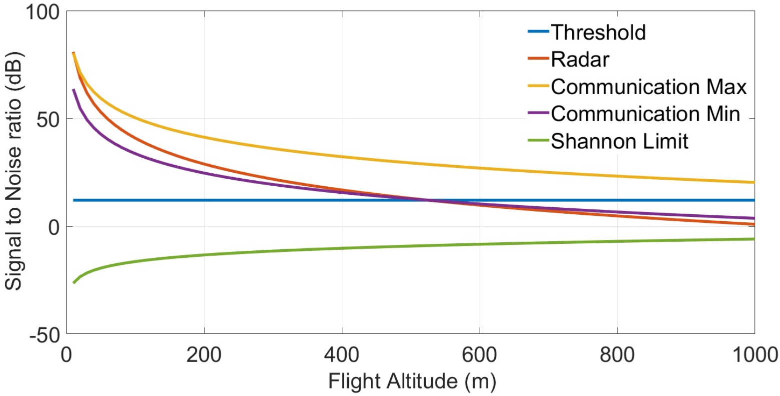


Figure 4.13: SNR of the radar part (red) and the communication part with two different power levels (purple and yellow) dependent on the flight altitude.

## 4.5 Discussion and Conclusion

This chapter is about the minimizing the overall bandwidth of the FDM signal consisting of the radar band and of the communication band by choosing an adapted communication power and a maximized radar power. Therefore, the intermodulation products generated by the HPA can be suppressed and an optimized overall bandwidth is feasible.

Section 4.1 describes the influence of third-order non-linearities on the radar and on the communication signal. These effects can be reduced by the power-balancing of the signals. The first investigation uses a generator signal instead of the radar chirp with a power of 30 dBm. This signal is affected by the communication signal if its power is larger than approximately 18 dBm. By using only 12 dBm, no influence is detectable. In the second part of the investigation, the radar chirp has a negative influence on the communication signal if the output power of the radar is close to the saturated output power of the HPA of approximately 36 dBm. By using a power back-off of approximately 6 dB to the saturated output power of the HPA the effect can be reduced below the detectable threshold. For this operating point, the radar power is 30 dBm. The context regarding the mentioned power back-off is presented in more detail in the following chapter.

Section 4.2 presents a mathematical deduction of the power of the third-order intermodulation products.

Section 4.3 is about the power dependencies of the third-order intermodulation products from the power of the radar and the communication signal. These power values of the intermodulation products should be as low as possible to get optimal radar and communication performance by using minimized gaps between both frequency bands. The first Sub-section 4.3.1 describes the dependency of third-order intercept point on the intermodulation products. The result is that this point should be as high as possible. Increasing the TOI by 5 dB reduces the intermodulation products by 10 dB as described in Equations 4.12 and 4.13 by using constant values for the two desired tones. The influence of the TOI on the EVM of the communication signal is presented subsequently by using a simulation. The EVM decreases quadratically while increasing the TOI linearly. As a consequence, the higher the TOI, the better the communication performance in the mentioned FDM system. The second Sub-section 4.3.2 is about the varying the power of the communication signal to minimize the power of the intermodulation products. Simulations show that the upper intermodulation product decreases by 20 dB rapidly after decreasing the communication power by 10 dB. The EVM of the QPSK communication is simulated dependent on different communication power levels. By using a gap between the radar band and the communication band of 0 Hz, in combination with a radar power of 30 dBm and a TOI of 40 dBm, the minimum of the EVM value is achieved at a power level of the communication part of 17 dBm. This simulation result is verified with measurements. The optimal communication power is found to be approximately 16 dBm by using a power of the generator signal instead of the chirp of 30 dBm and a TOI of the HPA of approximately 40 dBm. The gap between both frequency bands can be reduced in the measurement by 70%, minimizing the overall bandwidth.

The last Section 4.4 presents the SNR of the mentioned CSAR part and the QPSK communication part. Simulation results show that the maximal flight altitude of the system is approximately 520 m based on system parameters including a radar power of 30 dBm and a communication power as low as 13.4 dBm. Here, the same minimal SNR of 12 dB for both frequency bands is assumed.
This chapter shows that the gap between the radar band and the communication band and therefore the overall bandwidth can be reduced by using an adapted communication power.

# 5 Analysis of the Power Efficiency of Joint Broadband Radar and Single-Carrier Communication in FDM

The analysis of communication and also radar signals in the time domain gives an indication of the power efficiency of the system. Therefore, this chapter for the first time shows the optimal power efficiency of the joint broadband radar and single-carrier communication signal in FDM in comparison with OFDM. To this end, the PAPR and also the complementary cumulative distribution function (CCDF) is formulated. Here, the behavior of OFDM regarding the power efficiency in the form of CCDF curves for a different amount of carrier frequencies and also for two non-distortion PAPR reduction methods is shown. The more carrier frequencies are used, the worse the PAPR and the power efficiency is. High effort is necessary for reducing the PAPR values. Subsequently, the comparison of the two different modulation formats 16-QAM and QPSK regarding the PAPR in the form of CCDF curves is shown. QPSK is more favorable regarding the PAPR and the power efficiency than 16-QAM, because the 16-QAM signal uses additional amplitude modulation. Joint FMCW radar and single carrier QPSK communication in FDM has an optimal PAPR behavior, which is shown in the form of a simulated CCDF curve. Here, a maximal PAPR value of 6 dB is measured. Additionally, the joint FMCW radar and QPSK communication signal is analyzed in the time domain by measuring it with an oscilloscope. The result is that the HPA affects the signal in the region of high chirp frequencies insignificantly. Finally, the CCDF curves of the signal before and after the HPA is measured. The result of this is that the maximal PAPR before the HPA is 7 dB and after the HPA 6.3 dB. These values are approximately the same as calculated and simulated and depend on the frequency response of the used analog signal chain. The conclusion of this chapter is that the new joint broadband FMCW radar and single-carrier QPSK communication waveform has an optimal PAPR behavior without any additional effort compared to OFDM.

## 5.1 Introduction to the Complementary Cumulative Distribution Function

A common way to investigate the signals processed by the digital and analogous signal chain regarding the power efficiency is the use of the complementary cumulative distribution function (CCDF), which indicates the probability that the instantaneous power of a signal is higher than the average power. The CCDF curve of a signal with an optimal power efficiency is placed at a low PAPR and also at low probabilities.

The PAPR itself is defined as the ratio of the maximum power to the average power as shown in [AJ16].

$$\mathrm{PAPR} = \frac{\max|x(n)|^2}{\mathrm{E}[|x(n)|^2]}, \tag{5.1}$$

where $|x(n)|$ is the magnitude of $x(n)$ and $\mathrm{E}[]$ the expectation operator. The maximal PAPR in dB dependent on the amount of simultaneous carrier frequencies $N$ is defined as follows [Mul20].

$$\mathrm{PAPR}_{\mathrm{max,dB}} = 10 \cdot log_{10}(2N). \tag{5.2}$$

If the information bits to transmit are scrambled the PAPR of the multi-carrier signal is close to $2 \cdot \ln(N)$ as described in [Bra14]. The higher the PAPR, the higher the requirements on the analog signal chain and the lower the power efficiency.

The probability that the current PAPR of a signal is larger than a given threshold defines the CCDF as follows [RS17]:

$$\mathrm{CCDF}(\mathrm{PAPR}(x(n))) = \mathrm{Prob}(\mathrm{PAPR}(x(n)) > \mathrm{PAPR}_0), \tag{5.3}$$

where $\mathrm{PAPR}_0$ is a PAPR threshold. The CCDF curves can be used to measure how much of the time the signal is equal or larger than a specific level. This is helpful to analyze the distortion of a signal because of the analog signal chain or for the correct power balancing of the signal for the analog signal processing.

### 5.1.1 Behavior of OFDM Regarding the Power Efficiency

As mentioned in the previous chapters, this thesis is about a broadband FMCW radar and a single-carrier QPSK communication for radar raw data transmission in FDM. Here, only two different frequency bands are used and are separated in the frequency domain. A more general case of FDM with for example 8 channels and equal bandwidth is visualized in Figure 5.1. This is usually used in communications for simultaneous data transmission of different users.

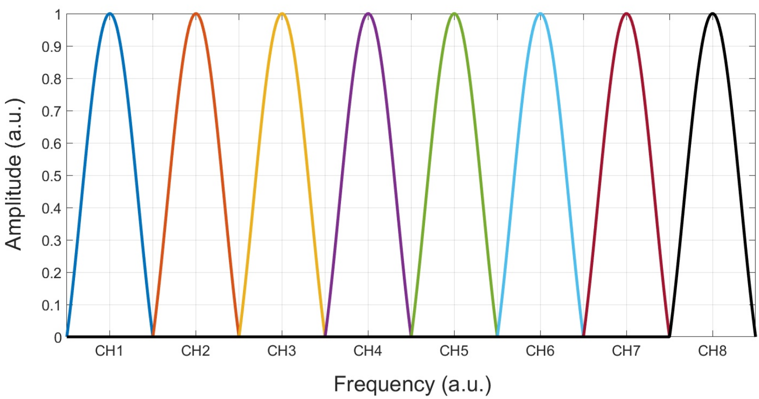


Figure 5.1: Frequency division multiplexing (FDM) of 8 channels.

Multiple channels are separated by using different center frequencies, and each channel can be filtered out, because the signals are not overlapping in the frequency domain. One of the main disadvantages of this approach is the non-optimal overall bandwidth utilization in the case of communication-only applications.

Modern communication systems use the OFDM principle. Here, multiple sub-carriers overlap, because the signals are orthogonal. This saves overall bandwidth compared to FDM for the same number of users in case of communications. A general case of OFDM with for example 8 channels and equal bandwidth is shown in the Figure 5.2.

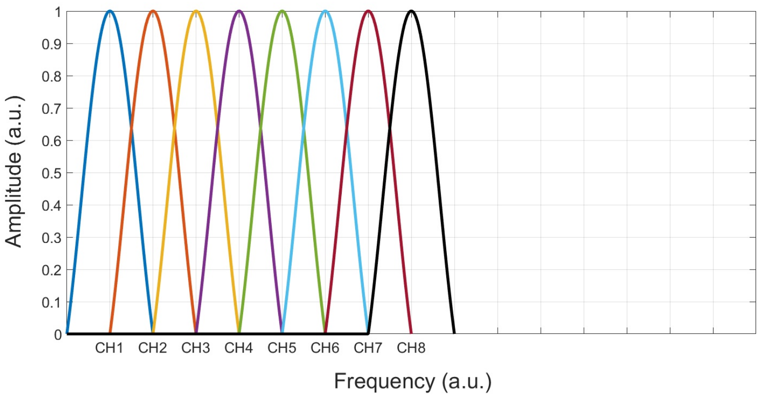


Figure 5.2: Orthogonal frequency division multiplexing (OFDM) of 8 channels.

Each channel can be separated, because the sub-carriers are orthogonal. It is possible to realize radar measurements with OFDM. In this process, the radar frequencies are used simultaneously and not one after another as in the case of a chirp used in an FMCW radar. Thus, OFDM uses very high numbers of simultaneous carrier frequencies and not only two as in the approach described in this thesis. Therefore, the PAPR of OFDM in comparison to the two-tone approach of this thesis (refer to Equation 5.2) with only about 6 dB is significantly higher, and the requirements on the analog signal chain are enormous. It is necessary in OFDM systems that the whole bandwidth of the signal must be digitized. This puts very high demands on the analog-to-digital converter and on the digital signal processing unit in case of broadband applications. Both disadvantages lead to poor power efficiency.

The sub-carriers of the OFDM signal are all orthogonal. This increases the requirements of the analog signal chain regarding linearity.
The behavior of an OFDM signal regarding the PAPR and therefore the power efficiency dependent on the amount of carrier frequencies is visualized in the following Figure 5.3. This figure is modified from [BP20].

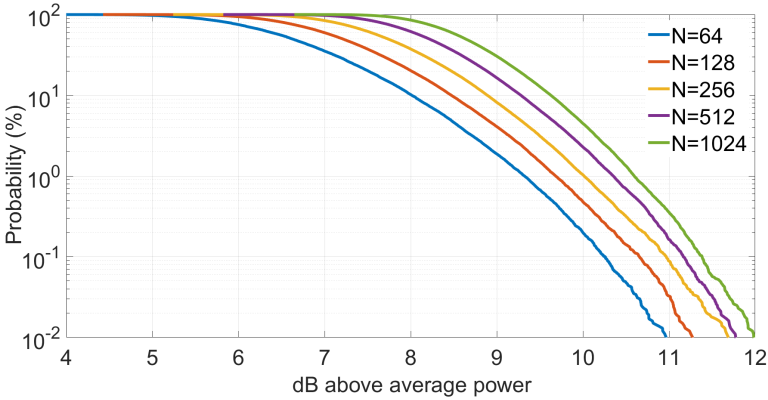


Figure 5.3: CCDF curves for a different amount of carrier frequencies N of an OFDM system. Modified from [BP20].

The optimal case regarding the power efficiency of the CCDF curve is at low probabilities (y-axis) and low PAPR values (x-axis). As expected, the higher the amount of carrier frequencies of the OFDM signal, the higher the probabilities and the higher the PAPR values. The more the curve is located at the top/right corner, the lower the power efficiency and the higher the requirements regarding the analog signal chain. The CCDF curve of the approach described in this thesis is presented later on in this chapter.
The PAPR values of the OFDM signal can be reduced with digital processing techniques. Figure 5.4 presents two non-distortion, but complex PAPR reduction techniques compared with the original OFDM signal with 1024 carrier frequencies. This figure is modified from [RS17].

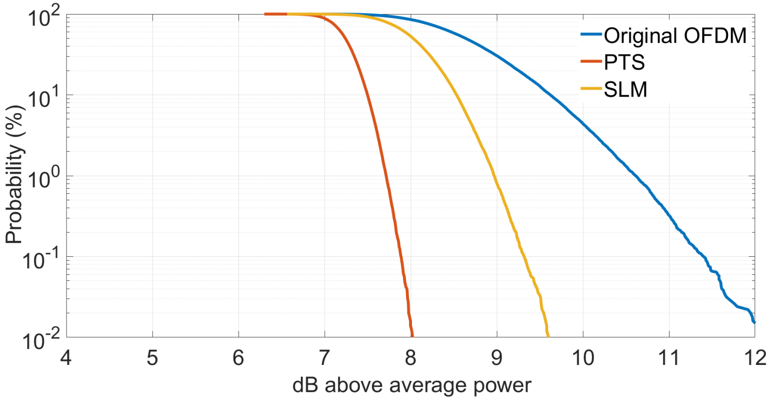


Figure 5.4: CCDF comparison of two different, non-distortion PAPR reduction techniques for an OFDM system with 1024 carriers. Modified from [RS17].

The blue curve of this figure shows the PAPR progression for the original OFDM signal. Here, a power back-off regarding the analogous signal chain of 11.5 dB and more is necessary. After reducing the PAPR with selected mapping (SLM) shown in yellow and partial transmit sequence (PTS) visualized in red the power back-off can be reduced by approximately 2 dB for SLM and approximately 3 dB for PTS. This increases the power efficiency of the OFDM system. These approaches for reducing the PAPR of an OFDM system can be very complex and require more or less processing power. However, FDM with two carrier frequencies as mentioned here has theoretically a PAPR of 6 dB without any PAPR reduction procedures as depicted in Figure 5.6. This is lower than the PAPR of OFDM systems with PAPR reduction techniques as shown in Figure 5.4. Therefore, the approach investigated in this thesis is more power-efficient than OFDM.

### 5.1.2 Comparison of 16-QAM and QPSK Regarding the Power Efficiency

One of the main objectives of this thesis is the joint use of broadband radar and single-carrier communication with high power efficiency to increase the operating time of the system. Therefore, it is necessary to chose a modulation format of the communication part with an optimal power efficiency. The most popular modulation formats nowadays are QPSK and QAM as mentioned in Chapter 2. Thus, the CCDF of both modulation formats are considered and depicted in the following Figure 5.5 with similar parameters and after the influence of an AWGN-channel. In this way, the necessary power back-off for the analog signal chain of the two modulation formats can be obtained.

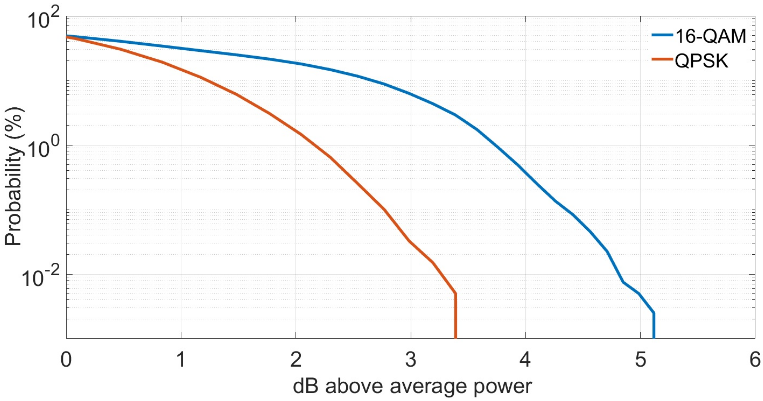


Figure 5.5: CCDF curves for the two different modulation formats QPSK and 16-QAM after the influence of an AWGN-channel.

The red curve shows the result for the QPSK modulation. The maximal PAPR is approximately 3.4 dB. The PAPR of the 16-QAM modulation format is maximal approximately 5.2 dB. This is 1.8 dB higher than the QPSK modulation because the amplitude of the signal is modulated. Regarding of a low PAPR of the whole system it makes sense to choose QPSK. Therefore, this thesis uses FMCW radar and QPSK communication in FDM mode.

## 5.2 CCDF of FMCW Radar and QPSK Communication in FDM

Similar to the analysis of OFDM and the modulation formats QPSK and QAM regarding CCDF and power efficiency, the waveform proposed in this thesis is considered. This is done with a simulation first, followed by measurements of the FDM signal before and after a HPA [JSK23b].

### 5.2.1 Simulative Validation

The joint broadband FMCW radar and single-carrier QPSK signal in FDM is simulated and the resulting CCDF curve is depicted in the following Figure 5.6.

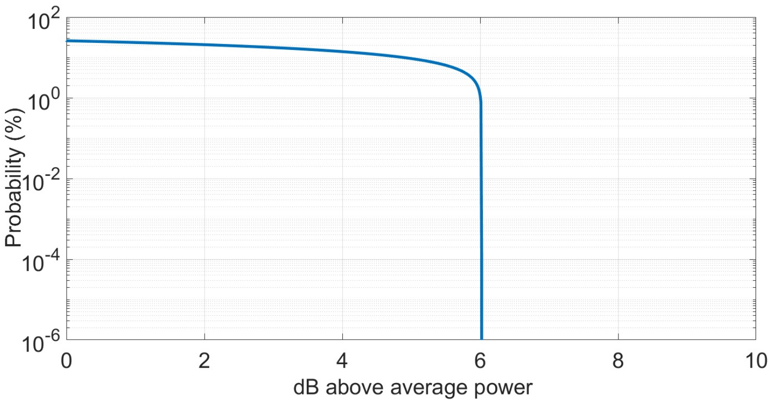


Figure 5.6: Simulated CCDF curve of the joint FMCW radar and QPSK communication signal in FDM.

The simulation uses a chirp with a center frequency of 35 GHz and a bandwidth of 2 GHz and a QPSK communication at 37.4 GHz with a bandwidth of 300 kHz in FDM simultaneously without noise. The maximal PAPR of this waveform approaches approximately 6 dB, because each of both signals has a PAPR of 3 dB. At worst, a PAPR of maximal 6 dB of the mentioned two-tone signal results.

### 5.2.2 Behavior of an Amplifier Regarding the CCDF

The result of the simulation shown in Figure 5.6 will be validated with measurements of the mentioned FDM waveform. Additionally, the influence on the waveform proposed in this thesis caused by a HPA will be shown with time domain analysis. For this analysis, the measurement setup of Figure 5.7 is used.

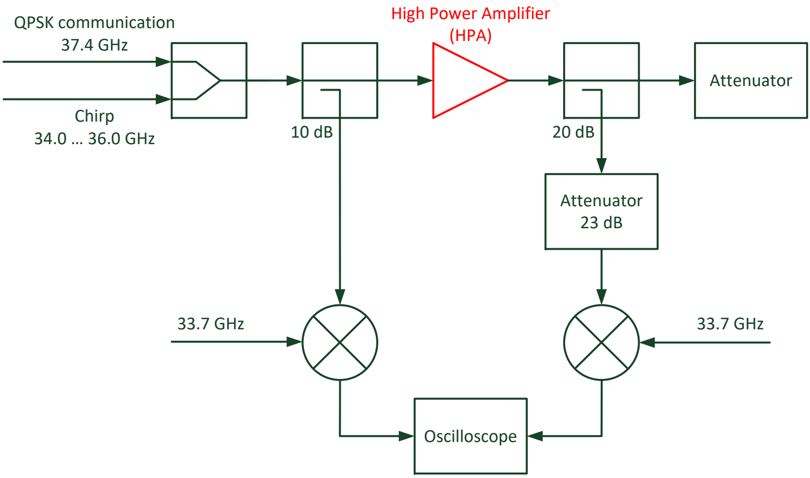


Figure 5.7: Measurement setup for measuring the FDM signal before and after the HPA in the time domain with an oscilloscope.

A power combiner at the top left of this figure combines the chirp of the FMCW radar and the QPSK communication signal to enable simultaneous operation of broadband radar and single-carrier communication in FDM. To measure the input signal of the amplifier with an oscilloscope the signal must be coupled out and down-converted with a mixer by using a local oscillator at 33.7 GHz. After amplification by using a HPA, the signal will be coupled out, attenuated by 23 dB and down-converted with a mixer by using the same local oscillator. Thus, the output signal of the amplifier can also be measured with the oscilloscope. The oscilloscope itself has a maximal analog bandwidth of 4 GHz and $10^7$ samples will be acquired in 1 ms. The following Table 5.1 summarizes the most important parameters used for the measurements.

Table 5.1: Parameters used for the measurement for the assessment of the signals before and after the HPA.

| **Parameter** | **Value** |
|---|---|
| Radar center frequency | 35.0 GHz |
| Radar bandwidth | 2.0 GHz |
| Chirp duration | 1 ms |
| Communication center frequency | 37.4 GHz |
| Communication bandwidth | 300 kHz |
| Saturated output power of HPA | 36 dBm |
| Power back-off of HPA input | 6 dB |

The saturated output power of the amplifier is approximately 36 dBm. As shown in Figure 5.6, a theoretical PAPR of approximately 6 dB is expected, thus, a power back-off of minimally 6 dB is necessary.
Figure 5.8 shows the measurement result of the input signal and the output signal of the HPA in the time domain measured with an oscilloscope.

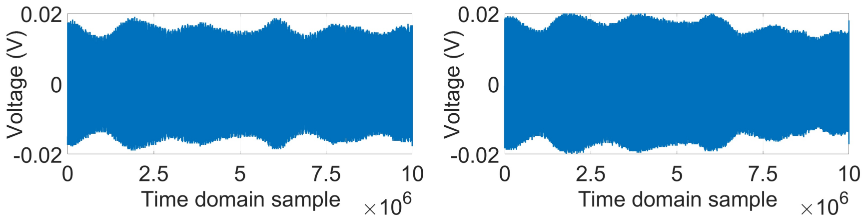


Figure 5.8: FDM signal before (left) and after (right) the HPA in the time domain.

The amplitudes of both signals are approximately +/- 0.02 V. The output signal of the HPA was attenuated. For this reason, the voltage of the input - and the output signal of the HPA is very similar. The DC component of the signals was reduced by post-processing with software. In both graphs, amplitude

perturbations are visible. This is mostly explained by the signal generation, up-conversion and frequency multiplication of the chirp signal. Because of the characteristics of the amplifier, the amplitude reduces at the right side of Figure 5.8 (right) at high frequencies of the chirp.
The last step is to analyze the CCDF curves of the signals before and after the HPA depicted in Figure 5.8. The resulting CCDF curves are visualized in the following Figure 5.9.

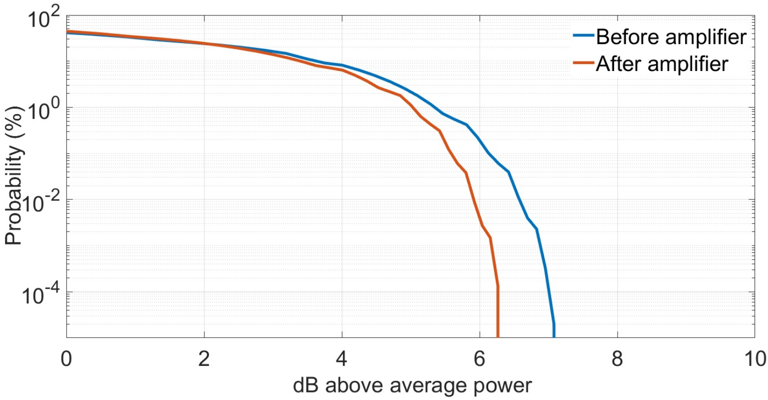


Figure 5.9: Measured CCDF curves of the FDM signal before and after the HPA.

The blue line of Figure 5.9 represents the CCDF of the FDM signal consisting of the chirp with 2 GHz bandwidth and the QPSK communication with 0.4 Mbit/s data rate respectively 300 kHz bandwidth at the input of the HPA. Here, the maximal PAPR is approximately 7.1 dB. This is approximately 1 dB higher than the theory and the simulation shown in Figure 5.6 because of the mentioned amplitude perturbation of the signal caused by the analog signal chain. The red line shows the CCDF of the signal after amplification with the HPA. Here, the maximal PAPR is approximately 6.2 dB. The difference between the signals before and after amplification is 0.9 dB and is found in the frequency dependent variations in the flatness of the gain of the amplifier.

Comparing Figure 5.9 with Figure 5.4 shows that the new approach investigated in this thesis has a significantly lower PAPR than OFDM. This is achieved without any additional effort. Supplementary, the PAPR is independent of the radar and communication bandwidth, because the amount of carrier frequencies is always two and not dependent on the application as in the case of OFDM.

# 6 Conclusions

In this thesis, a solution for an efficient, joint broadband SAR and wireless communication system in the millimeter-wave band for small airborne platforms is investigated. This new system is based on FDM of two simultaneous carrier frequencies: one for FMCW radar and one for QPSK communication.
Chapter 2 gives an introduction to the topic by presenting the fundamentals of radar and wireless communication and by formulating a mathematical description of this approach. After the description of the hardware used in this thesis, a first simulation with the tool SystemVue and the corresponding measurements are presented in the form of range profiles for radar and constellation diagrams for communication. This first setup works almost perfectly regarding the performance of the two system parts.
Radar measurements with an RF bandwidth of 2 GHz and simultaneous communication in an efficient manner is not described in the literature up to now (Refer to Section 1.2). Hence, a further investigation of the approach regarding the power levels of the two frequency bands and the resulting overall bandwidth makes sense.
The following Chapter 3 analyses the relations between the two frequency bands in the case of using a single HPA in the transmitter. This is useful for saving weight, size, power consumption and cost regarding the final system but the resulting intermodulation products have to be considered. For this purpose, the minimal gap between the radar band and the communication band is determined regarding the transmitted signal. Here, by using the minimal gap, equal to the communication bandwidth, no influence of the intermodulation products on the two useful bands occur. Sub-section 3.1.3 presents the resulting overall bandwidth by using an assumed CSAR scenario dependent on the flight altitude of the airborne platform with the mentioned minimal gap. The overall bandwidth is only 5% larger than the radar bandwidth for a maximal flight

altitude of 1000 m. Here, raw data transmission of the FMCW SAR with the integrated communication link to a ground station is assumed. Sub-section 3.2.1 analyses the effect of different gaps on the communication performance in the receiver by using a simulation and a measurement. The gap in percentage of the communication bandwidth is reduced and the rmsEVM in percentage is measured. The minimal gap in percentage of the communication band is found to be approximately 80% in the simulation and approximately 63% in the measurement. These values are lower than the theoretical value of 100%, because of the usage of a pulse-shaping filter and the specific measurement setup. The effect of different gaps on the FMCW radar performance in the receiver without band selection filter is analyzed quantitatively in Sub-section 3.2.2. For this purpose, range-Doppler maps with different gaps between the two frequency bands are used. It turns out that the minimal gap must be larger than the maximal IF to prevent influences of the communication signal on the radar signal. In all other cases, the difference between the spurious signals and the signals caused by the targets in the measurement scene must be considered. This is done theoretically by calculating the ratio between the power of the spurious signal and the power of the signals corresponding to the targets in a first approximation. For a parameter set used for the simulation, this ratio amounts to 57.8 dB. Corresponding simulations show that the ratio amounts to approximately 60.5 dB. The ratio resulting from the measurements amounts to approximately 63.3 dB. The calculated value for the parameter set used for the measurements equals 65.7 dB. The last Section 3.3 presents two possibilities to determine the frequency of the local oscillator for down-conversion of the communication signal in the receiver without a band selection filter. The first approach is for the case of a minimal gap equal to the communication bandwidth between the two frequency bands. If the resulting IF gets too high for processing with the following SDR, the second approach can be used. Here, the gap must be larger than two times the communication bandwidth. Simulations and measurements are presented to show the mentioned effects. Finally, the communication performance is assessed with measurements with and without the chirp signal by using a loop-back cable and an attenuator between the transmitter and the receiving mixer. The EVM increases by only 1% rms

after including the radar chirp into the spectrum of the transmit signal.
The approach described in this thesis needs the radar bandwidth and additional bandwidth for the communication and a gap between the two frequency bands. The literature review, mentioned in Section 1.2, shows alternatives, but with disadvantages regarding the efficiency, the radar bandwidth and the communication data rate. In this thesis, the FMCW radar principle with analog de-ramping is used. This reduces the additional bandwidth required for the communication of radar raw data transmission to a minimum with less computational effort. So the only way to save overall bandwidth is by minimizing the gap between both frequency bands.
Chapter 4 is about minimizing the overall bandwidth by choosing an adapted power of the communication signal and a maximized radar power. First, Section 4.1 describes theoretically what the influence of third-order non-linearities close to the carrier frequencies of the radar and the communication signal is. This effect can be reduced by power balancing of the signals. It turns out for the described HPA that the maximal radar power must be 6 dB lower than the saturated output power. The power of the communication signal must be below 18 dBm. If this requirement is met, only minor influence on the desired frequency bands is detectable in the measurements. Section 4.2 shows the theory about the power of the intermodulation products dependent on the power of the two fundamental frequencies and the third-order intercept point. The dependency of the power of the intermodulation products from the power of the third-order intercept point is investigated in Sub-section 4.3.1. It turns out that the TOI must be as large as possible to suppress the intermodulation products as much as possible. This is shown with a simulation of the whole system of rmsEVM in percentage over TOI in dBm by using a relevant parameter set. The EVM decreases quadratically by increasing the TOI linearly. The mentioned joint CSAR and communication scenario allows the reduction of the power of the communication signal while using a maximal radar power. This reduces the influence of the intermodulation products on the communication signal by using gaps below the communication bandwidth. The rmsEVM in percentage dependent on different power levels of the communication signal is simulated and measured for relevant parameter sets. The optimal simulated

power level for the communication is 17 dBm by using a gap of 0 Hz. Here, the EVM curve has a minimum. In the measurement, a minimal gap of 30% of the communication bandwidth must be chosen, because of the mentioned effect of non-linearities close to the carrier frequencies, as mentioned at the beginning of this chapter. Here, the influence of the intermodulation products on the communication signal is recognizable and can be minimized by reducing the power of the communication signal. The best value for this operating point is by using a power of the communication signal of approximately 16 dBm. As mentioned earlier, the CSAR scenario allows the reduction of the power of the communication signal by using a maximized radar power. This is analyzed in Section 4.4 by calculating the SNR of the radar and the communication part. It turns out for this parameter set with a radar power of 30 dBm and a power of the communication signal of 13.4 dBm that the maximal flight altitude is 520 m. Here, the radar and the communication performance is still sufficient, because the SNR of both functions equals 12 dB.

This chapter shows that the gap between both frequency bands and therefore the overall bandwidth can be reduced by using an adapted communication signal power and a maximized radar power. Hence, broadband radar measurements and simultaneous communication for radar raw data transmission is possible in an efficient manner. Additionally, the radar bandwidth and also the communication data rate can be increased with less effort. This goes beyond the state of the art described in Section 1.2.

Chapter 5 presents the power efficiency of the proposed approach in comparison to the popular OFDM method by using the CCDF analysis. The PAPR of the OFDM signal depends on the measurement scenario as well as the parameter sets and must be reduced with more or less computationally intensive reduction methods. Modern communication systems can have PAPR values larger than 10 dB [Mul20]. The PAPR of the approach investigated in this thesis is only about 6 dB without any effort and is always identical. The lower the PAPR, the more efficient is the analog signal chain. Finally, the CCDF before and after the HPA is analyzed with measurements. The maximal PAPR before the HPA is approximately 7.1 dB. This is 1.1 dB larger than the theoretical one because of amplitude perturbations caused by the analog signal chain. The

PAPR after the HPA is 6.2 dB and 1.1 dB lower than that of the signal at the input of the HPA. This is due to the fact that the amplifier gain has a frequency dependency.

The PAPR of the signals of the approach investigated in this thesis without any effort is significantly lower than the PAPR of the signals of OFDM with reduction techniques. Therefore, the power efficiency of this two-tone FDM consisting of a broadband FMCW radar and a single-carrier QPSK communication simultaneously is essentially better than OFDM.

# Bibliography


[AEK+21] W. A. Ahmad, A. Ergintav, M. Kucharski, D. Kissinger, H. J. Ng. “Scalable 2×2 MIMO Radar Demonstrator with BPSK Data Communication at 79 GHz”. In: *2020 17th European Radar Conference (EuRAD)*. Jan. 2021, pp. 234–237 (cit. on p. 8).

[AJ16] P. P. Ann, R. Jose. “Comparison of PAPR reduction techniques in OFDM systems”. In: *2016 International Conference on Communication and Electronics Systems (ICCES)*. Oct. 2016, pp. 1–5 (cit. on p. 98).

[AON+20] M. B. Alabd, L. G. de Oliveira, B. Nuss, W. Wiesbeck, T. Zwick. “Time-Frequency Shift Modulation for Chirp Sequence based Radar Communications”. In: *2020 IEEE MTT-S International Conference on Microwaves for Intelligent Mobility (ICMIM)*. Nov. 2020, pp. 1–4 (cit. on p. 7).

[Bal66] A. H. Ballard. “A New Multiplex Technique for Communication Systems”. In: *IEEE Transactions on Power Apparatus and Systems* PAS-85.10 (Oct. 1966), pp. 1054–1059 (cit. on p. 3).

[BEJ07] P. Barrenechea, F. Elferink, J. Janssen. “FMCW radar with broadband communication capability”. In: *2007 European Radar Conference*. Oct. 2007, pp. 130–133 (cit. on p. 8).

[BKRS23] H. K. Boddapati, K. Kumar, A. K. Reddy Chavva, M. Saquib Khan. “Joint Communication and Sensing for MIMO Systems with Overlapped OFDM and FMCW”. In: *2023 IEEE 98th Vehicular Technology Conference (VTC 2023-Fall)*. Oct. 2023, pp. 1–5 (cit. on p. 4).

[BMRP16] J.-Y. Baudais, S. Méric, V. Riché, É. Pottier. “MIMO-OFDM signal optimization for SAR imaging radar”. In: *EURASIP Journal on Advances in Signal Processing* 2016.1 (2016), p. 103. URL: https://doi.org/10.1186/s13634-016-0402-7 (cit. on p. 8).

[BP20] S. Bharati, P. Podder. “Adaptive PAPR Reduction Scheme for OFDM Using SLM with the Fusion of Proposed Clipping and Filtering Technique in Order to Diminish PAPR and Signal Distortion”. In: *Wireless Personal Communications* 113.4 (2020), pp. 2271–2288. URL: https://doi.org/10.1007/s11277-020-07323-0 (cit. on p. 101).

[BPG+21] A. N. Barreto, T. M. Pham, S. George, P. Sen, G. Fettweis. “Analysis of a Chirp-Based Waveform for Joint Communications and Radar Sensing (JC&S) using Non-Linear Components”. In: *2021 15th European Conference on Antennas and Propagation (EuCAP)*. Mar. 2021, pp. 1–5 (cit. on p. 6).

[Bra14] K. M. Braun. “OFDM Radar Algorithms in Mobile Communication Networks”. PhD thesis. 2014 (cit. on p. 98).

[BSBF21] F. Bozorgi, P. Sen, A. N. Barreto, G. Fettweis. “RF Front-End Challenges for Joint Communication and Radar Sensing”. In: *2021 1st IEEE International Online Symposium on Joint Communications & Sensing (JC&S)*. Feb. 2021, pp. 1–6 (cit. on p. 6).

[CBP+17] M. Caris, T. Brehm, S. Palm, S. Sieger, F. Klöppel, R. Sommer, D. Janssen, V. Port, S. Stanko. “High resolution dual-channel SAR-system for airborne applications”. In: *2017 18th International Radar Symposium (IRS)*. June 2017, pp. 1–7 (cit. on p. 24).

[CSM+14] M. Caris, S. Stanko, M. Malanowski, P. Samczyński, K. Kulpa, A. Leuther, A. Tessmann. “mm-Wave SAR demonstrator as a test bed for advanced solutions in microwave imaging”. In: *IEEE Aerospace and Electronic Systems Magazine* 29.7 (July 2014), pp. 8–15 (cit. on pp. 2, 6).

[CTRO23] M.-E. Chatzitheodoridi, A. Taylor, O. Rabaste, H. Oriot. “A Cooperative SAR-Communication System Using Continuous Phase Modulation Codes and Mismatched Filters”. In: *IEEE Transactions on Geoscience and Remote Sensing* 61 (2023), pp. 1–14 (cit. on p. 9).

[DBSF19] S. Dwivedi, A. N. Barreto, P. Sen, G. Fettweis. “Target Detection in Joint Frequency Modulated Continuous Wave (FMCW) Radar-Communication System”. In: *2019 16th International Symposium on Wireless Communication Systems (ISWCS)*. Aug. 2019, pp. 277–282 (cit. on p. 7).

[DCJ+23] W. Deng, Z. Chen, H. Jia, P. Guan, T. Ma, A. Yan, S. Sun, X. Huang, G. Chen, R. Ma, S. Dong, L. Duan, Z. Wang, B. Chi. "A D-Band Joint Radar-Communication CMOS Transceiver". In: *IEEE Journal of Solid-State Circuits* 58.2 (Feb. 2023), pp. 411–427 (cit. on p. 8).

[FFW+20] Z. Feng, Z. Fang, Z. Wei, X. Chen, Z. Quan, D. Ji. "Joint radar and communication: A survey". In: *China Communications* 17.1 (Jan. 2020), pp. 1–27 (cit. on p. 3).

[GCI+16] D. Gaglione, C. Clemente, C. V. Ilioudis, A. R. Persico, I. K. Proudler, J. J. Soraghan. "Fractional fourier based waveform for a joint radar - communication system". In: *2016 IEEE Radar Conference (RadarConf)*. May 2016, pp. 1–6 (cit. on p. 7).

[GCI+18] D. Gaglione, C. Clemente, C. V. Ilioudis, A. R. Persico, I. K. Proudler, J. J. Soraghan, A. Farina. "Waveform design for communicating radar systems using fractional Fourier transform". English. In: *Digital Signal Processing* 80 (Sept. 2018), pp. 57–69 (cit. on p. 7).

[Gen23] Y. Geng. "A Novel Waveform Design for OFDM-Based Joint Sensing and Communication System". In: *2023 IEEE 3rd International Symposium on Joint Communications & Sensing (JC&S)*. Mar. 2023, pp. 1–6 (cit. on p. 4).

[GNA+22] L. Giroto de Oliveira, B. Nuss, M. B. Alabd, A. Diewald, M. Pauli, T. Zwick. "Joint Radar-Communication Systems: Modulation Schemes and System Design". In: *IEEE Transactions on Microwave Theory and Techniques* 70.3 (Mar. 2022), pp. 1521–1551 (cit. on p. 3).

[HHM+18] Y. Huang, S. Hu, S. Ma, Q. Luo, D. Huang, Y. Gao, R. Shi. "Constant envelope OFDM RadCom fusion system". In: *EURASIP Journal on Wireless Communications and Networking* 2018.1 (2018), p. 104. URL: https://doi.org/10.1186/s13638-018-1105-6 (cit. on p. 5).

[HHM+22] Y. Huang, S. Hu, S. Ma, Z. Liu, M. Xiao. "Designing Low-PAPR Waveform for OFDM-Based RadCom Systems". In: *IEEE Transactions on Wireless Communications* 21.9 (Sept. 2022), pp. 6979–6993 (cit. on p. 5).

[HKH23] K. Han, S. Kang, S. Hong. "Sub-Nyquist Sampling OFDM Radar". In: *IEEE Transactions on Radar Systems* 1 (2023), pp. 669–680 (cit. on p. 4).

[HL05] S. H. Han, J. H. Lee. “An overview of peak-to-average power ratio reduction techniques for multicarrier transmission”. In: *IEEE Wireless Communications* 12.2 (Apr. 2005), pp. 56–65 (cit. on p. 5).

[HLZ+22] Q. Huang, Z. Luo, J. Zhang, W. Wang, Q. Zhang. “LoRadar: Enabling Concurrent Radar Sensing and LoRa Communication”. In: *IEEE Transactions on Mobile Computing* 21.6 (June 2022), pp. 2045–2057 (cit. on p. 7).

[HRT+17] R. Hadani, S. Rakib, M. Tsatsanis, A. Monk, A. J. Goldsmith, A. F. Molisch, R. Calderbank. “Orthogonal Time Frequency Space Modulation”. In: *2017 IEEE Wireless Communications and Networking Conference (WCNC)*. Mar. 2017, pp. 1–6 (cit. on p. 5).

[JDW+21] G. Jin, Y. Deng, W. Wang, Y. Zhang, D. Liang, R. Wang. “A Novel Spaceborne MIMO-SAR Imaging Scheme Based on Improved OFDM Waveforms”. In: *IEEE Geoscience and Remote Sensing Letters* 18.12 (Dec. 2021), pp. 2122–2126 (cit. on p. 9).

[JSK22] W. Johannes, S. Stanko, I. Kallfass. “Investigation of an RF Frontend at 35 GHz for Joint Broadband Radar and Communication Applications”. In: *2022 14th German Microwave Conference (GeMiC)*. May 2022, pp. 204–207 (cit. on pp. 28, 30, 79).

[JSK23a] W. Johannes, S. Stanko, I. Kallfass. “Efficient Joint Broadband Radar and Single Carrier Communication System in Frequency Division Multiplexing for High-Range Applications”. In: *2023 24th International Radar Symposium (IRS)*. May 2023, pp. 1–10 (cit. on pp. 65, 66).

[JSK23b] W. Johannes, S. Stanko, I. Kallfass. “Time Domain Analysis of Joint Broadband Radar and Single Carrier Communication in Frequency Division Multiplexing”. In: *2023 20th European Radar Conference (EuRAD)*. Sept. 2023, pp. 278–281 (cit. on p. 104).

[JSW+14] W. Johannes, S. Stanko, A. Wahlen, R. Sommer, N. Pohl, P. Wellig, C. Sennhauser, E. Meier, I. Kallfass. “Implementation of a 35 GHz SAR sensor and a high resolution camera to enable real-time observation”. In: *EUSAR 2014; 10th European Conference on Synthetic Aperture Radar*. June 2014, pp. 1–4 (cit. on p. 2).

[JW08] T. Jiang, Y. Wu. "An Overview: Peak-to-Average Power Ratio Reduction Techniques for OFDM Signals". In: *IEEE Transactions on Broadcasting* 54.2 (June 2008), pp. 257–268 (cit. on p. 5).

[KBM17] L. Kocjancic, A. Balleri, T. Merlet. "Study of the frequency slope effect on the chirp waveform orthogonality". In: *International Conference on Radar Systems (Radar 2017)*. Oct. 2017, pp. 1–6 (cit. on p. 22).

[KD21] S. Kumar, S. Deshwal. "A Review on Orthogonal Time Frequency Space Modulation". In: 2021. URL: `https://api.semanticscholar.org/CorpusID:235754549` (cit. on p. 5).

[Key24] Keysight. *PathWave System Design (SystemVue)*. 2024. URL: `https://www.keysight.com/de/de/products/software/pathwave-design-software/pathwave-system-design-software.html` (cit. on p. 10).

[KPVY23a] U. Kumbul, N. Petrov, C. S. Vaucher, A. Yarovoy. "Performance Analysis of Phase-Coded FMCW for Joint Sensing and Communication". In: *2023 24th International Radar Symposium (IRS)*. 2023, pp. 1–10 (cit. on p. 6).

[KPVY23b] U. Kumbul, N. Petrov, C. S. Vaucher, A. Yarovoy. "Smoothed Phase-Coded FMCW: Waveform Properties and Transceiver Architecture". In: *IEEE Transactions on Aerospace and Electronic Systems* 59.2 (Apr. 2023), pp. 1720–1737 (cit. on p. 6).

[KPZ+21] U. Kumbul, N. Petrov, F. van der Zwan, C. S. Vaucher, A. Yarovoy. "Experimental Investigation of Phase Coded FMCW for Sensing and Communications". In: *2021 15th European Conference on Antennas and Propagation (EuCAP)*. Mar. 2021, pp. 1–5 (cit. on p. 6).

[LCM+22] F. Liu, Y. Cui, C. Masouros, J. Xu, T. X. Han, Y. C. Eldar, S. Buzzi. "Integrated Sensing and Communications: Toward Dual-Functional Wireless Networks for 6G and Beyond". In: *IEEE Journal on Selected Areas in Communications* 40.6 (June 2022), pp. 1728–1767 (cit. on p. 3).

[Lev00] N. Levanon. "Multifrequency radar signals". In: *Record of the IEEE 2000 International Radar Conference [Cat. No. 00CH37037]*. May 2000, pp. 683–688 (cit. on p. 3).

[LHN09] D.-W. Lim, S.-J. Heo, J.-S. No. "An overview of peak-to-average power ratio reduction schemes for OFDM signals". In: *Journal of Communications and Networks* 11.3 (June 2009), pp. 229–239 (cit. on p. 5).

[Lil25] J. Liller. *The Shannon-Hartley-Theorem*. 2025. URL: https://www.vcalc.com/wiki/vcalc/Shannon-Hartley-Theorem/ (cit. on p. 93).

[LMP+20] F. Liu, C. Masouros, A. P. Petropulu, H. Griffiths, L. Hanzo. “Joint Radar and Communication Design: Applications, State-of-the-Art, and the Road Ahead”. In: *IEEE Transactions on Communications* 68.6 (June 2020), pp. 3834–3862 (cit. on p. 3).

[LRBV21] S. D. Liyanaarachchi, T. Riihonen, C. B. Barneto, M. Valkama. “Optimized Waveforms for 5G–6G Communication With Sensing: Theory, Simulations and Experiments”. In: *IEEE Transactions on Wireless Communications* 20.12 (Dec. 2021), pp. 8301–8315 (cit. on p. 3).

[LTAW19] F. Lampel, R. F. Tigrek, A. Alvarado, F. M. Willems. “A Performance Enhancement Technique for a Joint FMCW RadCom System”. In: *2019 16th European Radar Conference (EuRAD)*. Oct. 2019, pp. 169–172 (cit. on p. 6).

[LUT+20] F. Lampel, F. Uysal, F. Tigrek, S. Orru, A. Alvarado, F. Willems, A. Yarovoy. “System Level Synchronization of Phase-Coded FMCW Automotive Radars for RadCom”. In: *2020 14th European Conference on Antennas and Propagation (EuCAP)*. Mar. 2020, pp. 1–5 (cit. on p. 6).

[M I80] M. I. Skolnik. *Introduction to radar systems*. 2nd edition. McGraw-Hill Kogakusha, 1980 (cit. on pp. 1, 92).

[MAA20] S. Mazahir, S. Ahmed, M.-S. Alouini. “A Survey on Joint Communication-Radar Systems”. In: *Frontiers in Communications and Networks*. 2020. URL: https://api.semanticscholar.org/CorpusID:23204185 (cit. on p. 3).

[Mar25] Marki microwave. *IP3 Intermodulation Calculator*. 2025. URL: https://markimicrowave.com/technical-resources/tools/ip3-intermodulation-calculator/ (cit. on pp. 74, 81).

[MBK+19] K. V. Mishra, M. Bhavani Shankar, V. Koivunen, B. Ottersten, S. A. Vorobyov. “Toward Millimeter-Wave Joint Radar Communications: A Signal Processing Perspective”. In: *IEEE Signal Processing Magazine* 36.5 (Sept. 2019), pp. 100–114 (cit. on p. 3).

[MCW+22] T. Mao, J. Chen, Q. Wang, C. Han, Z. Wang, G. K. Karagiannidis. “Waveform Design for Joint Sensing and Communications in Millimeter-Wave and Low Terahertz Bands”. In: *IEEE Transactions on Communications* 70.10 (Oct. 2022), pp. 7023–7039 (cit. on p. 5).

[MSA22] E. Memisoglu, M. M. Sahin, H. Arslan. “Orthogonal Coexistence of Overlapped Radar and Communication Waveforms”. In: *2022 IEEE Wireless Communications and Networking Conference (WCNC)*. Apr. 2022, pp. 2190–2195 (cit. on p. 4).

[MSBM19] P. M. McCormick, C. Sahin, S. D. Blunt, J. G. Metcalf. “FMCW Implementation of Phase-Attached Radar-Communications (PARC)”. In: *2019 IEEE Radar Conference (RadarConf)*. Apr. 2019, pp. 1–6 (cit. on p. 6).

[MSH+20a] D. Ma, N. Shlezinger, T. Huang, Y. Liu, Y. C. Eldar. “Automotive Dual-Function Radar Communications Systems: An Overview”. In: *2020 IEEE 11th Sensor Array and Multichannel Signal Processing Workshop (SAM)*. June 2020, pp. 1–5 (cit. on p. 3).

[MSH+20b] D. Ma, N. Shlezinger, T. Huang, Y. Liu, Y. C. Eldar. “Joint Radar - Communication Strategies for Autonomous Vehicles: Combining Two Key Automotive Technologies”. In: *IEEE Signal Processing Magazine* 37.4 (July 2020), pp. 85–97 (cit. on p. 3).

[MSM10] R. Mohseni, A. Sheikhi, M. A. Masnadi-Shirazi. “Multicarrier constant envelope OFDM signal design for radar applications”. In: *AEU - International Journal of Electronics and Communications* 64.11 (2010), pp. 999–1008. URL: `https://www.sciencedirect.com/science/article/pii/S1434841109002623` (cit. on p. 5).

[Mul20] T. Multerer. “Development of a spectrum-efficient OFDM MIMO radar for future urban air mobility applications”. PhD thesis. Jan. 2020 (cit. on pp. 5, 98, 112).

[MW13a] J. Moghaddasi, K. Wu. “Improved joint radar-radio (RadCom) transceiver for future intelligent transportation platforms and highly mobile high-speed communication systems”. In: *2013 IEEE International Wireless Symposium (IWS)*. Apr. 2013, pp. 1–4 (cit. on p. 7).

[MW13b] J. Moghaddasi, K. Wu. “Unified radar-communication (RadCom) multi-port interferometer transceiver”. In: *2013 European Microwave Conference*. Oct. 2013, pp. 1791–1794 (cit. on p. 7).

[NMMZ20] B. Nuss, J. Mayer, S. Marahrens, T. Zwick. "Frequency Comb OFDM Radar System With High Range Resolution and Low Sampling Rate". In: *IEEE Transactions on Microwave Theory and Techniques* 68.9 (Sept. 2020), pp. 3861–3871 (cit. on p. 4).

[P A13] P. A. Höher. *Grundlagen der digitalen Informationsübertragung*. 2. Auflage. Springer Vieweg, 2013 (cit. on pp. 18, 23).

[Pal21] S. M. Palm. "Mapping of urban scenes by single-channel mmW FMCW SAR on circular flight and curved car trajectories". en. PhD thesis. Technische Universität München, 2021, p. 153 (cit. on pp. 1, 42).

[PBF20] T. M. Pham, A. N. Barreto, G. P. Fettweis. "Efficient Communications for Overlapped Chirp-Based Systems". In: *IEEE Wireless Communications Letters* 9.12 (Dec. 2020), pp. 2202–2206 (cit. on p. 6).

[QQGZ14] S. Quan, W. Qian, J. Guq, V. Zhang. "Radar-communication integration: An overview". In: *The 7th IEEE/International Conference on Advanced Infocomm Technology*. Nov. 2014, pp. 98–103 (cit. on p. 3).

[R J00] R. J. Sullivan. *Microwave Radar: Imaging and Advanced Concepts*. Artech House Publishers, 2000 (cit. on p. 1).

[RB03] M. Roberton, E. Brown. "Integrated radar and communications based on chirped spread-spectrum techniques". In: *IEEE MTT-S International Microwave Symposium Digest, 2003*. Vol. 1. June 2003, pp. 611–614 (cit. on p. 7).

[RS17] J. Ravisankar, S. Suryanarayana. "Analysis of PAPR Reduction techniques in OFDM System". In: *International Journal of Creative Research Thoughts* 5.4 (2017), pp. 948–955 (cit. on pp. 98, 101, 102).

[RSM+18] T. F. Rahman, C. Sacchi, S. Morosi, A. Mazzinghi, N. Bartolomei. "Constant-Envelope Multicarrier Waveforms for Millimeter Wave 5G Applications". In: *IEEE Transactions on Vehicular Technology* 67.10 (Oct. 2018), pp. 9406–9420 (cit. on p. 5).

[SAC19] G. D. Surabhi, R. M. Augustine, A. Chockalingam. "Peak-to-Average Power Ratio of OTFS Modulation". In: *IEEE Communications Letters* 23.6 (June 2019), pp. 999–1002 (cit. on p. 5).

[Sem25] Semtech. *LoRa*. 2025. URL: `https://www.semtech.com/lora/` (cit. on p. 7).

[SFH+16] W. Scheiblhofer, R. Feger, A. Haderer, S. Scheiblhofer, A. Stelzer. "In-chirp FSK communication between cooperative 77-GHz radar stations integrating variable power distribution between ranging and communication system". In: *International Journal of Microwave and Wireless Technologies* 8.4-5 (2016), pp. 825–832 (cit. on p. 7).

[SFHS15] W. Scheiblhofer, R. Feger, A. Haderer, A. Stelzer. "Method to embed a data-link on FMCW chirps for communication between cooperative 77-GHz radar stations". In: *2015 European Radar Conference (EuRAD)*. Sept. 2015, pp. 181–184 (cit. on p. 7).

[SJS08] A. Stelzer, M. Jahn, S. Scheiblhofer. "Precise distance measurement with cooperative FMCW radar units". In: *2008 IEEE Radio and Wireless Symposium*. Jan. 2008, pp. 771–774 (cit. on p. 7).

[SPZW09] C. Sturm, E. Pancera, T. Zwick, W. Wiesbeck. "A novel approach to OFDM radar processing". In: *2009 IEEE Radar Conference*. May 2009, pp. 1–4 (cit. on p. 3).

[SRI06] R. A. Shafik, M. S. Rahman, A. R. Islam. "On the Extended Relationships Among EVM, BER and SNR as Performance Metrics". In: *2006 International Conference on Electrical and Computer Engineering*. Dec. 2006, pp. 408–411 (cit. on p. 92).

[SSB07] G. N. Saddik, R. S. Singh, E. R. Brown. "Ultra-Wideband Multifunctional Communications-Radar System". In: *IEEE Transactions on Microwave Theory and Techniques* 55.7 (2007), pp. 1431–1437 (cit. on p. 7).

[Sto92] A. G. Stove. "Linear FMCW radar techniques". In: *IEE Proceedings* 139 (1992), pp. 343–350 (cit. on p. 2).

[TAP+08] S. C. Thompson, A. U. Ahmed, J. G. Proakis, J. R. Zeidler, M. J. Geile. "Constant Envelope OFDM". In: *IEEE Transactions on Communications* 56.8 (Aug. 2008), pp. 1300–1312 (cit. on p. 5).

[TDJ+21] R. Thomä, T. Dallmann, S. Jovanoska, P. Knott, A. Schmeink. "Joint Communication and Radar Sensing: An Overview". In: *2021 15th European Conference on Antennas and Propagation (EuCAP)*. Mar. 2021, pp. 1–5 (cit. on p. 3).

[TLY+22] Y. Tan, Z. Li, J. Yang, X. Yu, H. An, J. Wu, J. Yang. “Joint Communication and SAR Waveform Design Method via Time-Frequency Spectrum Shaping”. In: *IEEE Transactions on Geoscience and Remote Sensing* 60 (2022), pp. 1–13 (cit. on p. 9).

[UO20] F. Uysal, S. Orru. “Phase-Coded FMCW Automotive Radar: Application and Challenges”. In: *2020 IEEE International Radar Conference (RADAR)*. Apr. 2020, pp. 478–482 (cit. on p. 6).

[Uys20] F. Uysal. “Phase-Coded FMCW Automotive Radar: System Design and Interference Mitigation”. In: *IEEE Transactions on Vehicular Technology* 69.1 (Jan. 2020), pp. 270–281 (cit. on p. 6).

[VBS23] P. Varshney, P. Babu, P. Stoica. “Low-PAPR OFDM Waveform Design for Radar and Communication Systems”. In: *IEEE Transactions on Radar Systems* 1 (2023), pp. 69–74 (cit. on p. 5).

[WA18] C.-H. Wang, O. Altintas. “Demo: A Joint Radar and Communication System Based on Commercially Available FMCW Radar”. In: *2018 IEEE Vehicular Networking Conference (VNC)*. Dec. 2018, pp. 1–2 (cit. on p. 7).

[WBV21] T. Wild, V. Braun, H. Viswanathan. “Joint Design of Communication and Sensing for Beyond 5G and 6G Systems”. In: *IEEE Access* 9 (2021), pp. 30845–30857 (cit. on p. 3).

[WCL+15] J. Wang, L.-Y. Chen, X.-D. Liang, C.-b. Ding, K. Li. “Implementation of the OFDM Chirp Waveform on MIMO SAR Systems”. In: *IEEE Transactions on Geoscience and Remote Sensing* 53.9 (Sept. 2015), pp. 5218–5228 (cit. on p. 8).

[WLC+19] J. Wang, X.-D. Liang, L.-Y. Chen, L.-N. Wang, K. Li. “First Demonstration of Joint Wireless Communication and High-Resolution SAR Imaging Using Airborne MIMO Radar System”. In: *IEEE Transactions on Geoscience and Remote Sensing* 57.9 (Sept. 2019), pp. 6619–6632 (cit. on p. 9).

[WLCL23] J. Wang, X.-D. Liang, L.-Y. Chen, Y.-L. Li. “Waveform Designs for Joint Wireless Communication and Radar Sensing: Pitfalls and Opportunities”. In: *IEEE Internet of Things Journal* 10.17 (Sept. 2023), pp. 15252–15265 (cit. on p. 3).

[Wol25] C. Wolff. *The Radar Equation*. 2025. URL: `https://www.radartutorial.eu/01.basics/!rb02.en.html` (cit. on p. 90).

[WQW+23] Z. Wei, H. Qu, Y. Wang, X. Yuan, H. Wu, Y. Du, K. Han, N. Zhang, Z. Feng. “Integrated Sensing and Communication Signals Toward 5G-A and 6G: A Survey”. In: *IEEE Internet of Things Journal* 10.13 (July 2023), pp. 11068–11092 (cit. on p. 3).

[XZD+23] B. Xue, G. Zhang, Q. Dai, Z. Fang, H. Leung. “Waveform Diversity Design of OFDM Chirp for Miniature Millimeter-Wave MIMO Radar Based on Dechirp”. In: *IEEE Transactions on Geoscience and Remote Sensing* 61 (2023), pp. 1–16 (cit. on p. 8).

[YWZT18] C. Yang, M. Wang, L. Zheng, C. Tang. “Dual Function System With Shared Spectrum Using FMCW”. In: *IEEE Access* 6 (2018), pp. 79026–79038 (cit. on p. 7).

[ZLM+21] J. A. Zhang, F. Liu, C. Masouros, R. W. Heath, Z. Feng, L. Zheng, A. Petropulu. “An Overview of Signal Processing Techniques for Joint Communication and Radar Sensing”. In: *IEEE Journal of Selected Topics in Signal Processing* 15.6 (Nov. 2021), pp. 1295–1315 (cit. on p. 3).

[ZRW+22] J. A. Zhang, M. L. Rahman, K. Wu, X. Huang, Y. J. Guo, S. Chen, J. Yuan. “Enabling Joint Communication and Radar Sensing in Mobile Networks—A Survey”. In: *IEEE Communications Surveys & Tutorials* 24.1 (Firstquarter 2022), pp. 306–345 (cit. on p. 3).

[ZWD+21] Y. Zhang, W. Wang, Y. Deng, R. Wang, G. Jin, Y. Zhou, Y. Long. “Implementation of a MIMO-SAR Imaging Mode Based on OFDM Chirp Waveforms”. In: *IEEE Geoscience and Remote Sensing Letters* 18.7 (July 2021), pp. 1249–1253 (cit. on p. 8).

[ZX15] T. Zhang, X.-G. Xia. “OFDM Synthetic Aperture Radar Imaging With Sufficient Cyclic Prefix”. In: *IEEE Transactions on Geoscience and Remote Sensing* 53.1 (2015), pp. 394–404 (cit. on p. 8).

[ZZCW22] W. Zhou, R. Zhang, G. Chen, W. Wu. “Integrated Sensing and Communication Waveform Design: A Survey”. In: *IEEE Open Journal of the Communications Society* 3 (2022), pp. 1930–1949 (cit. on p. 3).